Dissertation presented to the Instituto Tecnológico de Aeronáutica, in partial fulfillment of the requirements for the degree of Master of Science in the Program of Aeronautics and Mechanical Engineering, Field of Materials and Manufacturing Processes.

Lucas Barreiros Robatto

RESIDUAL STRESSES HETEROGENEITY ASSESSMENT OF HIGH PERFORMANCE POWDER METALLURGY GEARS

Dissertation approved in its final version by signatories below:

Prof. Dr. Anderson Vicente Borille
Advisor

Prof. Dr. Luiz Carlos Sandoval Góes
Prorector of Graduate Studies and Research

Campo Montenegro
São José dos Campos, SP - Brazil
2017

Cataloging-in Publication Data
Documentation and Information Division

Robatto, Lucas Barreiros
Residual stresses heterogeneity assessment of high performance powder metallurgy gears / Lucas Barreiros Robatto.
São José dos Campos, 2017.
100f.

Dissertation of Master of Science – Course of Aeronautics and Mechanical Engineering. Area of Materials and Manufacturing Processes – Instituto Tecnológico de Aeronáutica, 2017. Advisor: Prof. Dr. Anderson Vicente Borille.

1. Tensão residual. 2. Engrenagens. 3. Metalurgia do pó. 4. Fabricação de aço. 5. Heterogeneidade. 6. Metalurgia. I. Instituto Tecnológico de Aeronáutica. II. Residual stresses heterogeneity assessment of high performance powder metallurgy gears.

BIBLIOGRAPHIC REFERENCE

ROBATTO, Lucas Barreiros. **Residual stresses heterogeneity assessment of high performance powder metallurgy gears**. 2017. 100f. Dissertation of Master of Science – Instituto Tecnológico de Aeronáutica, São José dos Campos.

CESSION OF RIGHTS

Lucas Barreiros Robatto
DCTA - Departamento de Ciência e Tecnologia Aeroespacial, Praça Marechal Eduardo Gomes, n° 50 - Vila das Acácias
12.228-900 – São José dos Campos-SP-Brazil

RESIDUAL STRESSES HETEROGENEITY ASSESSMENT OF HIGH PERFORMANCE POWDER METALLURGY GEARS

Lucas Barreiros Robatto

Thesis Committee Composition:

Prof. Dr.	Alfredo Rocha de Faria	Chairperson	-	ITA
Prof. Dr.	Anderson Vicente Borille	Advisor	-	ITA
Prof. Dr.	Rodnei Bertazzoli		-	ITA
Dr.	Arnaldo Freitas Camarão		-	Engineering Consultant

ITA

Acknowledgments

Several people contributed in different ways for the realization of this Master Thesis, and I owe many thanks to them. My parents, grandparents and brothers for their example, love and support. My love Amanda Acioli, for being my inspiration. The parents of Amanda, for the friendship. My advisor, Prof. Anderson Borille, for all the incentive since I was an undergraduate freshman. My mentor Prof. Ronnie Rego, for the incalculable teachings. My research collaborators, André D'Oliveira, André Maia, José Moreira, Nathianne Andrade and Patrícia Helena for being the best team. Prof. Gilmar Thim, Dr. Tiago Moreira and Dr. Victor Righetti of the Physics department of ITA, for the support in X-ray diffractometry. Mr. Manjeet Dhiman and Dr. Philipp Kauffmann for the support in powder metallurgy issues. ITA, CCM and CAPES for the knowledge and resources provided. God, for everything.

Resumo

A implementação da metalurgia do pó (MP) em engrenagens de transmissões automotivas tem o potencial de substituir a cadeia convencional de aço forjado em um futuro próximo. Diversos estudos mostram os possíveis benefícios dessa implementação em termos de custos, tempo de fabricação e desempenho de produto. O principal desafio para essa transição é a resistência mecânica inferior das engrenagens da MP, o que implica em uma menor vida em fadiga. Com o avanço da técnica, contudo, a resistência mecânica de tais componentes tem sido aumentada, se aproximando daquela de engrenagens forjadas. Não obstante, a cadeia da MP tem como característica efeitos de heterogeneidade microestrutural, devido à porosidade e à orientação de grão induzida pela etapa de densificação de superfície. Como consequência, tem-se um estado heterogêneo de tensões residuais (TR), que pode afetar o comportamento em fadiga. A presente dissertação então tem como objetivo a compreensão do estado de TR de engrenagens da MP, baseando-se na hipótese de que tais heterogeneidades podem ser avaliadas por métodos de difração de raios X. Portanto, duas perguntas de pesquisa foram formuladas como guia. A primeira delas é sobre qual é o método mais apropriado para essa avaliação. A segunda é sobre quão significante é o efeito da cadeia da MP na heterogeneidade de TR de engrenagens. De acordo com essas perguntas, mapeamentos de TR e métodos de alargamento de perfil de difração foram aplicados à superfície de flancos de engrenagens correspondentes a etapas sucessivas das cadeias de MP e de aço forjado. Análises correlacionais de integridade de superfície foram também realizadas para suportar os resultados de TR. Da análise da metodologia, o método de alargamento de perfil foi o mais apropriado para investigação de etapas de processo isoladas, enquanto que ambos métodos são indicados para comparações entre etapas de processo e cadeias de manufatura. Foi possível então observar que as heterogeneidades de TR de engrenagens se manifestam em dois níveis (macro e micro) e de acordo com a distribuição (ao longo da linha de flanco, da evolvente e difusa). Da análise da evolução da heterogeneidade na cadeia da MP, verificou-se que cada etapa do processo é associada a uma heterogeneidade de TR característica. Constatou-se também a propagação das heterogeneidades ao longo das cadeias. O presente estudo, portanto, contribui para o conhecimento de engrenagens da MP para a otimização de sua vida em fadiga, cujas consequências podem beneficiar as indústrias da metalurgia do pó e automotiva.

Abstract

The implementation of powder metallurgy (PM) for high performance automotive transmission gears has the potential to replace the conventional wrought steel manufacturing chain in a near future. Several studies have shown the possible benefits of this implementation in terms of manufacturing costs, times and product performance. The main limitation of this transition is the inferior mechanical strength of the PM gears, which may implicate in shorter fatigue life. With the advance of the technique, however, the strength of PM gears have been improved, getting closer to that of the wrought steel ones. Nonetheless, the powder metallurgy chain has as characteristic effects of microstructural heterogeneity, due to the porosity and the grain orientation caused by surface densification. A consequence of this is a heterogeneous state of residual stresses (RS), that may affect the fatigue behavior of such gears. The present dissertation, then, has as objective the comprehension of the RS heterogeneity state of PM gears. It is based on the hypothesis that such heterogeneity can be assessed through X-ray diffraction methods. Hence, two research questions were formulated to guide this study. The first question is about the most suitable method for this assessment. The second question is about how significant is the effect of the PM chain on the RS heterogeneity of gears. According to these questions, RS mappings and X-ray diffraction line broadening analysis were applied to the surface of the flank of gear teeth correspondent to successive steps of the PM and wrought steel manufacturing chains. Correlational surface integrity assessments, such as metallography, topography analysis and hardness mapping, were also performed to support the RS results. From the methodology analysis, the line broadening was the most suitable method for investigating single process steps, and both methods are indicated for comparing different manufacturing steps and chains. It could then be observed that the RS heterogeneity of gears is manifested in two levels (macro and micro RS) and three types of distribution (along the lead, along the involute and diffuse). From the evolution of the heterogeneity along the PM chain, it was found that each of the process steps is associated to a characteristic RS heterogeneity. It could also be perceived that the heterogeneity of RS is propagated along the chains analyzed. Therefore, the present study contributes to the knowledge of PM gears for their lifetime optimization, whose consequences can benefit the powder metallurgy and automotive industries.

List of Figures

FIGURE 1.1 – Gear industry scenario 18

FIGURE 1.2 – Logical sequence for the study's objective and approach definition . 21

FIGURE 1.3 – Structure of the dissertation 22

FIGURE 2.1 – Common process steps in the conventional and powder metallurgy chains for gears manufacturing (KLOCKE *et al.*, 2005; KAUFFMANN, 2012; KLOCKE *et al.*, 2014) 23

FIGURE 2.2 – Process steps of the conventional and PM chains in detail (KLOCKE *et al.*, 2005; KAUFFMANN, 2012; KLOCKE *et al.*, 2014) 24

FIGURE 2.3 – Atomization method for producing metal powder (BOLJANOVIC, 2010) 25

FIGURE 2.4 – Types of powders of alloys. From left to right: elemental powder mixture, diffusion bonded powder and pre-alloyed powder (ORLANDIN *et al.*, 2009) 25

FIGURE 2.5 – Compaction tools. Left: compaction tools schematic for spur gears (DAVIS, 2005). Right: compaction tools for helical gears (SIGL *et al.*, 2005) 26

FIGURE 2.6 – Compaction techniques and the resultant density gradients (IERVOLINO; BULLA, 2009) 27

FIGURE 2.7 – Schematic of a continuous sintering furnace (UPADHYAYA, 2002) . . 28

FIGURE 2.8 – Stresses on gears (KLOCKE *et al.*, 2010) 28

FIGURE 2.9 – Methods of gear surface densification. Left: translatory rolling method (NEUGEBAUER *et al.*, 2007). Right: rotary rolling method (KLOCKE *et al.*, 2013) 29

FIGURE 2.10 –Comparison of the processes for gear manufacturing in terms of raw material utilization and energy demand (NARASIMHAN; BORECZKY, 2006; ANDERSON; IMBROGNO, 2014) 30

FIGURE 2.11 –Estimation of costs in the manufacturing of PM and conventional gears (STREHL, 1997 apud RAU *et al.*, 2003) 31

FIGURE 2.12 –PM gears with multifunctional features. Left: (KAUFFMANN, 2015). Right: (WHITTAKER, 2016) 31

FIGURE 2.13 –Surface comparison of a finish hobbed gear and a surface densified PM gear (KAUFFMANN, 2015) 31

FIGURE 2.14 –Summary of the potentials of PM gears 33

FIGURE 2.15 –Schematic for the comprehension of the surface integrity of PM gears 34

FIGURE 2.16 –Residual stress generating mechanisms models (GRIFFITHS, 2001) . 35

FIGURE 2.17 –Origins of residual stresses in the conventional and PM gear manufacturing chains (INOUE, 2014) 35

FIGURE 2.18 –(a) Macro residual stress composed by the contribution of each phase; (b) Schematic of all levels of residual stresses (HAUK; NIKOLIN, 1988; WHITERS; BADHESIA, 2001; SPIESS *et al.*, 2014) 36

FIGURE 2.19 –Gear fatigue failure modes: bending and contact stresses (LECHNER; NAUNHEIMER, 1999; DING; RIEGER, 2003; BELSAK; FLASKER, 2006) 37

FIGURE 2.20 –Relationship between the residual stress profile and the crack propagation (MITSUBAYASHI *et al.*, 1994) 37

FIGURE 2.21 –X-ray diffraction in crystal lattice and the resultant diffractogram. Adapted from (SHACKELFORD, 2014) 38

FIGURE 2.22 –Angles used in residual stress measurement by X-ray diffraction. Adapted from (FITZPATRICK *et al.*, 2005) 40

FIGURE 2.23 –Diffraction from strained material, tension axis horizontal. Lattice planes shown belong to the same *(hkl)* set. N = diffraction-plane normal. Adapted from (CULLITY; STOCK, 2014) 41

FIGURE 2.24 –Different types of d vs $\sin^2\psi$ plots (NOYAN; COHEN, 1987) 41

FIGURE 2.25 –Residual stresses heterogeneity induced by shot peening. (a) Heterogeneity in centimeters scale vs a 2 mm measurement spot (ZHAN *et al.*, 2013); (b) Heterogeneity in tenths of millimeters vs a 2 mm measurement spot (SCHOLTES, 2000) 43

FIGURE 2.26 –The fatigue results of ground discs conflict with the expected effect of the residual macrostresses. A potential explanation is given by the RS heterogeneity, by means of the *Gauss* integral breadth (REGO, 2016) 43

FIGURE 2.27 –Methods for residual stresses heterogeneity assessment, proposed by Rego (2016) 44

FIGURE 2.28 –Contributions of the material's microstructure to the line broadening of diffraction profiles (NOYAN; COHEN, 1987; COCKROFT; BARNES, 2001). On the bottom right, an example of the broadening caused by shot peening (ZHAN *et al.*, 2012) 45

FIGURE 2.29 –Contributions of the surface densification step to the heterogeneity of the microstructure. Effect of the material flow (GRÄSER, 2013) and of the stock (KLOCKE *et al.*, 2013) 46

FIGURE 2.30 –The resultant microstructure after surface densification. Preferred grain orientation can be seen at the dedendum and addendum regions of the gear tooth (KLOCKE *et al.*, 2013) 47

FIGURE 3.1 – Overall experimental scope 48

FIGURE 3.2 – Powder metallurgy and wrought steel gear workpieces 49

FIGURE 3.3 – Experimental diffraction arrangement 50

FIGURE 3.4 – Residual stress mapping 51

FIGURE 3.5 – Fluxogram of curves treatment steps for residual stress determination 53

FIGURE 3.6 – Line broadening analysis procedure 56

FIGURE 3.7 – Metallography analysis 57

FIGURE 3.8 – Hardness mapping 58

FIGURE 3.9 – Topography analysis 59

FIGURE 4.1 – Structure of the results presentation 60

FIGURE 4.2 – Classification of the gears surface residual stresses heterogeneity according to levels (macro and micro) and distribution 61

FIGURE 4.3 – Variations of the macro RS σ_y and the broadening parameters FWHM and ε along the lead profile of PM gears, according to each manufacturing step 62

FIGURE 4.4 – Comparison between the RS variations and the microstrain intensities in the PM and wrought steel chains 63

FIGURE 4.5 – The answer to the first research question of this study on the most suitable method for RS heterogeneity assessment 64

FIGURE 4.6 – Multiple peaks available for the line broadening analysis of this study 65

FIGURE 4.7 – Sensitivity of the different peaks of αFe to broadening. The peaks of higher 2θ angles (211) are the most sensitive 65

FIGURE 4.8 – Results of the residual stress mapping along the lead of the gear tooth after sintering 66

FIGURE 4.9 – RS heterogeneity along the PM gear lead profile as a result of the compaction step 67

FIGURE 4.10 –Line broadening analysis along the lead of the gear tooth after sintering 67

FIGURE 4.11 –Results of the residual stress mapping along the involute of the gear tooth after sintering 68

FIGURE 4.12 –Topography analysis of the flank of the sintered gear tooth. a) SEM image showing heterogeneous pores distribution. b) Different porosity distribution along the lead profile, as calculated by an image analysis software. c) The bands of pores evidenced in a profilometry image 69

FIGURE 4.13 –Roughness mapping along the involute of the sintered gear tooth . . 69

FIGURE 4.14 –Hardness mapping along the involute of the sintered gear tooth . . . 70

FIGURE 4.15 –Metallography showing the transition from sintering to surface densification. 50x magnification 70

FIGURE 4.16 –Results of the residual stress mapping along the lead of the gear tooth after surface densification 70

FIGURE 4.17 –Line broadening analysis along the lead of the gear tooth after surface densification 71

FIGURE 4.18 –Results of the residual stress mapping along the involute of the gear tooth after surface densification 72

FIGURE 4.19 –Metallography showing the different surface densification depths along the involute. 50x magnification 72

FIGURE 4.20 –Metallography showing the non-lamellar bainitic microstructure evolution from sintering to surface densification (200x magnification). In detail, the different grain orientation at the addendum and dedendum of the surface densified gear tooth (500x magnification) . . 73

FIGURE 4.21 –Hardness mapping along the involute of the surface densified gear tooth 73

FIGURE 4.22 –Topography results of the surface densified gear tooth. a) SEM images. b) Profilometry images and roughness mapping 74

FIGURE 4.23 –Results of the residual stress mapping along the lead of the gear tooth after heat treatment 74

FIGURE 4.24 –Line broadening analysis along the lead of the gear tooth after heat treatment 75

FIGURE 4.25 –Results of the residual stress mapping along the involute of the gear tooth after heat treatment 75

FIGURE 4.26 –Metallography showing the microstructure evolution from surface densification to heat treatment (50x magnification). Oriented grains are indicated by the arrows. In detail, the different orientation of the retained austenite at the addendum and dedendum of the heat treated gear tooth (200x magnification) 76

FIGURE 4.27 –Hardness mapping along the involute of the heat treated gear tooth 77

FIGURE 4.28 –Topography results of the heat treated gear tooth. a) Profilometry images and rougness mapping. b) SEM images showing randomly oriented marks 77

FIGURE 4.29 –Comparison of RS heterogeneity along the lead of PM and wrought steel specimens before heat treatment 78

FIGURE 4.30 –Line broadening analysis results along the lead of PM and wrought steel specimens before heat treatment 79

FIGURE 4.31 –Comparison of RS heterogeneity along the involute of PM and wrought steel specimens before heat treatment 80

FIGURE 4.32 –Comparison of RS heterogeneity along the lead of PM and wrought steel specimens after heat treatment 81

FIGURE 4.33 –Line broadening analysis results along the lead of PM and wrought steel specimens after heat treatment 82

FIGURE 4.34 –Comparison of RS heterogeneity along the involute of PM and wrought steel specimens after heat treatment 83

FIGURE 4.35 –Evolution of the RS heterogeneity along the PM manufacturing chain 84

FIGURE 4.36 –Resultant residual stress gradient at the surface of the gear tooth flank of the powder metallurgy manufacturing chain 85

FIGURE 4.37 –Resultant residual stress gradient at the surface of the gear tooth flank of the powder metallurgy manufacturing chain 85

FIGURE A.1 –Gear nomenclature for macrogeometry (AGMA, 2011; MAZZO, 2013) 100

List of Tables

TABLE 2.1 – Weight and inertia reduction for the redesigned transmission (SKOGLUND; LITSTRÖM, 2013) 32

TABLE 2.2 – Types of X-ray diffraction analysis of engineering interest. Adapted from (BALZAR, 1993) 39

TABLE A.1 – PM_S residual stresses values 97

TABLE A.2 – PM_D residual stresses values 97

TABLE A.3 – PM_HT residual stresses values 98

TABLE A.4 – W_C residual stresses values 98

TABLE A.5 – W_HT residual stresses values 98

TABLE A.6 – W_SP residual stresses values 99

TABLE A.7 – W_G residual stresses values 99

List of Abbreviations and Acronyms

FWHM	Full width at half maximum
HV	*Vickers* hardness
MP	Metalurgia do pó
PM	Powder metallurgy
PM_S	Powder metallurgy specimen after sintering
PM_D	Powder metallurgy specimen after surface densification
PM_HT	Powder metallurgy specimen after heat treatment
RS	Residual stresses
RPM	Revolutions per minute
SEM	Scanning electron microscopy
TR	Tensões residuais
XEC	X-ray elastic constants
W_C	Wrought steel specimen after cutting
W_HT	Wrought steel specimen after heat treatment
W_SP	Wrought steel specimen after shot peening
W_G	Wrought steel specimen after grinding

List of Symbols

Capital letters

E	[GPa]	Modulus of elasticity
I	[counts]	Intensity
$K\alpha_1$	[-]	X-ray radiation
$K\alpha_2$	[-]	X-ray radiation
L	[mm]	Length of the irradiated area
N	[Å]	Crystallite size
R	[mm]	Radius of the goniometer
Sa	[μm]	Arithmetical mean height of a surface
W	[mm]	Width of the irradiated area

Small letters

d	[Å]	Distance between lattice planes
d_0	[Å]	Distance between undeformed lattice planes
h	[mm]	Width set in the crossed slits assembly
h	[-]	Function of the observed profile
f	[mm]	Distance from the focus of the X-ray tube to the crossed slits
f	[-]	Function of the physical profile
g	[-]	Function of the instrumental profile
n	[-]	Number of wavelengths
s_1	[10^{-6} MPa^{-1}]	X-ray elastic constant
s_2	[10^{-6} MPa^{-1}]	X-ray elastic constant

Greek letters

β	[° (2θ)]	Integral breadth
β_C	[° (2θ)]	*Cauchy* integral breadth
β_C^f	[° (2θ)]	*Cauchy* integral breadth of the physical profile
β_C^g	[° (2θ)]	*Cauchy* integral breadth of the instrumental profile
β_C^h	[° (2θ)]	*Cauchy* integral breadth of the observed profile

β_G	[° (2θ)]	*Gauss* integral breadth
β_G^f	[° (2θ)]	*Gauss* integral breadth of the physical profile
β_G^g	[° (2θ)]	*Gauss* integral breadth of the instrumental profile
β_G^h	[° (2θ)]	*Gauss* integral breadth of the observed profile
ε	[%]	Microstrain
θ	[°]	Diffraction angle
λ	[Å]	Wavelength
σ	[MPa]	Normal stress
τ	[MPa]	Shear stress
ν	[-]	*Poisson*'s ratio
ϕ	[°]	Angle of rotation of the sample about its surface normal
χ	[°]	Angle of rotation in the plane normal to that of ω and 2θ
ψ	[°]	Tilt angle
ω	[°]	Angle between the incident beam and the sample surface

Chemical elements

Cr	Chromium
Fe	Iron
Mn	Manganese

Contents

1 Introduction 18

1.1 Motivation 18

1.2 Objective and approach 20

1.3 Structure of the dissertation 22

2 Literature review 23

2.1 Powder metallurgy for gears manufacturing 23

2.1.1 The powder metallurgy manufacturing chain 23

2.1.2 Potentials and challenges of PM gears 30

2.2 Surface integrity 33

2.2.1 Residual stresses: definition and relationship with fatigue strength . . 35

2.2.2 X-ray diffraction for residual stress measurement 38

2.2.3 The state of the art of RS heterogeneity investigation 42

2.3 The connection between residual stress heterogeneity and PM gears 46

3 Materials and methods 48

3.1 Workpieces description 49

3.2 RS heterogeneity assessment methods 49

3.2.1 Residual stress mapping 49

3.2.2 Line broadening method 53

3.3 Correlational surface integrity assessment 57

4 Results and discussion 60

4.1 Evaluation of the methods for the assessment of RS heterogeneity 61

4.2 Evolution of RS heterogeneity in the gears manufacturing chains 66

4.2.1 Powder metallurgy chain 66

4.2.2 Manufacturing chains comparison 77

4.2.3 Summary 84

5 Conclusions and outlook 87

Bibliography 89

Appendix A – RS values 97

Annex A – Gears terminology 100

1 Introduction

1.1 Motivation

Gears are machine elements whose function is the transmission of rotary motion and power between shafts through successive engagement of projections called teeth. Gears exist for more than three thousand years and nowadays they are an important element in all machinery in a wide range of applications, among which are gears for machine tools, land transportation, ships, aircrafts and wind turbines (MAITRA, 1994; DAVIS, 2005; RADZEVICH, 2004). Billions of gears are produced every year and the world gear demand is estimated to be of about US$ 217 billion in 2018. The automotive industry is the main gears consumer corresponding to about 70 percent of the market, and automotive transmissions alone account for 45 percent of the entire gear market (MCGUINN, 2011; RADZEVICH, 2004). Figure 1.1 summarizes the present scenario of the gear industry.

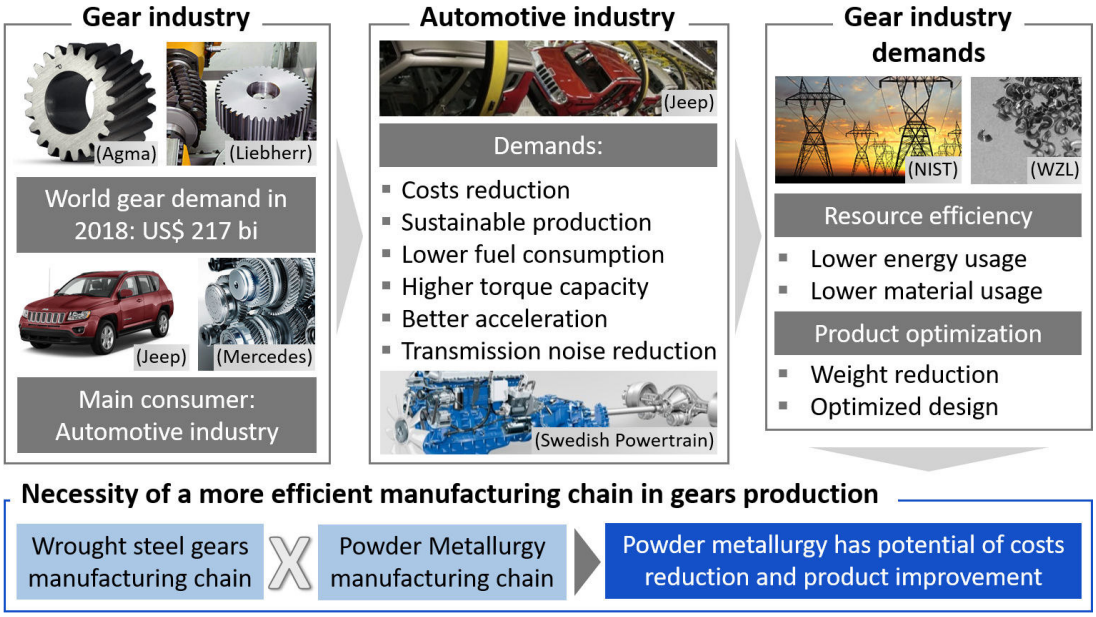

FIGURE 1.1 – Gear industry scenario

Automotive transmission gears are high performance elements, since high power transmission, high dimensional accuracy and long service life must be met. Continuous efforts of the automotive industry point towards costs reduction, sustainable production, lower vehicle fuel consumption, higher torque capacity, better vehicle acceleration and transmission noise reduction. There is also a recent trend in improving the number of speeds in transmissions, which requires higher gear production. Other trend of electrification and hybridization in automotive drivetrains demands reduction in noise emission and increase in power density (SKOGLUND; LITSTRÖM, 2013; WHITTAKER, 2016). Therefore, the gear industry must follow these efforts in terms of resource efficiency (lower energy and material usage) and product optimization (weight reduction, mechanical strength improvement and optimized design). It is remarkable then that gear design and manufacturing require careful treatment, since cost savings in the range of just 10 cents in the production of every gear would imply in total cost savings of hundreds of millions of dollars per year (RADZEVICH, 2004).

In this context, powder metallurgy arises as a potential advantageous alternative process for automotive transmission gears manufacturing in comparison to the conventional wrought steel manufacturing chain. The use of powder metallurgy in the mass production of gears can be associated to significant costs reduction, less environmental impact and also product improvement (RAU *et al.*, 2003; SIGL *et al.*, 2005; ENGSTRÖM; MILLIGAN, 2006; KLOCKE *et al.*, 2007; SKOGLUND; LITSTRÖM, 2013). For the past 30 years, academic and industrial researches have gradually put a lot of focus on making powder metallurgy gears for automotive transmissions a reality (WHITTAKER, 1991; LAWCOCK *et al.*, 1999; FLODIN, 2016). The market potential of automotive transmission gear is a strong motivator for the powder metallurgy industry, since the gear market is believed to be nearly the size of the entire powder metallurgy market (Metal Powder Industries Federation, 2012). Thereupon, in the following years, powder metallurgy gears are expected to be introduced in the least loaded stages of automotive transmissions, where the technology will prove itself as reliable before replacing more heavily loaded gears (FLODIN, 2016).

Despite all the benefits to which powder metallurgy gears can be associated, the challenge of its implementation is related to the material porosity, which can lead to inferior mechanical properties in comparison to wrought steels. Therefore, many present research efforts have been directed to the understanding and improvement of performance of powder metallurgy gears, mainly in terms of fatigue behavior. In this context, residual stresses and its heterogeneity on the surface play an important role in crack initiation and propagation, therefore, affecting the fatigue strength of mechanical components (SCHOLTES, 2000; REGO, 2016). Powder metallurgy steel and the inherent porosity are associated to a higher level of structural heterogeneity, which can be reflected in the non-uniformity of residual stresses in the microscale. Up to the present time, such heterogeneities and the

complexity of their experimental evaluation have not been systematically described in the literature.

The present study hence provide answers on the heterogeneity of residual stresses of powder metallurgy gears, assessed through X-ray diffraction methods. Consequences of this knowledge can give basis to the application of the concept of *Design for Residual Stress* described by REGO (2016) for powder metallurgy gears and to the optimization of surface integrity and fatigue strength of such components. Therefore, these contributions can be a small step in making the implementation of powder metallurgy in automotive transmission gears a reality.

1.2 Objective and approach

The implementation of high performance powder metallurgy gears for automotive transmissions can be associated to economical, ecological and technical advantages in comparison to the conventional wrought steel gears. However, the material porosity and the grain orientation induced by the surface densification manufacturing step can lead to microstructural non-uniformity, which in turn can be reflected into a heterogeneous state of residual stresses. The heterogeneity of such stresses can have a significant effect on fatigue behavior, since variations of intensity of micro residual stresses are linked to crack initiation. As the challenge of applying powder metallurgy gears is mainly related to the fatigue performance, the knowledge of the associated residual stress and its heterogeneity must be dominated to achieve the control of such features for the gears lifetime optimization.

The problematic of assessing the residual stress heterogeneity is based on the complexity of its experimental evaluation and on finding a robust and accurate method for this purpose. In gears engineering applications, however, residual stresses are generally assessed in a macro scale by X-ray diffraction (GENZEL, 1997; KLOCKE *et al.*, 2016). Micro residual stresses and microstructural properties of the material, which are reachable through the potential of the diffraction technique and which could be useful for analyzing structurally heterogeneous materials, are in most cases not explored (GENZEL, 1997). Under these circumstances, having as assumption that the non-uniform microstructure in powder metallurgy gears lead to a heterogeneous residual stresses state, the research hypothesis of this study was formulated:

> *"Methods of X-ray diffraction based on surface residual stress mapping and diffraction microstructural line broadening analysis can be appropriate for the residual stress heterogeneity assessment of powder metallurgy gears."*

If the hypothesis is proved, the application of these methods can provide knowledge on how the powder metallurgy manufacturing steps influence these heterogeneities. Accordingly, the objective of this study is the comprehension of the residual stress heterogeneity state of gears manufactured by powder metallurgy. As consequence of the hypothesis and objective, the following research questions were drawn up to orient this Master Thesis:

1st Research question: What is the most suitable method for the assessment of residual stress heterogeneity of powder metallurgy gears?

2nd Research question: How significant is the effect of the powder metallurgy chain on the evolution of the residual stress heterogeneity of a gear?

The approach to answer these questions was the X-ray diffraction measurement at the flank surface of powder metallurgy and wrought steel gears at different steps of the correspondent manufacturing chains. The residual stress mapping and the line broadening analysis methods were applied for residual stresses heterogeneity assessment. Topography, metallography and hardness distribution investigations were also performed for correlation with the residual stresses findings. The residual stress heterogeneity assessment methods were then evaluated to provide the answer to the first research question. In sequence, the results were analyzed in-between the manufacturing chains to answer the second research question on the evolution of the residual stresses heterogeneity with the processes steps. Figure 1.2 summarizes the objective of this study and the approach to its achievement.

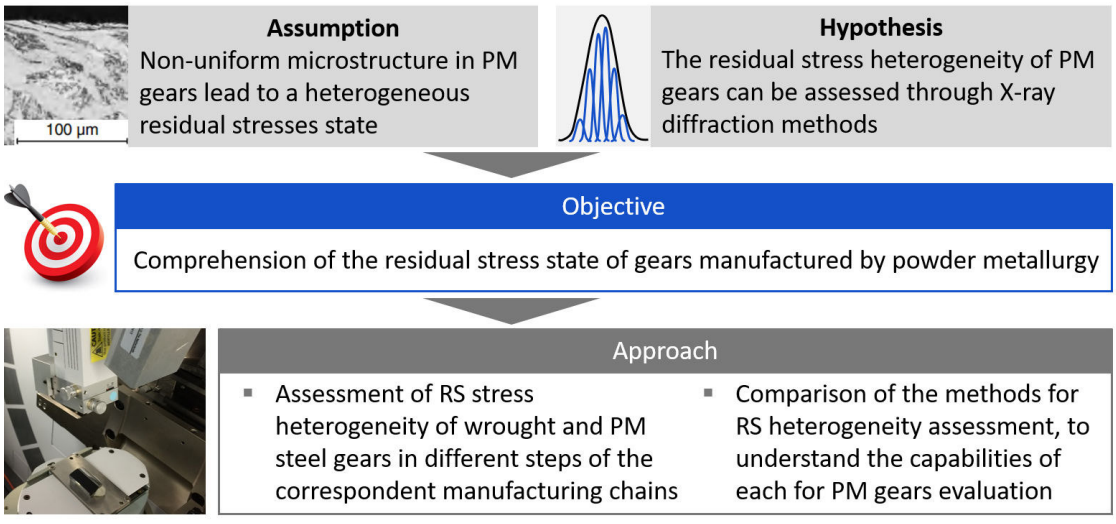

FIGURE 1.2 – Logical sequence for the study's objective and approach definition

1.3 Structure of the dissertation

The structure of this Master Thesis is oriented to answer the research questions in the most logical manner. After the study introduction in **Chapter 1**, in which the motivation, objective and approach are delineated, the theoretical fundamentals and state of the art are described in **Chapter 2**. This chapter provides basic and updated knowledge of what has been developed in scientific and industrial scenarios. It starts with a description of the powder metallurgy manufacturing chain for gears and with a detailing of the potential and challenges of this non-conventional process. In sequence, the importance of surface integrity for mechanical components performance is highlighted, and finally the topic residual stresses and their heterogeneity is explored. Chapter 2 is then concluded with a section connecting the main themes of powder metallurgy gears and residual stresses heterogeneity.

To answer the research question appropriately, it is fundamental to have well defined and directed methods. Therefore, **Chapter 3** exposes the materials, the experiments and analytic methods of this study. An overview of the experimental and analytical scope is firstly done, and next the workpieces studied are described. The methodology description is then divided into residual stress heterogeneity assessment, whose described methods are the core of this study, and correlational surface integrity assessment (material characterization, topography and hardness distribution analysis).

In **Chapter 4**, the exposal of the results is divided according to the research questions. In its first section, focus is given on the first question, and the methods for residual stresses heterogeneity assessment are analyzed and compared. In the other section, the results and discussion are directed to the second question, and the evolution of residual stress heterogeneity is analyzed along the manufacturing chains steps. Finally, the conclusions of this Master Thesis are made in **Chapter 5**, in which the objective and research questions are recalled and the contributions of the study are emphasized. The dissertation is then closed with proposals of future developments for the continuation of the research of residual stresses heterogeneity in powder metallurgy gears. Figure 1.3 illustrates and summarizes the whole structure described.

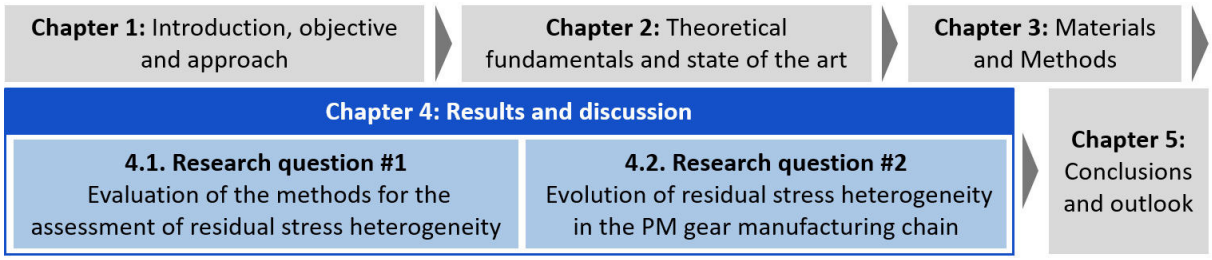

FIGURE 1.3 – Structure of the dissertation

2 Literature review

2.1 Powder metallurgy for gears manufacturing

2.1.1 The powder metallurgy manufacturing chain

In the conventional manufacturing chain of automotive gears, the material of choice is normally a wrought steel alloy (SIGL *et al.*, 2007; NIGARURA *et al.*, 2015b; KHODAEE *et al.*, 2016). The conventional manufacturing starts with a forged blank that passes through successive machining steps and heat treatment. Different machining processes for teeth cutting and heat treatments can be employed, depending on the product specifications. The alternative powder metallurgy chain, in contrast, is totally different until the heat treatment step, after which the processes can be similar for both chains (KAUFFMANN, 2012). A comparison of the conventional and powder metallurgy chains steps is shown in Figures 2.1 and 2.2. As the conventional route is widely known in the gear industry, a more detailed description of the powder metallurgy chain steps is done in the following paragraphs.

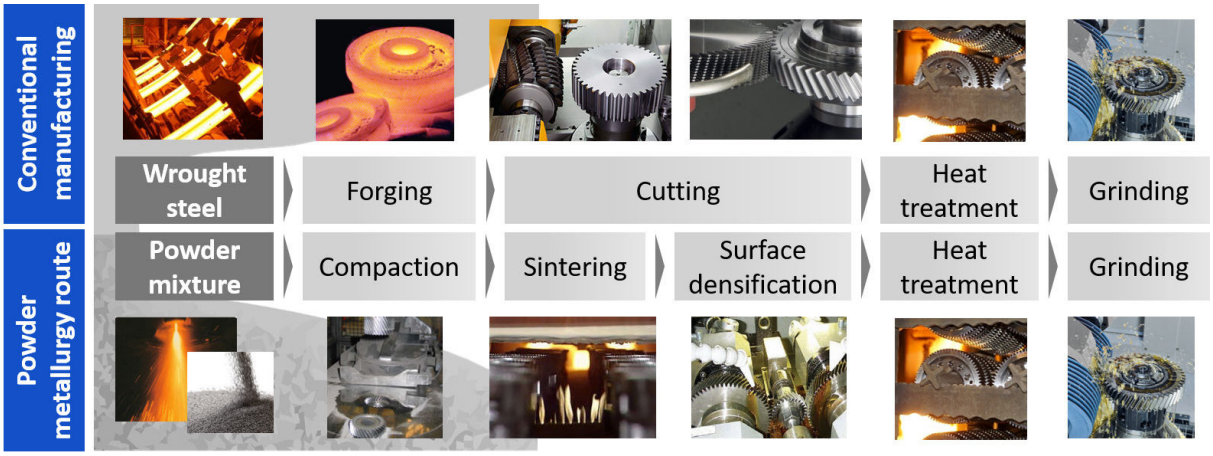

FIGURE 2.1 – Common process steps in the conventional and powder metallurgy chains for gears manufacturing (KLOCKE *et al.*, 2005; KAUFFMANN, 2012; KLOCKE *et al.*, 2014)

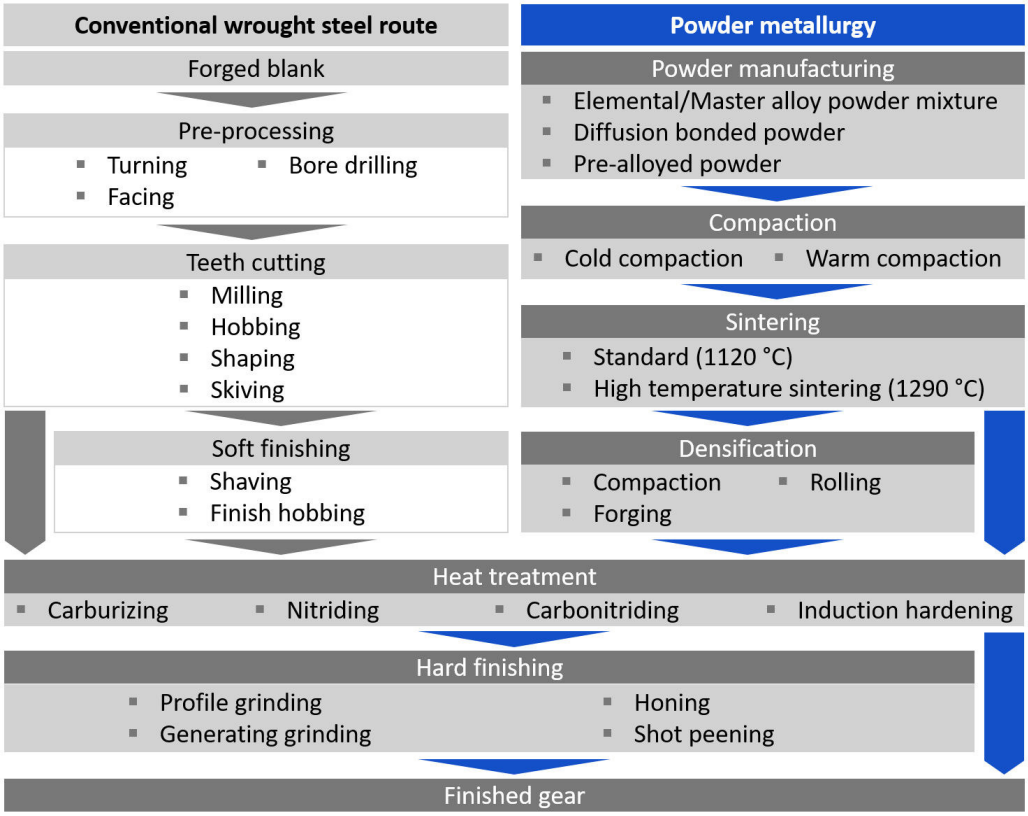

FIGURE 2.2 – Process steps of the conventional and PM chains in detail (KLOCKE *et al.*, 2005; KAUFFMANN, 2012; KLOCKE *et al.*, 2014)

Powder manufacturing

The raw material in powder metallurgy is a determinant factor of quality, mainly in terms of material uniformity. Therefore, the powder characteristics must be known under a rigorous control and its quality is dependent on how it is manufactured. The powder manufacturing methods can be classified in four groups: chemical methods, atomization, electrolytic deposition and mechanical methods. The chemical and atomization methods are the most important in practice, since they are more cost effective and attend the requirements of most powder metallurgy products (CHIAVERINI, 2001). Chemical methods are commonly based on reduction of oxides or on chemical decomposition. The chemical reduction, however, produces powder with interior porosity, which reduces the reached density after compaction, and the chemical decomposition is suitable only in special applications (CHIAVERINI, 2001; UPADHYAYA, 2002; KAUFFMANN, 2012).

The atomization method is the most important of all and consists on passing a molten metal through an orifice and then submitting it to a high pressure stream of water, gas or centrifugal force (CHIAVERINI, 2001; CAMPBELL, 2013), according to Figure 2.3. Atomization is also the dominant method for producing powders of steel, because of the high production rates associated and due to the fact that pre-alloying powders can only be produced by this process (BOLJANOVIC, 2010). Particularly, the water atomization

variant is appropriate for PM gears manufacturing (KAUFFMANN, 2012). The advantages of water atomized powders are freedom to alloy, lower cost, higher purity, control of particle shape, size and structure and also the uniformity in composition of all particles (GUMMESON, 1972 apud UPADHYAYA, 2002).

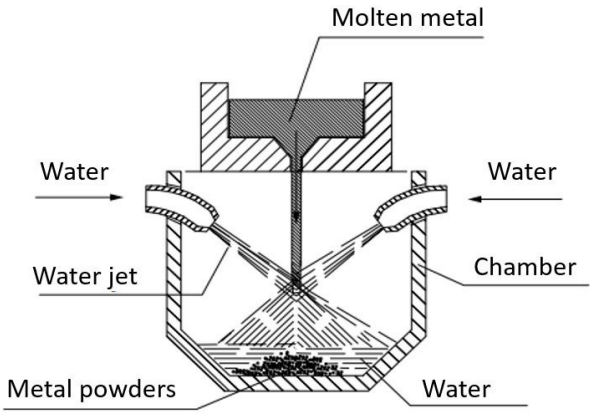

FIGURE 2.3 – Atomization method for producing metal powder (BOLJANOVIC, 2010)

Powders of alloys can be of different types: elemental powder mixture (admixed), diffusion bonded or pre-alloyed, as shown in Figure 2.4. The elemental powder mixture is versatile and present good compressibility, but is easily susceptible to segregation and tend to be more heterogeneous, even after sintering. In the diffusion bonded, the powder mixture is heated and the particles bonded, which eliminates the possibility of segregation. In the pre-alloyed, the powder is usually produced directly by atomization and every particle consist of a more homogeneous alloy. Despite the higher quality homogeneous microstructure, pre-alloyed powders present lower compressibility, which can be solved by additional efforts in compaction and sintering (THÜMMLER; OBERACKER, 1993; SCHATT *et al.*, 2006; KAUFFMANN, 2012; CAMPBELL, 2013). Powders can also be hybrid, for example, a combination of water atomized pre-alloy of iron molybdenum can be diffusion bonded with other alloying elements and carbon can be added by powder mixing (KLOCKE *et al.*, 2007). Before proceeding to compaction, lubricants are added to the powder mixture to reduce the friction between particles and between the mixture and the compaction tools.

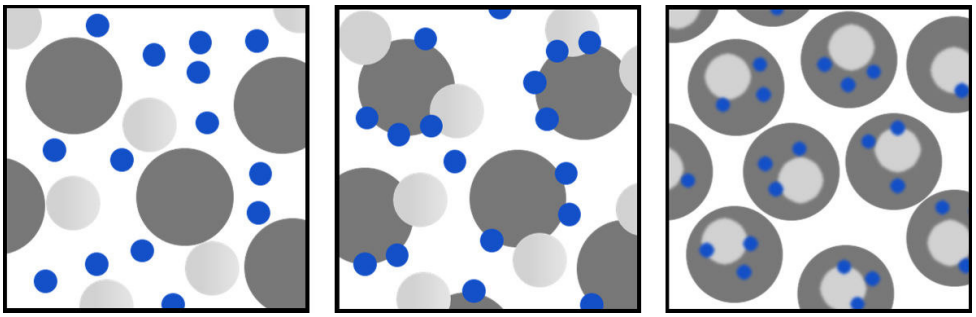

FIGURE 2.4 – Types of powders of alloys. From left to right: elemental powder mixture, diffusion bonded powder and pre-alloyed powder (ORLANDIN *et al.*, 2009)

Compaction

The compaction has the functions of consolidating the powder into the desired shape, reaching the desired level of porosity and providing adequate strength for subsequent handling (UPADHYAYA, 2002). Axial pressing is the most practical method of compaction and is very economical for the mass production of precision parts (THÜMMLER; OBERACKER, 1993). In Figure 2.5, the tools for spur helical gears compaction are shown. The compaction sequence is die filling, compaction and ejection of the compacted component, which is called "green compacted" at this stage. The operation requires mechanical or hydrostatical presses. Mechanical presses are generally associated to higher production rates and hydrostatic presses guarantee a better control of pressure and of the punches position (THÜMMLER; OBERACKER, 1993; UPADHYAYA, 2002; SCHATT *et al.*, 2006). For higher production rates and to reach density homogeneity, mechanical presses with hydraulic adaptors can be employed (SCHATT *et al.*, 2006; KAUFFMANN, 2012).

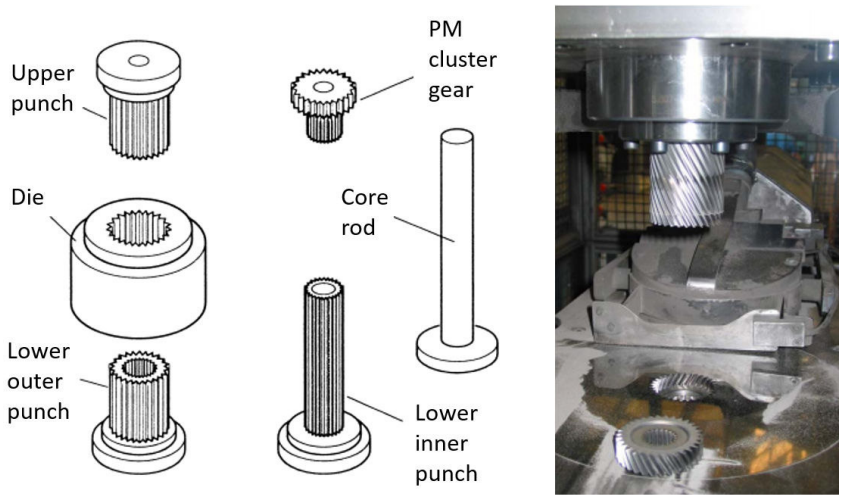

FIGURE 2.5 – Compaction tools. Left: compaction tools schematic for spur gears (DAVIS, 2005). Right: compaction tools for helical gears (SIGL *et al.*, 2005)

Powders tend to not assume the same density in the compact. Due to friction between the powder particles and the die and between individual particles, the transmission of pressure is hindered. The density uniformity can be improved and depends on the compaction technique, the pressed material and lubricants. The pressing technique can be classified into single action pressing and double action pressing, depending on the movement between the tool elements. In single action pressing, the lower punch and the die are stationary and the upper punch moves. It results in a higher density on the top than on the bottom of the compact. In double action pressing, the upper and lower punches moves into the die. The result is a high density at the top and bottom of the compact, while the centre remains as a neutral zone, which is relative weak. Figure 2.6 illustrates these two kinds of compaction techniques and the resultant density distributions (UPADHYAYA, 2002).

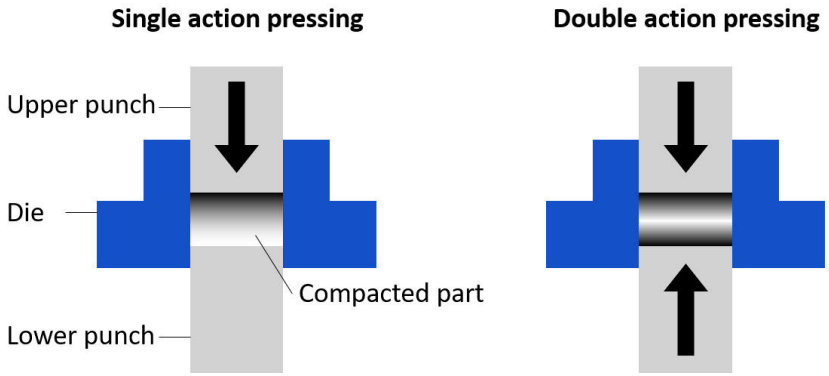

FIGURE 2.6 – Compaction techniques and the resultant density gradients (IERVOLINO; BULLA, 2009)

Compaction can be performed either at room temperature (cold compaction) or at elevated temperature (warm compaction, at temperatures between 120°C and 150°C) to improve the powder compressibility (SALAK; RIECANSKY, 1995; SIMCHI; NOJOOMI, 2013; JAMES; NARASIMHAN, 2013). Warm compaction can also provide better pore morphology in comparison to cold compaction, resulting in smaller, rounder and more uniformly distributed pores (SIMCHI; NOJOOMI, 2013). For cold or warm compaction, precision and durability are requirements for the tooling. Therefore, the material of the tools is normally cemented carbide and the prices associated to them are very high. For the production of helical PM gears, for example, the tools investment can reach more than a hundred thousand dollars (KAUFFMANN, 2012).

Sintering

Sintering can be defined as the heat treatment of a powder compact at temperatures high enough to enable diffusional mass transport at relatively fast rates, which results in growth of particle contacts, shrinkage of pore volume and pore geometry. The temperature is normally below the melting point of the major constituent but enough to get metal in the recrystallization zone, in which the metal particles recrystallize into each other. Sintering has the objective of changing the mechanical strength of the powder compact towards that of the pore free body. In the case of atomized pre-alloyed powders, most of the micro segregation, if there is any, can be eliminated in sintering (THÜMMLER; OBERACKER, 1993; UPADHYAYA, 2002; RAMAKRISHNAN, 2002; SCHATT *et al.*, 2006; BOLJANOVIC, 2010).

Before sintering, the lubricant that is still in the green body is burned in temperatures between 500 °C and 600 °C and the space previously occupied by it remains as porosity. Common sintering temperatures for steel are around 1120 °C. High temperature sintering (HTS) at temperatures between 1180 °C and 1350 °C in special furnaces is more expensive, but it increases the diffusion rate and better mechanical properties can be achieved due to more spherical pores and higher bonding strength. Shrinkage of the component can occur in the process, which can be avoided by using appropriate sintering temperatures, part

density and alloy composition. After sintering, the part is cooled at specified rates, in a protective atmosphere to avoid oxidation in contact with air. The cooling step is important because the phase transformations involved will affect the mechanical properties of the material (SCHATT *et al.*, 2006; KLOCKE *et al.*, 2007; BOLJANOVIC, 2010; KAUFFMANN, 2012; TROSS, 2016). In Figure 2.7, a schematic of a type of continuous furnace is shown, which illustrates the steps of the heat treatment.

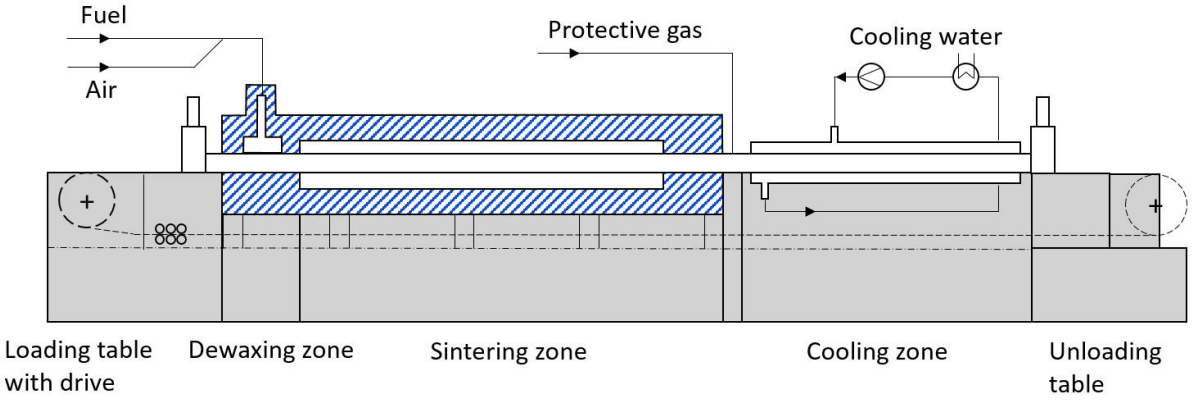

FIGURE 2.7 – Schematic of a continuous sintering furnace (UPADHYAYA, 2002)

Surface densification

After sintering, densification processes for increasing the mechanical strength of high performance PM gears are usually required. Densification can be global or selective. For global densification, compaction or forging can be applied. However, the critical loads to which gears are submitted are Hertzian contact and sliding contact stresses at the tooth flank and bending stresses at the tooth root, which are essentially concentrated at the surface and subsurface, as shown in Figure 2.8. Therefore, a selective densification at the surface in an appropriate depth can lead to fatigue properties equivalent to those of a wrought steel gear. Hence, with surface densification it is possible to produce high strength gears with low cost in comparison to the global densification. Additionally the surface densification preserves the benefits of a porous core in terms of weight and noise damping (SLATTERY *et al.*, 2004; CAPUS, 2008; KAUFFMANN, 2012; KLOCKE *et al.*, 2013; TROSS, 2016).

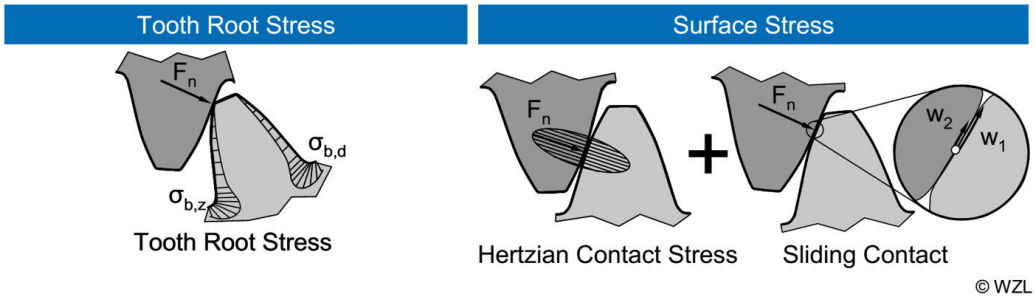

FIGURE 2.8 – Stresses on gears (KLOCKE *et al.*, 2010)

There are translatory and rotary methods for surface densification, as illustrated in Figure 2.9. The most common method of gears surface densification is the rotary rolling process, in which the spur or helical sintered gear with stock material at flank and root is mounted between two tool gears. In the process, the tool gears apply pressure on the gear teeth, while the center distance between the gears is progressively reduced. The applied pressure produces a plastic strain at the surface, which reduces the tooth thickness and generates a fully dense layer up to a depth of approximately 0.3 to 1 mm. Additional benefits of rolling are excellent surface finish at the tooth flanks (smoother than ground gears), improved gear geometry and tolerance and the possibility to crown the tooth (BONETTI *et al.*, 2000; SLATTERY *et al.*, 2004; SIGL *et al.*, 2005; CAPUS, 2006; KAUFFMANN, 2012; KLOCKE *et al.*, 2013; TROSS, 2016). Further secondary effects of the surface densification process are described in section 2.3.

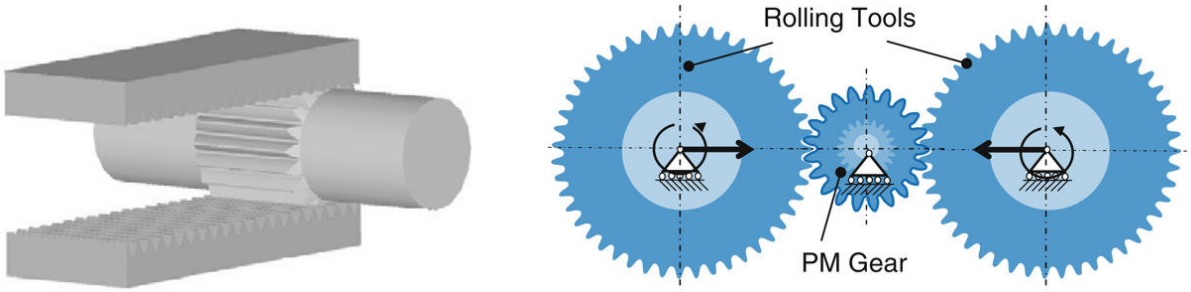

FIGURE 2.9 – Methods of gear surface densification. Left: translatory rolling method (NEUGEBAUER *et al.*, 2007). Right: rotary rolling method (KLOCKE *et al.*, 2013)

Heat treatment

In order to enhance the mechanical properties of the gears, it is necessary to perform a suitable heat treatment after surface densification. The same types of treatment of wrought steel gears are indicated to PM gears, but the process parameters are different and have to be specially tailored, due to the pores and the connectivity between them. The high reactivity with the atmosphere due to the large specific surface of the porous material permits much shorter processing times to be used, which in turn demands a more refined process control. The reduced thermal conductivity of the pores is another characteristic that influences the heat treatment of PM materials (BONETTI *et al.*, 2000; KLOCKE *et al.*, 2007; FLODIN, 2016).

Gears are usually heat treated by case hardening. For PM gears, low pressure carburizing with gas quenching or plasma carburizing are the most suitable heat treatment methods (KLOCKE *et al.*, 2007). Carburizing consists on adding carbon in the surface layers of a low-carbon steel gear at temperatures at which austenite is the stable crystal structure (generally between 850 °C and 950 °C) and the carbon solubility is high. Hardening of the component is followed by quenching and tempering, resulting in a pre-

dominant martensitic structure. The resulting carbon gradient below the surface causes a hardness gradient, which is translated into a hard case and a relatively soft but tough core of the gear (RAKHIT, 2000; DAVIS, 2002; DAVIS, 2005).

2.1.2 Potentials and challenges of PM gears

Powder metallurgy for gears manufacturing has the potential of being technically, economically and environmentally more advantageous in relation to the conventional wrought steel manufacturing chain. The impact can be even more significant in the field of automotive transmissions, the largest gear market. As the powder metallurgy manufacturing chain was described, the process is near net shape, and no other process that could be used for gear manufacturing has a so optimized raw material utilization (NARASIMHAN; BORECZKY, 2006; ANDERSON; IMBROGNO, 2014; KAUFFMANN, 2015). Chip disposal and the use of machining fluids are likewise dramatically reduced. In terms of energy consumption, there is also no other process more economical than powder metallurgy and the plant CO_2 emissions of this process are in the same way smaller (NARASIMHAN; BORECZKY, 2006; ANDERSON; IMBROGNO, 2014; KAUFFMANN, 2015). This is better exposed in Figure 2.10, where it can be seen that powder metallurgy overcomes the other processes and the conventional machining chain is the most disadvantageous considering material and energy utilization.

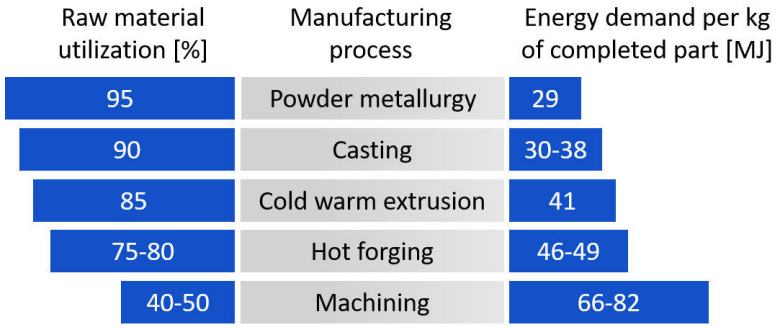

FIGURE 2.10 – Comparison of the processes for gear manufacturing in terms of raw material utilization and energy demand (NARASIMHAN; BORECZKY, 2006; ANDERSON; IMBROGNO, 2014)

Regarding manufacturing costs, there is also an estimation of costs reduction of 25% to 30% in comparison to the conventional route, as shown in Figure 2.11 (STREHL, 1997; RAU *et al.*, 2003). Furthermore, multifunctional gear features such as those in Figure 2.12 can be manufactured without expected additional machining operations in powder metallurgy. Therefore, the more complex and detailed is the gear geometry, the highest is the potential of costs reduction.

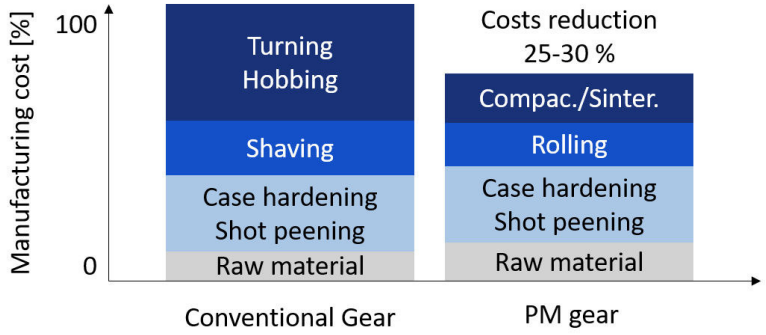

FIGURE 2.11 – Estimation of costs in the manufacturing of PM and conventional gears (STREHL, 1997 apud RAU *et al.*, 2003)

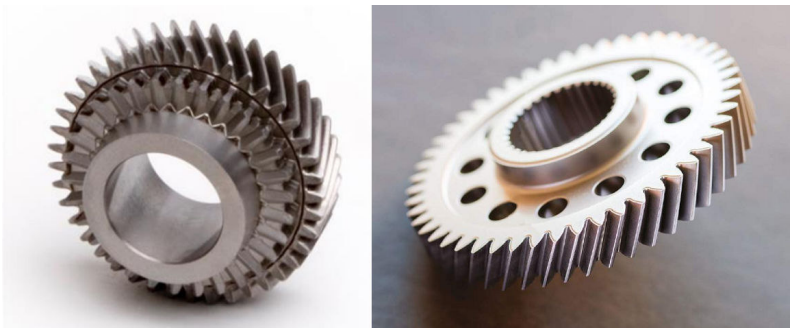

FIGURE 2.12 – PM gears with multifunctional features. Left: (KAUFFMANN, 2015). Right: (WHITTAKER, 2016)

The production rates are likewise higher than in the conventional chain and less finishing operations are also usually required in PM gears, due to the manufacturing precision and better surface properties, as illustrated in Figure 2.13 (NIGARURA *et al.*, 2015a; KAUFFMANN, 2015). However, due to the high costs of the compaction tools, the application of this process is feasible especially for mass production. Furthermore, investments costs in new plants of PM gears manufacturing can be reduced by around 30% in comparison to a conventional plant, because much of soft machining equipment do not have to be part of the investment (FLODIN, 2016).

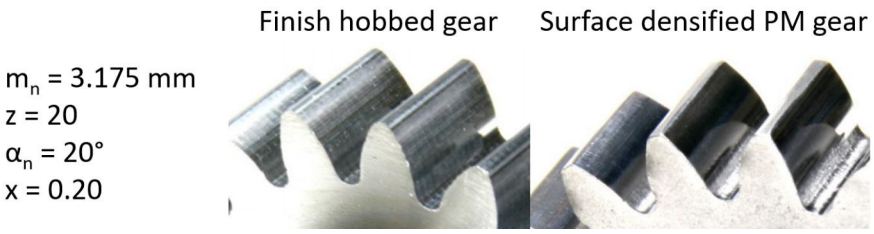

FIGURE 2.13 – Surface comparison of a finish hobbed gear and a surface densified PM gear (KAUFFMANN, 2015)

Aside the economical and sustainability gains, PM gears can also be technically superior. If the same design of a wrought steel gear is applied to a PM gear, 5% to 10%

of weight can be reduced (KAUFFMANN, 2015). Nevertheless, Skoglund and Litström (2013) redesigned the gears of an automotive transmission for powder metallurgy with an optimized geometry and achieved reductions from 8% to 23% in weight and inertia, reducing the total mass of the transmission in 1.1 kg, as shown in Table 2.1. Weight and inertia reductions are very important, since it results in improvement of fuel economy, lower CO_2 footprint, lower material costs and reduces the losses while accelerating the gear every time the RPM is shifted. Additionally, with gear reduced inertia, synchronization packages could also be redesigned to be simpler and smaller (SKOGLUND; LITSTRÖM, 2013).

TABLE 2.1 – Weight and inertia reduction for the redesigned transmission (SKOGLUND; LITSTRÖM, 2013)

	Inertia M32 steel vs PM [kgm^{2}x10^{-6}]				Mass [kg]		
Gear	M32	Copied PM	Optimized PM	Diff. [%]	M32	PM	Diff. [%]
1st	2154	1769	1670	22	1.097	0.896	18
2nd	1285	1114	1090	15	0.953	0.819	14
3rd	1991	1605	1532	23	1.159	0.930	20
4th	983	860	848	14	0.831	0.730	12
5th	244	224	224	8	0.323	0.297	8
6th	213	196	196	8	0.387	0.355	8
R	1336	1140	1109	17	0.946	0.791	16

If the gears are properly designed for powder metallurgy, the potentials of the process can be fully explored and the benefits can be even higher. Powder metallurgy allows the implementation of features in high production rates that would be impeditive by machining, either by kinematical, economical or production times limitations. In the traditional gear hobbing, for example, the root of the gear have the shape of a trochoid curve limited by the tool geometry and the process kinematics. By using powder metallurgy, the freedom of design is much higher. The tooth root can be redesigned to imply in root stress reduction up to 30%, in a way that would not be possible by conventional machining at the same speed as is possible by powder metallurgy. Other more advanced design could be also possible through powder metallurgy, such as non-involute gearing and asymmetric gear teeth designed for reduced contact and bending stresses (SKOGLUND; LITSTRÖM, 2013). Additionally, the characteristic pores in the core of PM gears can also have beneficial effects of vibration and noise damping, resulting in quieter transmissions (DAVIS, 2005; SIMCHI; NOJOOMI, 2013; LÖPENHAUS, 2016). All the potentials of PM gears described hitherto are summarized in Figure 2.14.

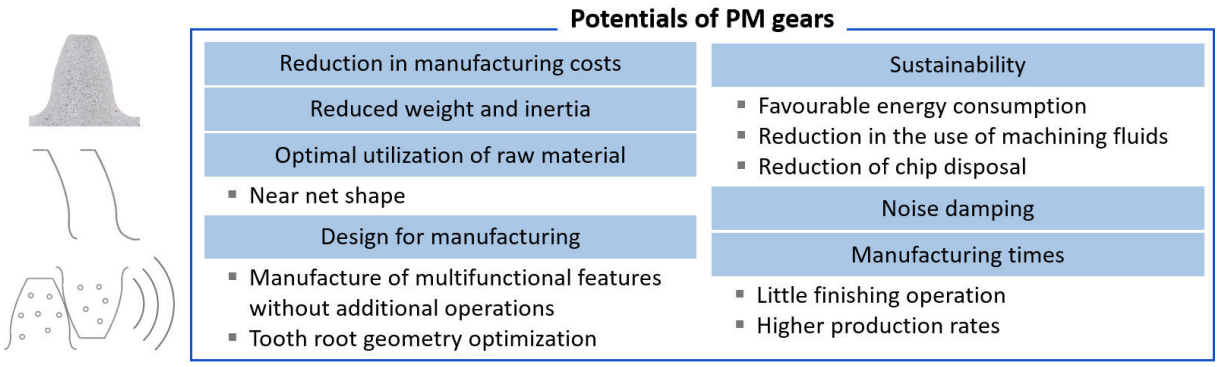

FIGURE 2.14 – Summary of the potentials of PM gears

Despite all the benefits that could be associated to powder metallurgy for gears manufacturing, there are of course challenges in its implementation. The porous material is associated to inferior mechanical properties in relation to wrought steel. However, as described before, with optimized design and with appropriate processing, PM gears can have similar or even superior performance in comparison to conventional gears. Several powder metallurgy industries and research centers have applied efforts towards making PM gears a reality (CAPUS, 2006; CAPUS, 2008; KAUFFMANN, 2012; FLODIN, 2016; WHITTAKER, 2016). Nevertheless, as for every technology that is not yet mature, technical difficulties are being overcome and a more systematic understanding of the complexity of variables involved is being gradually achieved. The core necessity is to comprehend how the material, processes and design criteria can influence the load capacity, transmission error, transmission efficiency, noise and fatigue behavior of PM gears to reach an optimized performance. Part of this comprehension involves the residual stresses in PM gears, which is directly associated to the fatigue behavior of the component. This topic is approached in the next sections.

2.2 Surface integrity

Surface integrity can be defined as the topographical, mechanical, chemical and metallurgical condition of a manufactured surface and its relationship to the functional performance (FIELD; KAHLES, 1964; GRIFFITHS, 2001; ASTAKHOV, 2010). As stated in the definition, it is a result of the manufacturing processes. The mechanical, thermal and chemical loads imposed on the material during processing affect the surface properties, which can be divided in external or internal (GRIFFITHS, 2001). Topography is one of the features of the surface that can be considered external, because it is at the interface with the environment. Roughness, waviness and form are the expressions of topography that are differentiated according to the extension of periodicity. Internal features are microstructure, crystallographic texture, residual stresses, hardness and others. Features

can also be mixed, for example cracks, which in the cases of worn gears can be found at the surface or subsurface.

The assessment of surface integrity is essential for assuring the quality of high performance gears, since external and internal surface features affect the fatigue behavior, wear, load capacity, lubrication, noise emission and accuracy. A wide comprehension of surface integrity involves understanding two correlations. The first one is related to the influence of material and process parameters on the surface features. The second one is related to how these surface integrity conditions affect the functional performance. After these correlations are understood, a third and more practically important one can be done directly: how the material and process parameters affect the functional performance of the component. An example of this concept for high performance gears is illustrated in Figure 2.15.

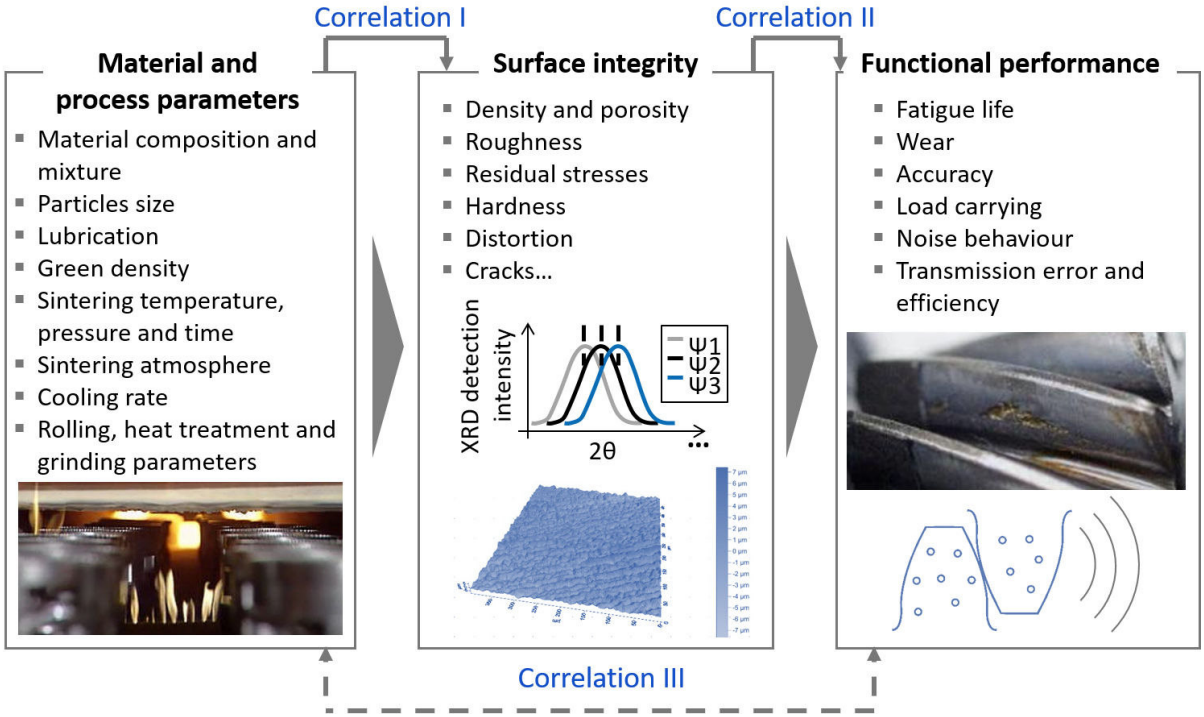

FIGURE 2.15 – Schematic for the comprehension of the surface integrity of PM gears

The present study focuses on the understanding of how the powder metallurgy process steps influence the residual stresses heterogeneity. Therefore, the investigations actuate on the first correlation mentioned. In the next sections, the topic residual stresses and its heterogeneity is then approached.

2.2.1 Residual stresses: definition and relationship with fatigue strength

Residual stresses are an important feature of surface integrity and they are defined as internal stresses caused by mechanical, thermal and microstructural phenomena inherent to the manufacturing process of components. They originate from elastic accommodation of misfits between different regions in a structure, as a result of inhomogeneous plastic strains (LÖHE *et al.*, 2002; BOUCHARD; WHITERS, 2006). For these reasons, residual stresses exist independently of externally applied loads and their basic characteristic is the equilibrium principle, in which the sum of the compressive residual stresses compensates the sum of the tensile ones (HEYN, 1914; BEHNKEN, 1997). In Figure 2.16, simplistic models of residual stresses generating mechanisms are shown. Figure 2.17, in turn, exposes the causes of residual stresses in the conventional and powder metallurgy manufacturing chains of gears.

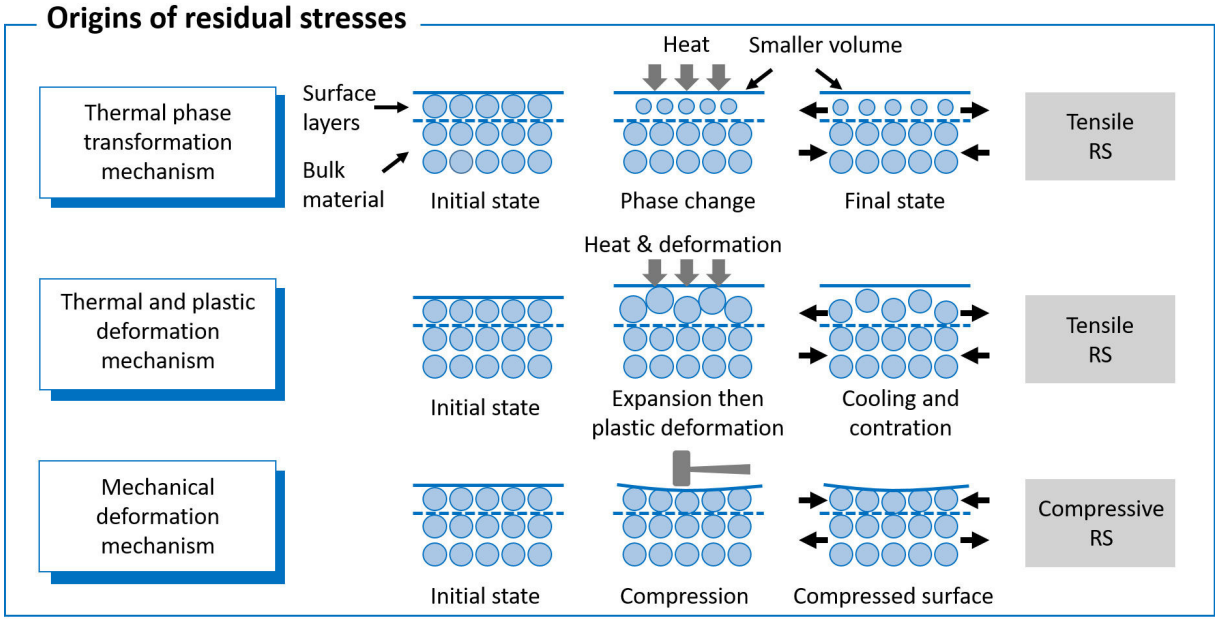

FIGURE 2.16 – Residual stress generating mechanisms models (GRIFFITHS, 2001)

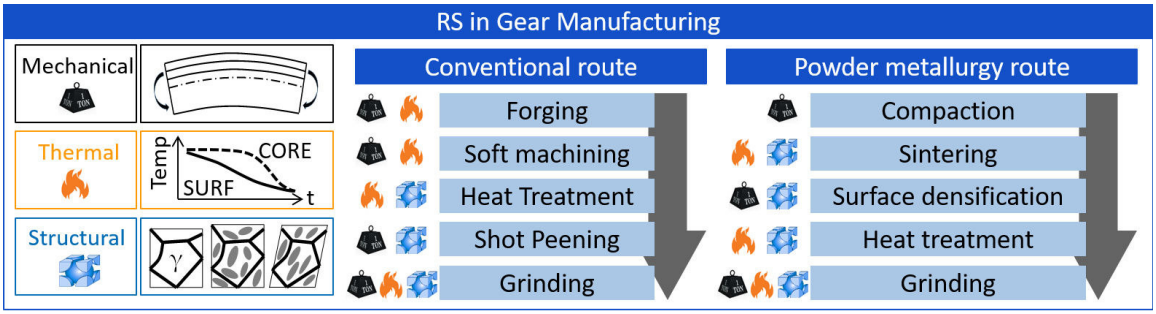

FIGURE 2.17 – Origins of residual stresses in the conventional and PM gear manufacturing chains (INOUE, 2014)

Residual stresses can be classified according to the size of their analysis domain. Macro residual stresses (or type I) are those considered to be an average of stresses in a volume of several crystal grains in a material, even of different phases. Additionally, a separation into type I residual stresses for each of the material phases can be made. In turn, micro residual stresses can be considered those that are the average of stresses in the crystal grain scale (type II) or even at sub microscopic scale (type III) as the average of stresses in the range of some atomic distances inside the grain (WHITERS; BADHESIA, 2001; FITZPATRICK *et al.*, 2005; SHACKELFORD, 2014; SPIESS *et al.*, 2014; REGO, 2016). Those classifications of residual stresses are well illustrated in Figure 2.18.

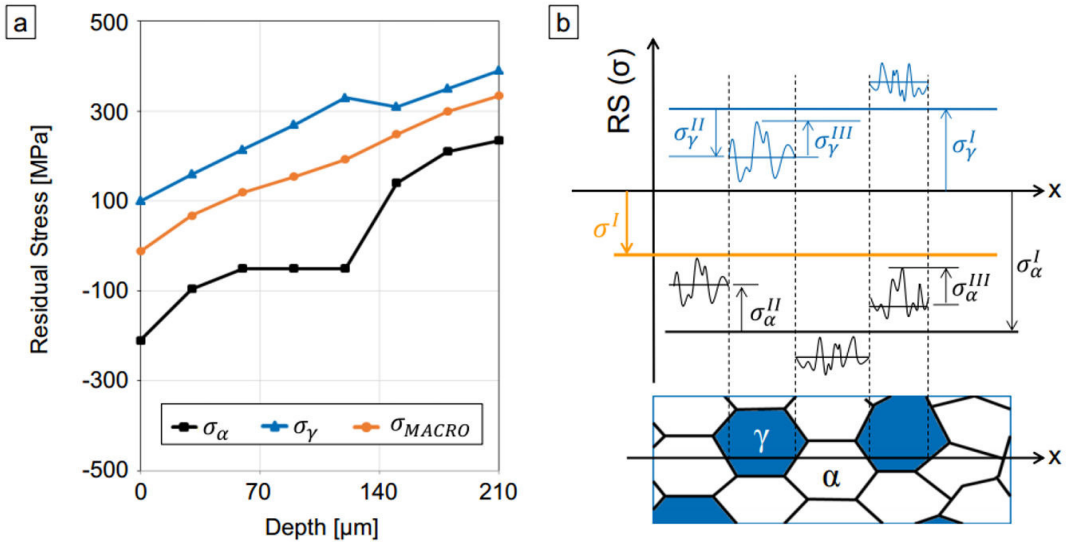

FIGURE 2.18 – (a) Macro residual stress composed by the contribution of each phase; (b) Schematic of all levels of residual stresses (HAUK; NIKOLIN, 1988; WHITERS; BADHESIA, 2001; SPIESS *et al.*, 2014)

It is well established that no component is free of micro residual stresses and that almost all technical components have macro residual stresses to a certain extent. Residual stresses can have favorable or detrimental effects on mechanical behavior and are one of the most important parameters that influence the fatigue resistance, since they may promote or retard crack initiation and accelerate or decelerate crack propagation. The effective stress in a mechanical part in service is a result of the superposition of residual and externally applied stresses. Therefore, the manufacturing processes and parameters have to be selected in order to induce the proper sign, magnitude and distribution of residual stresses that counterbalance the external load in the critical parts of the component. For accomplishing that, the critical applied stresses and failure modes of a component must be well known and a broad comprehension on how to induce the proper residual stresses is a requirement (HAUK, 1997; SCHOLTES, 2000; LÖHE *et al.*, 2002).

Bending and contact fatigue are the most common gear failure modes, which are illustrated in Figure 2.19. The cause of those failures are Hertzian contact and sliding contact stresses at the tooth flank and bending stresses at the tooth root. Those cyclic stresses at the surface and subsurface are normally lower than the ultimate strength of the material. However, they harden the material locally and the concentration of dislocations form crack nucleations, which grow until a critical size for failure (ALBAN, 2002; ASHBY *et al.*, 2007). In the case of gears, compressive residual stresses at the surface have a benefic effect on the component life. Mitsubayashi *et al.* (1994) showed that the compressive residual stress peak in the surface depth coincides with the depth at which cracks have the lowest propagation rate, as shown in Figure 2.20. However, attention should be given not only to the residual stress depth profile, but also on how the residual stress is distributed along the surface, or how heterogeneous it is (REGO, 2016). The importance of the heterogeneity of residual stresses is discussed in the following sections.

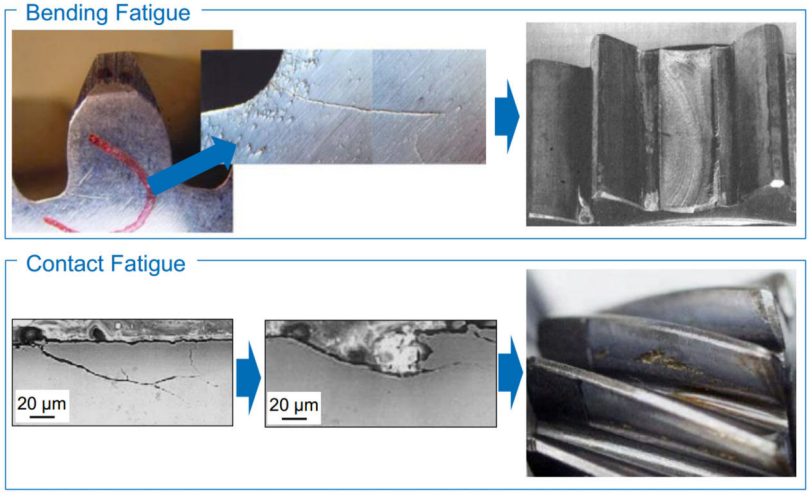

FIGURE 2.19 – Gear fatigue failure modes: bending and contact stresses (LECHNER; NAUNHEIMER, 1999; DING; RIEGER, 2003; BELSAK; FLASKER, 2006)

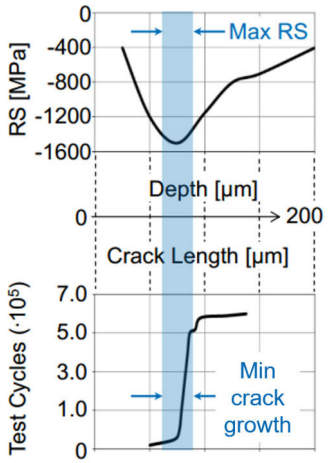

FIGURE 2.20 – Relationship between the residual stress profile and the crack propagation (MITSUBAYASHI *et al.*, 1994)

Even so, the relation between residual stresses and fatigue strength is not unique and simple. The same processes that generate residual stresses also lead to other alterations in the material that have impact on fatigue behavior, such as topography modifications, phase transformations, texturing, strain hardening or softening. Another reason for this is that residual stresses may suffer relaxation during the fatigue process, as a consequence of cyclic plastic deformations (SCHOLTES, 2000). Hence, for a broader comprehension on the fatigue behavior of gears and other mechanical components, residual stresses depth profile, heterogeneity and stability must be analyzed together with other surface features investigations.

2.2.2 X-ray diffraction for residual stress measurement

X-ray diffraction is the most common method of measuring residual stresses in gears. It is a nondestructive method in which X-rays diffract according to specific angles after the incidence in crystal lattices. Diffraction consists on the deviation of a wave trajectory as it encounters an obstacle with a similar size of its wavelength. This phenomenon is explained by the *Huygens-Fresnel* principle, in which each point of the wave front can be considered as a wave source, and by the superposition of waves principle (BARBOSA *et al.*, 2012). X-rays are used for material investigation because the wavelength of these radiations is of the same order of magnitude of the dimensions of atoms and ions (CALLISTER; RETHWISCH, 2007). Therefore, the disposal of atoms in crystals acts as a diffraction grating, as showed in Figure 2.21.

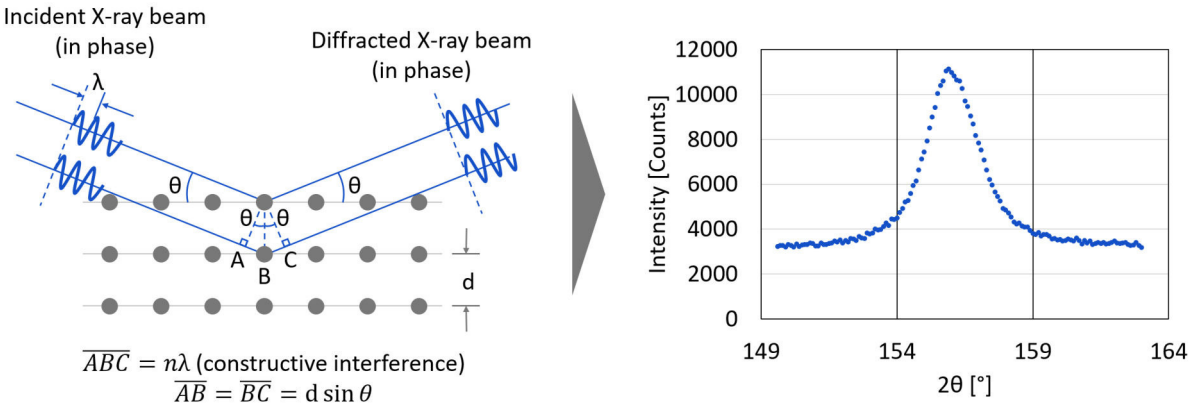

FIGURE 2.21 – X-ray diffraction in crystal lattice and the resultant diffractogram. Adapted from (SHACKELFORD, 2014)

The X-rays scattered by diffraction can interfere constructively or destructively. For having constructive interference and for being possible the measurement of the diffracted radiation intensity, the value of the difference between the path lengths of the waves must be equal to an integer multiple of the wavelength, as described by the Bragg's law in Equation 2.1:

$$n\lambda = 2d\sin\theta \tag{2.1}$$

in which n is an integer, λ is the radiation wavelength, d is the distance between the crystalline planes and θ is the diffraction angle. The detection of radiation beams after the incidence in a material allows the obtainment of profiles of radiation intensity according to the diffraction angles, also called diffractograms, as shown in Figure 2.21.

Several methods permit the characterization of materials through diffractograms. The main analysis of engineering interest are listed in Table 2.2, together with the characteristics of the peak profiles used for their execution.

TABLE 2.2 – Types of X-ray diffraction analysis of engineering interest. Adapted from (BALZAR, 1993)

Peak characteristic					
Position	Intensity	Form	Shift	Method	Identification
++	++			Phase analysis	Material identification and quantification
		+	++	Peak shift analysis	Macro residual stresses
+		++		Peak form analysis	Microstrain, crystallite size, lattice defects

In gear technology, X-ray diffraction is generally used with the peak shift analysis for macro residual stresses measurements. The residual stresses are measured indirectly, because diffraction allows the obtainment of the distance between lattice planes. In a simplistic way, residual stresses could be calculated by knowing the distances between the planes of atoms in stressed and stress-free conditions, d and d_0 respectively. The difference between those distances could be used to calculate the strain and consequently, the residual stress. However, obtaining d_0 experimentally is not practical and it cannot be obtained accurately from the lattice parameter of a similar stress-free material from handbooks, for example. The calculations must, therefore, follow the fundamental equation of X-ray

stress determination (Equation 2.2) (HAUK, 1997).

$$\begin{aligned}\frac{d_{\phi\psi}-d_0}{d_0} =& \frac{1}{2}s_2\left(\sigma_{11}\cos^2\phi\sin^2\psi+\sigma_{22}\sin^2\phi\sin^2\psi+\sigma_{33}\cos^2\psi\right)\\ &+\frac{1}{2}s_2\left(\sigma_{12}\sin 2\phi\sin^2\psi+\sigma_{13}\cos\phi\sin 2\psi+\sigma_{23}\sin\phi\sin 2\psi\right)\\ &+s_1\left(\sigma_{11}+\sigma_{22}+\sigma_{33}\right)\end{aligned} \tag{2.2}$$

In which $d_{\phi\psi}$ is the measured lattice distance at angles ψ and ϕ described in Figure 2.22, d_0 is the stress-free lattice distance and s_1 and s_2 are the X-ray Elastic Constants (XEC), which depend on the interference plane *(hkl)*. The averages of the XEC taken over all lattice planes, however, are connected to the macroscopic constants of modulus of elasticity E and *Poisson*'s ratio υ, as in Equations 2.3 and 2.4.

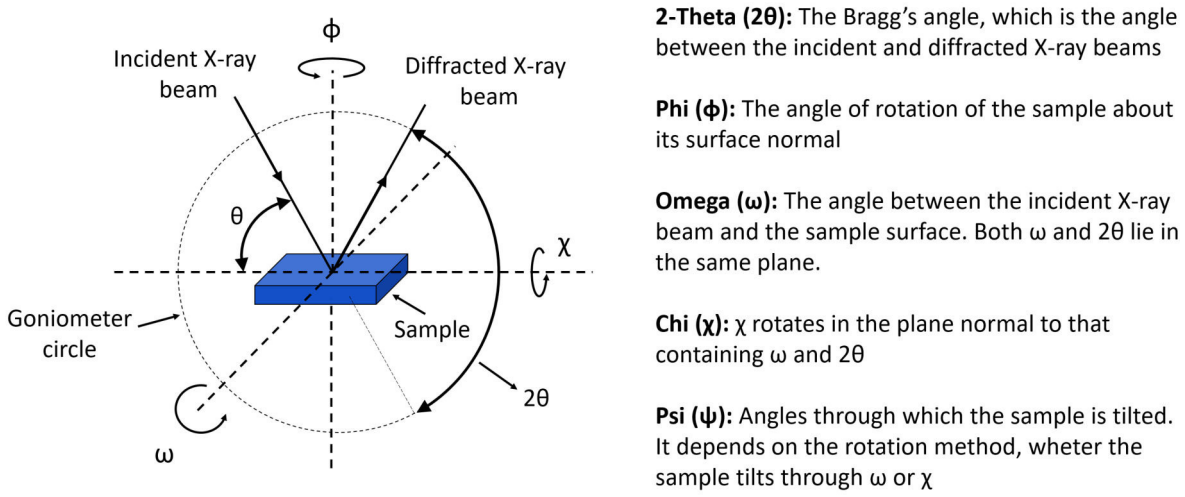

FIGURE 2.22 – Angles used in residual stress measurement by X-ray diffraction. Adapted from (FITZPATRICK *et al.*, 2005)

$$s_1 = -\frac{\upsilon}{E} \tag{2.3}$$

$$\frac{1}{2}s_2 = \frac{1+\upsilon}{E} \tag{2.4}$$

When the stresses are biaxial, the peak shift analysis by means of the $\sin^2\psi$ method is a solution for this problem. In this method, at least two measurements of plane spacing on the stressed material permit the calculation of the residual stress through Equation 2.5 (CULLITY; STOCK, 2014).

$$\frac{d_{\phi\psi}-d_0}{d_0} = \frac{1+\upsilon}{E}\sigma_\phi\sin^2\psi - \frac{\upsilon}{E}(\sigma_{11}+\sigma_{22}) \tag{2.5}$$

In which σ_{11} and σ_{22} are the normal stresses in the reference plane. In this case, d_0 can be considered as equal to the experimentally measured d-spacing at $\psi = 0$, an assumption that causes errors less than 0,1% in the curve slope, smaller than that caused by other sources (NOYAN; COHEN, 1987; CULLITY; STOCK, 2014). Figure 2.23 illustrates the peak shift method.

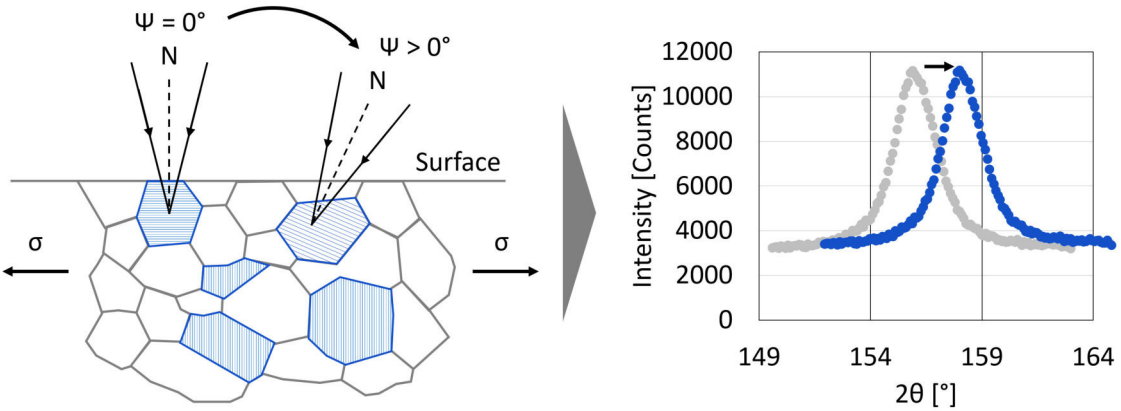

FIGURE 2.23 – Diffraction from strained material, tension axis horizontal. Lattice planes shown belong to the same *(hkl)* set. N = diffraction-plane normal. Adapted from (CULLITY; STOCK, 2014)

Finally, the residual stress in the direction of interest σ_ϕ can be determined by the d vs $\sin^2\psi$ curve slope, as shown in Figure 2.24 (a). Other patterns of d vs $\sin^2\psi$ curves can be found in practice, the "ψ-splitting" shown in Figure 2.24 (b) indicates that triaxial stresses are present, and the oscillatory behavior in Figure 2.24 (c) indicates a significant level of texture. The assumptions of Equation 2.5 of the $\sin^2\psi$ method are not valid for these two different patterns, which require special approaches for their analysis (CULLITY; STOCK, 2014).

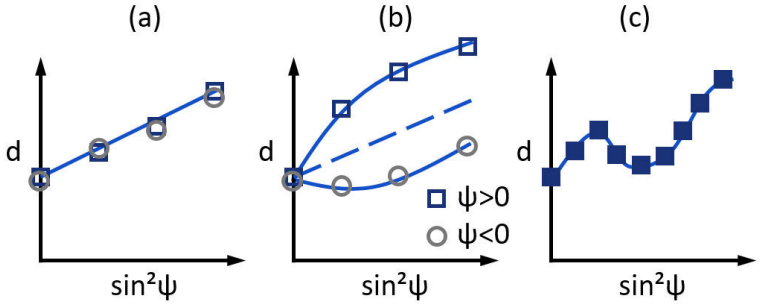

FIGURE 2.24 – Different types of d vs $\sin^2\psi$ plots (NOYAN; COHEN, 1987)

In the case of "ψ-splitting", shear stresses may exist and the residual stress tensor can be determined by the *Dölle-Hauk* method. According to this method, Equations 2.6 and 2.7 may be used, and data over a range $\pm\psi$ at three ϕ tilts (0°, 45° and 90°) must be

obtained (NOYAN; COHEN, 1987; HAUK, 1997).

$$\begin{aligned} a_1 =& \{\frac{d_{\phi\psi+} + d_{\phi\psi-}}{2d_0} - 1\} \\ &= \frac{1+\upsilon}{E}\{\sigma_{11}\cos^2\phi + \sigma_{12}\sin 2\phi + \sigma_{22}\sin^2\phi - \sigma_{33}\}\sin^2\psi \\ &+ \frac{1+\upsilon}{E}\sigma_{33} - \frac{\upsilon}{E}(\sigma_{11}+\sigma_{22}+\sigma_{33}) \end{aligned} \tag{2.6}$$

$$a_2 = \{\frac{d_{\phi\psi+} - d_{\phi\psi-}}{2d_0} - 1\} = \frac{1+\upsilon}{E}\{\sigma_{13}\cos\phi + \sigma_{23}\sin\phi\}\sin|2\psi| \tag{2.7}$$

a_1 is a mean value for $\psi > 0$ and $\psi < 0$, while a_2 is a deviation. Thus, the stresses σ_{11}, σ_{12}, σ_{22} and σ_{33} can be obtained from the slope and intercept of a_1 vs $\sin^2\psi$ for $\phi = 0°$, 45° and 90°. The slope of a_2 vs $\sin|2\psi|$ for $\phi = 0°$ and 90°, respectively, provides the shear stresses σ_{13} and σ_{23}. For the oscillatory d vs $\sin^2\psi$ behavior, Equation 2.2 cannot be used and special techniques for the analysis of these curves are described in (NOYAN; COHEN, 1987).

2.2.3 The state of the art of RS heterogeneity investigation

In the mechanical engineering field, residual stresses analysis is often focused in punctual macrostresses evaluations. In the same way, for gears investigation, residual stress measurements are usually made by X-ray diffraction in spots with diameter between 1 and 3 mm through the peak shift method. The study of Rego (2016), however, points out that this conventional analysis may not be enough for a complete prediction of the fatigue behavior of mechanical components. According to the study, the punctual measurement may not represent the stress variations along the entire surface nor the mean residual stress value may represent the local deviations. Mappings of residual stresses were performed by Scholtes (2000) and Zhan *et al.* (2013) on shot peened surfaces and illustrate these two kinds of deviations, as shown in Figure 2.25.

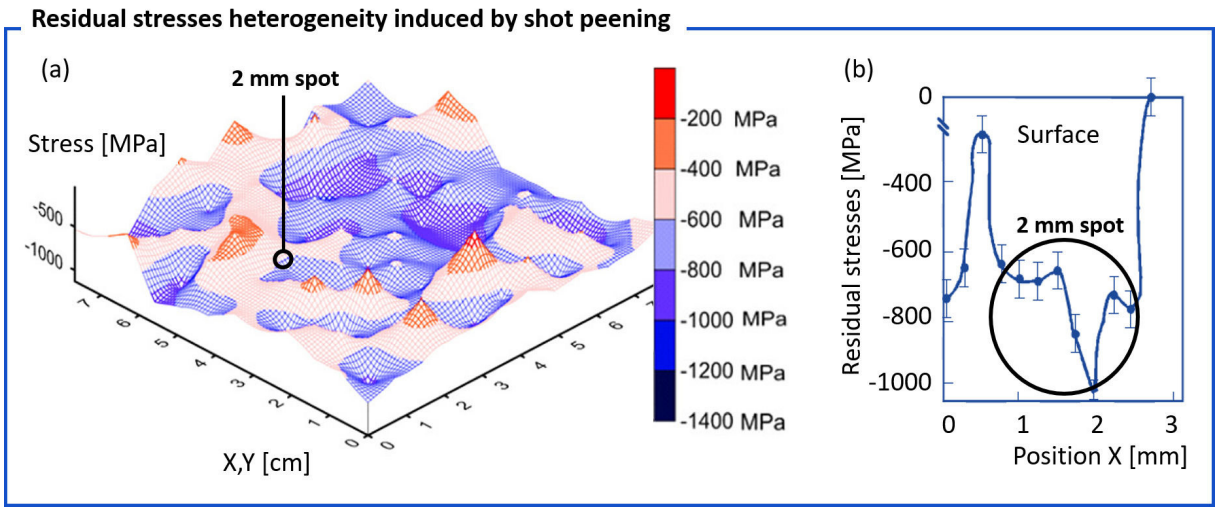

FIGURE 2.25 – Residual stresses heterogeneity induced by shot peening. (a) Heterogeneity in centimeters scale vs a 2 mm measurement spot (ZHAN *et al.*, 2013); (b) Heterogeneity in tenths of millimeters vs a 2 mm measurement spot (SCHOLTES, 2000)

Rego (2016) then proposes that the heterogeneity of those macro residual stresses is a result of the micro residual stresses intensities and should also be assessed for fatigue comprehension. This assertive agrees with the study of Scholtes (2000), in which the micro residual stresses importance is highlighted for crack initiation, while it indicates that macro residual stresses have a more dominant importance in the case of crack propagation. The relevance of the residual stress heterogeneity is also confirmed by Rego (2016) through experimental results, in which the lifetime of discs ground with different parameters is not explained by the macro residual stresses, as shown in Figure 2.26. Differently from what would be conventionally expected, the specimen with less compressive macro residual stresses showed higher lifetime, but a lower residual stress heterogeneity level.

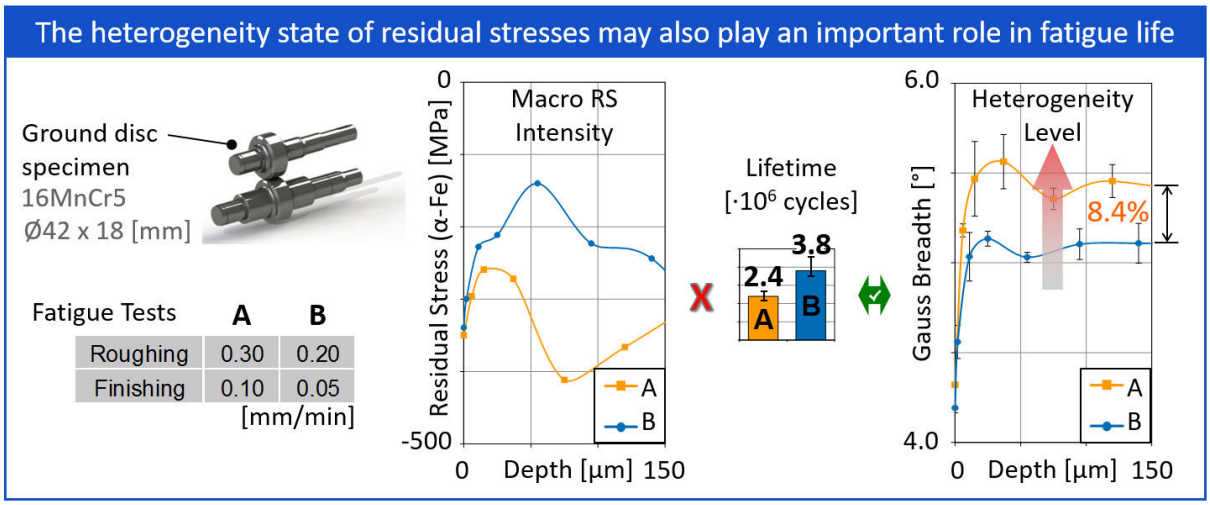

FIGURE 2.26 – The fatigue results of ground discs conflict with the expected effect of the residual macrostresses. A potential explanation is given by the RS heterogeneity, by means of the *Gauss* integral breadth (REGO, 2016)

The methods proposed by Rego (2016) for assessing the residual stresses heterogeneity were the residual macrostress mapping and the line broadening analysis, which are illustrated in Figure 2.27. By means of the residual stress mapping, the mentioned study obtained residual stresses values of 1 mm spots inside 3 mm spots, which also had the residual stresses measured. Thus, the local stresses deviation could be assessed to a certain extent. The line broadening analysis is based on the full width at half maximum (FWHM) of the difractograms and on the integral breadth (peak area/maximum intensity, β) defined by equation 2.8 (GENZEL, 1997). Through this method, information about the microstrains could be obtained. Rego (2016) then found a satisfactory correlation between these two methods, indicating that the residual macrostress heterogeneity can be assessed by microstrain intensities. In addition to providing information on a microstructural level, the line broadening analysis experiments are considerably less time consuming than the residual stress mapping.

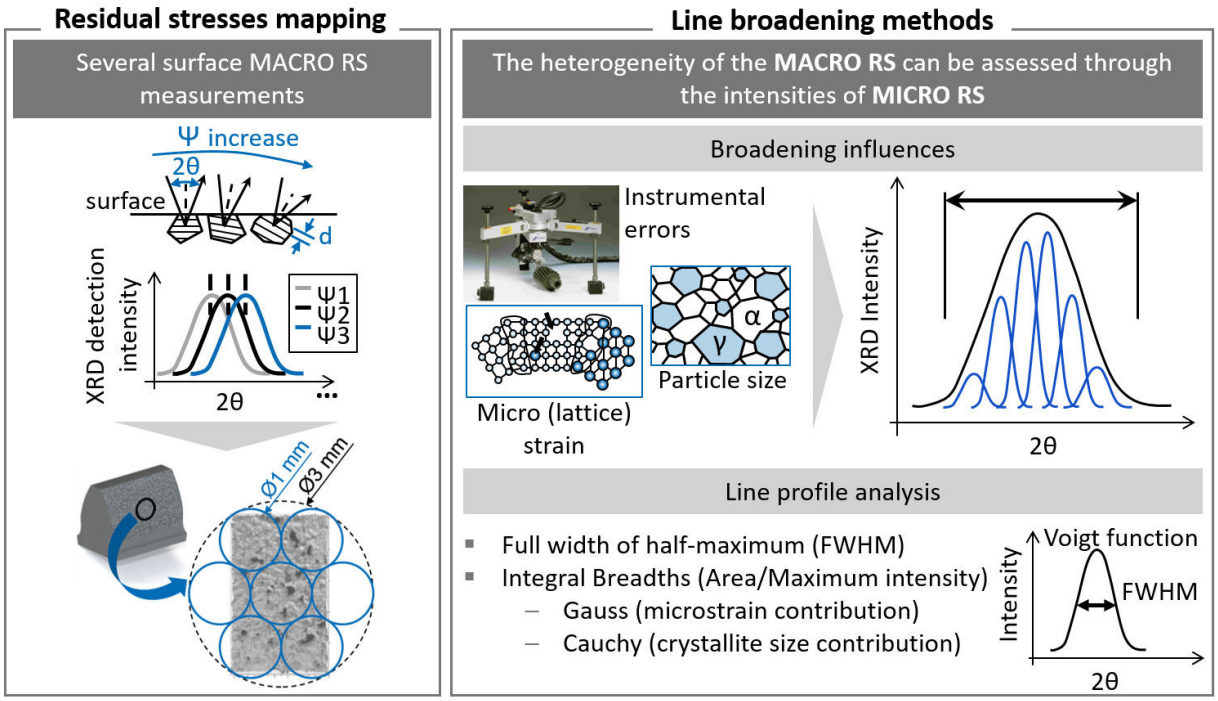

Sources: (Rego, 2016)

FIGURE 2.27 – Methods for residual stresses heterogeneity assessment, proposed by Rego (2016)

$$\beta = \frac{\int I(2\theta) 2\theta d2\theta}{\int I(2\theta) d2\theta} \tag{2.8}$$

According to Genzel (1997) and Ichikawa (2013), microstrains, crystallite size and also instrumental contributions determine the shape and width of diffraction profiles. The smaller the crystallite sizes and more heterogeneous the microstrains, the more broadened

is the diffraction peak. This is well illustrated in Figure 2.28, in which these contributions and an example of the effect of shot peening treatments on the broadening of diffraction curves are shown.

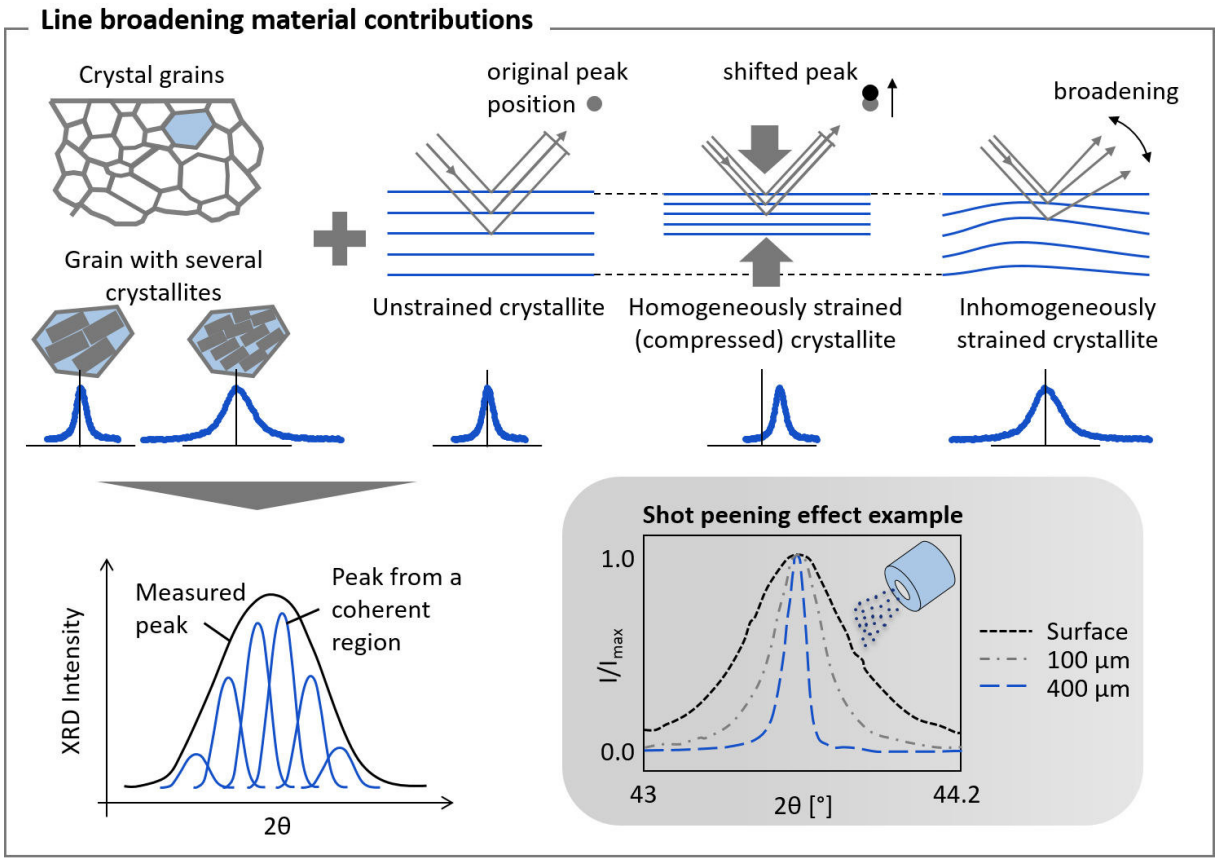

FIGURE 2.28 – Contributions of the material's microstructure to the line broadening of diffraction profiles (NOYAN; COHEN, 1987; COCKROFT; BARNES, 2001). On the bottom right, an example of the broadening caused by shot peening (ZHAN *et al.*, 2012)

As stated in (SCHOLTES, 2000), the association between residual stress state and fatigue strength, however, is not simple. Other surface features such as topography, strain hardening, softening, phase transformations and texturing also have a great impact on the mechanical component lifetime. Furthermore, residual stresses may also suffer relaxation during service. Many of these features can be analyzed by X-ray diffraction and can be equally important for the performance of the material (GENZEL, 1997; SCHOLTES, 2000). Therefore, with an appropriate knowledge of the X-ray diffraction techniques, it is possible to explore the macro residual stresses, their heterogeneity, their stability and the material's microstructure. In such manner, a more complete understanding of gears fatigue behavior can be achieved.

2.3 The connection between residual stress heterogeneity and PM gears

Two aspects of powder metallurgy gears may be of relevance in terms of residual stress heterogeneity. The first is the inherent porosity, which is a structural heterogeneity that can have impact on the residual stress distribution. The second aspect is related to the kinematics of the surface densification step. The process kinematics results in an uneven distribution of the applied stresses on the tooth flank profile during the densification. Due to different sliding velocities from the root to the tip, a material flow from the pitch diameter to the tooth root and tip directions can be observed. The study of Klocke *et al.* (2013) shows that one consequence of this effect is that if an uniform stock of material is used along the flank profile, the resultant densification depth is not uniform. However, it is also shown that this non-uniform density can be predicted and compensated by using an appropriate design of stock (KLOCKE *et al.*, 2013). The material flow and the influence of the stock on the density distribution are illustrated in Figure 2.29.

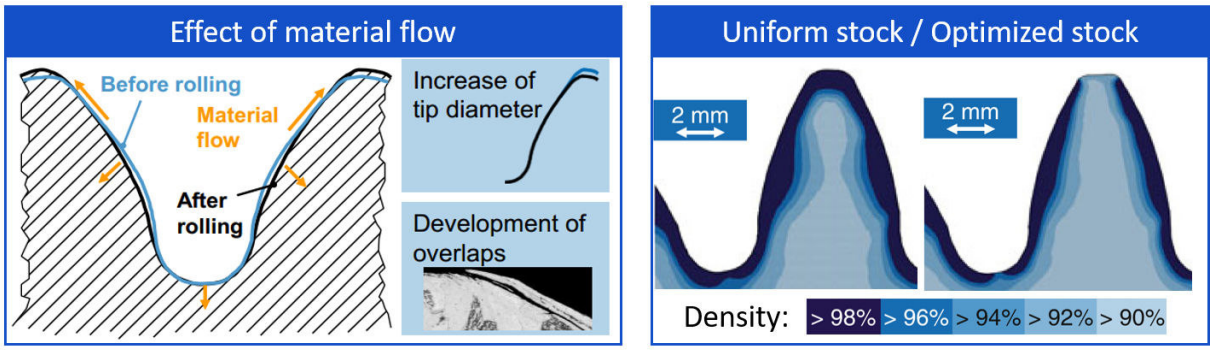

FIGURE 2.29 – Contributions of the surface densification step to the heterogeneity of the microstructure. Effect of the material flow (GRÄSER, 2013) and of the stock (KLOCKE *et al.*, 2013)

The microstructural analysis of a surface densified PM gear tooth also reveals other possible consequences, which are the microstructural texturing at the dedendum and addendum regions and the possibility of surface defect of material overlap in these areas (the basic gear nomenclature is presented in Annex A, where these regions are shown). Therefore, the surface densification process also contributes to the structural heterogeneity of PM gears. Figure 2.30 shows the resultant microstructure after surface densification.

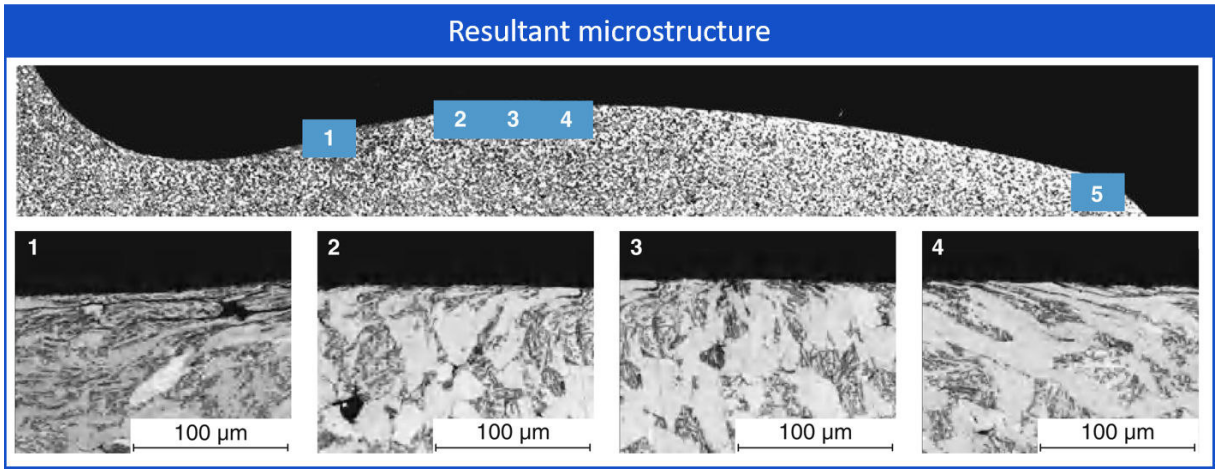

FIGURE 2.30 – The resultant microstructure after surface densification. Preferred grain orientation can be seen at the dedendum and addendum regions of the gear tooth (KLOCKE *et al.*, 2013)

Although changes on the residual stresses occur after heat treatment, Rego (2016) showed that the effects of the previous manufacturing steps also contributes to the residual stress state and are relevant to the final product. Therefore, the mentioned structural and residual stress heterogeneity of PM gears that are induced before heat treatment may be significant. Due to these evidences, the focus of the present study is to provide answers on how such stresses heterogeneity can be assessed and on how they evolve along the PM manufacturing chain. The next chapter then describes the methods used to achieve this.

3 Materials and methods

For the analysis of the evolution of residual stresses heterogeneity along the manufacturing chains, powder metallurgy and wrought steel gear teeth were evaluated. The experiments were then divided into RS heterogeneity and correlational surface integrity assessments. The RS heterogeneity experiments were based on the RS mapping and on the line broadening analysis of the gears flanks surface. The correlational surface integrity assessment consisted on the analysis of surface features that may correlate themselves with the RS findings. Those features were microstructure, topography and hardness distribution. Figure 3.1 summarizes the overall experimental scope. In the following sections, the workpieces studied and the mentioned methods are described.

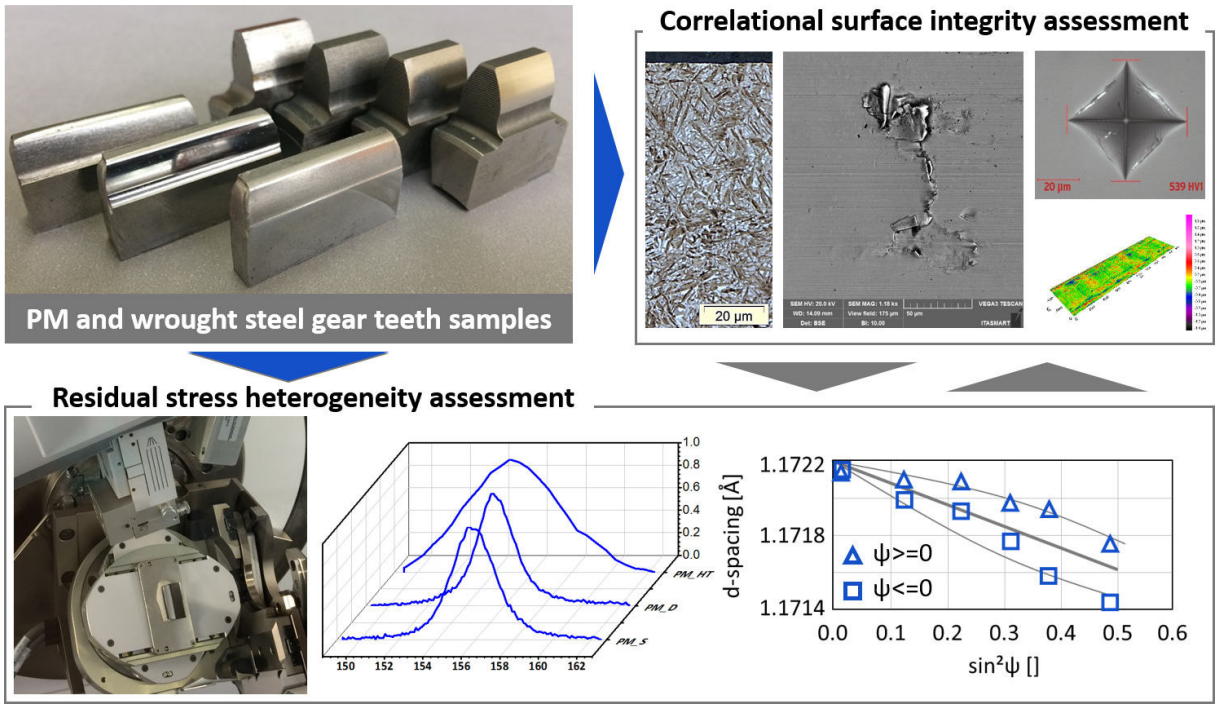

FIGURE 3.1 – Overall experimental scope

3.1 Workpieces description

Specimens of gears teeth correspondent to different manufacturing steps of the powder metallurgy and wrought steel chains were selected for the study. Figure 3.2 illustrates the manufacturing chains from which the workpieces were originated. For the PM chain, three workpieces of a PM steel alloy correspond to gear teeth after the steps of sintering, surface densification and heat treatment. The nomenclature of those samples are respectively PM_S, PM_D and PM_HT. From the wrought steel chain, four workpieces of DIN 16MnCr5 steel correspond to teeth after cutting, heat treatment, shot peening and grinding, of a FZG-C gear model. The nomenclature for wrought steel workpieces are then W_C, W_HT, W_SP and W_G, respectively.

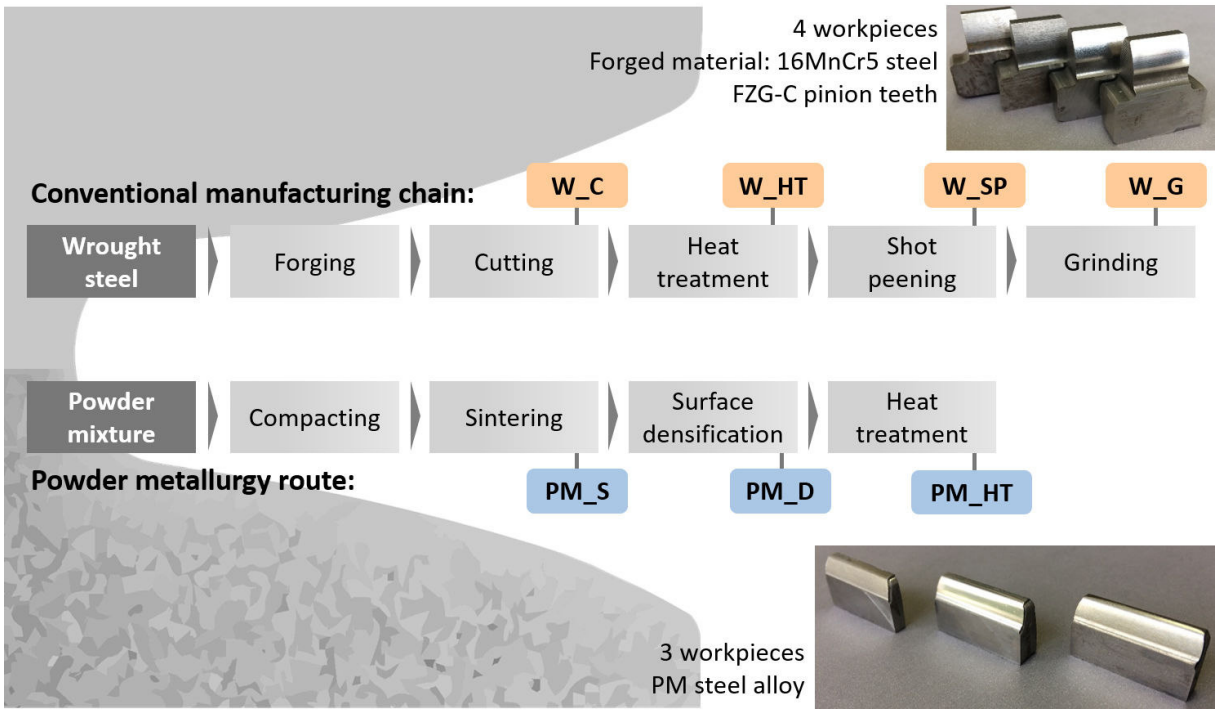

FIGURE 3.2 – Powder metallurgy and wrought steel gear workpieces

3.2 RS heterogeneity assessment methods

3.2.1 Residual stress mapping

Residual stresses were measured by X-ray diffractometry in a *Panalytical Empyrean* diffractometer with Cr $K\alpha_1$ anode radiation in point focus. The Cr tube voltage and current were set to 40 kV and 40 mA for the measurements, respectively. In the incident beam optics, an X-ray lens with a crossed slits assembly guaranteed a quasi-parallel beam with irradiated spot size control. The parallel beam geometry provided makes the mea-

surements insensitive to sample height misalignment (EMPYREAN REFERENCE MANUAL, 2010). On the diffracted beam side, a parallel plate collimator with an equatorial acceptance angle of 0.18° and a scintillation detector were used. The diffractometer and the accessories used are shown in Figure 3.3. The selected diffraction peak for the shift analysis was positioned around $2\theta = 156°$, which corresponds to the diffraction plane (211) of αFe (ferrite-martensite) (ALEXANDRU; BULANCEA, 2002; ASTM E2860-12, 2012). It is a general recommendation to select peaks with the highest 2θ for stress analysis, since they are more sensitive to strains and display a larger shift in 2θ (NOYAN; COHEN, 1987). The measurement range, step and counting time were then tried to be adjusted to provide a curve well defined in terms of peak intensity/position and background definition on both sides of the peak. For peaks correspondent to ferrite, a small step $2\theta = 0.1°$ was used. In the case of the broadened martensite profiles, bigger steps of $2\theta = 0.5°$ were used, as recommended by Jenkins and Snyder (1996).

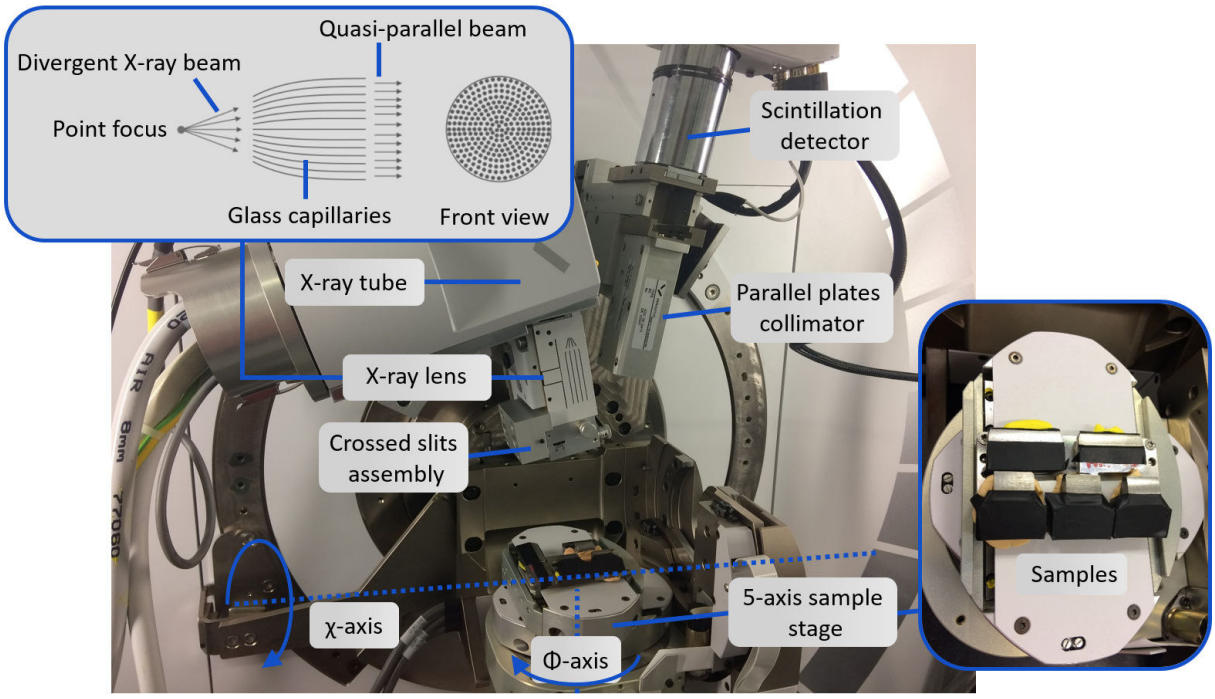

FIGURE 3.3 – Experimental diffraction arrangement

The measurement method consisted on obtaining data of d vs $sin^2\psi$ in the χ mode, in which negative and positive tilt angles χ were used to provide $sin^2\psi$ values of 0.0, 0.1, 0.2, 0.3, 0.4 and 0.5. The χ-tilt was preferred because, differently from the ω-tilt, the defocusing effects are the same for positive and negative ψ and absorption is not affected by the tilting (FITZPATRICK *et al.*, 2005; ASTM E2860-12, 2012). For performing these tilts, a 5-axis sample stage was used, which also allowed the automatic samples positioning for the batch of measurements. Squared spots of 3 mm and 1 mm sides were then chosen for the RS mappings. The larger spot of 3 mm was chosen because it comprises almost the entire involute profile of the PM gears (approximately 5 mm). The 1 mm spots

were selected because they represent smaller areas along the gear flank with a still good compromise solution in terms of signal amplitude and measurement time. The wrought steel gears present higher tooth height and lower tooth width, even so the spots sizes and positions were the same as those of PM gears, for comparison purposes.

The sizes of the irradiated spots were set by the aperture in the crossed slits, and their change with sample tilt was predicted through Equations 3.1 and 3.2 (EMPYREAN REFERENCE MANUAL, 2010). The varying spots sizes were also confirmed experimentally through the incidence of the X-rays on a fluorescent sample.

$$L = \frac{h + \delta(R - f)}{\sin \omega} + W \sin \chi \cot \omega \tag{3.1}$$

$$W = \frac{w + \delta(R - f)}{\cos \chi} \tag{3.2}$$

In which, L and W are the respective length and width of the irradiated area, R is the radius of the goniometer, h and w are the height and width set in the crossed slits assembly, f is the distance from the focus of the X-ray tube to the crossed slits and δ is the divergence of the X-ray beam emerging from the X-ray lens, in radians. Geometric calculations were also conducted to ensure that the irradiated spot would measure the areas of interest even with the change of the beam and sample angles.

The RS mapping was therefore performed by measuring three large spots of 3 mm and six 1 mm spots on each sample. Figure 3.4 illustrates the mapping spots positions.

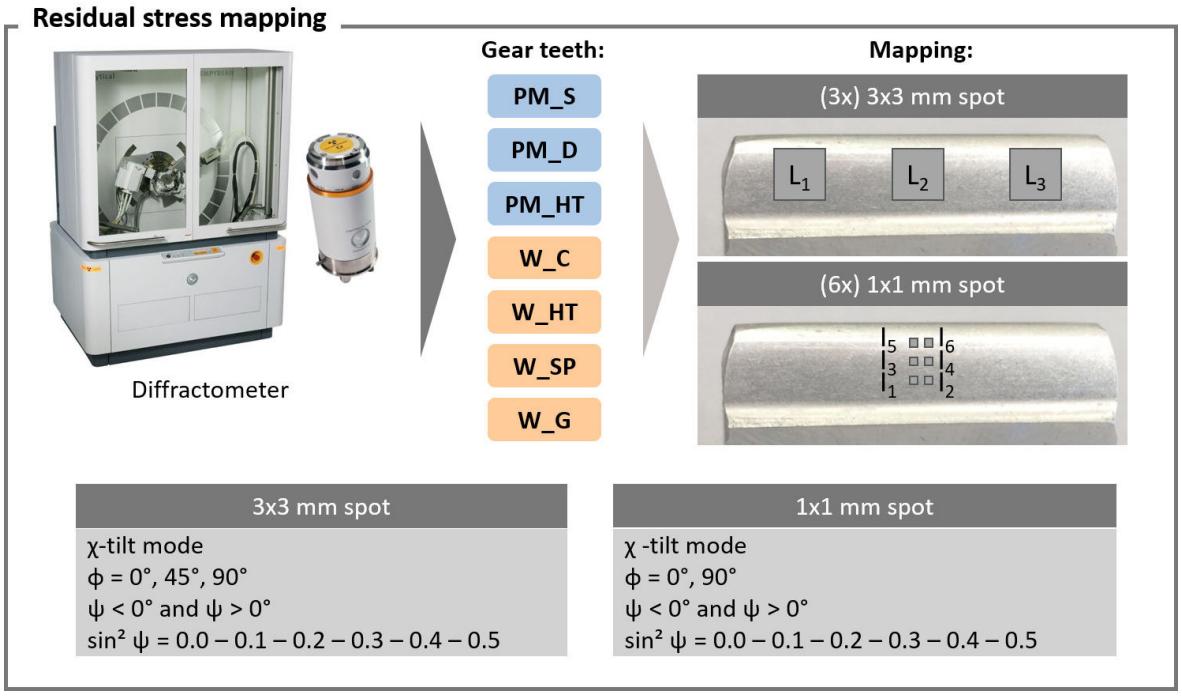

FIGURE 3.4 – Residual stress mapping

The spots of 3 mm were measured at adjacent regions of the teeth flanks to verify how the RS vary with the measurement position along the gear tooth lead (see Annex A for basic gear nomenclature definitions). The 1 mm spots were positioned at the center of the lead profile, to map the RS at the dedendum, pitch and addendum regions. The centered 3 mm spot result is expected to be approximately an average value of the six 1 mm spots results. Different values for the RS of the 1 mm spots are also expected for the powder metallurgy specimens, due to the heterogeneous microstructure described in the literature (KLOCKE *et al.*, 2013).

For the 3 mm spots, the measurements were performed at $\phi = 0°$, 45° and 90° and the RS tensor could be determined by the *Dölle-Hauk* method. The X-ray elastic constants (XEC) used in the calculations were $s_1 = -1.25$ [10^{-6} MPa^{-1}] and $(1/2)s_2 = 5.76$ [10^{-6} MPa^{-1}] (HAUK, 1997). Those values may not represent accurately the investigated materials, but for comparison purposes this choice is suitable. The stress normal to the surface (σ_{33}) was assumed to be insignificant due to the small depth of penetration of X-rays at the free surface, which lays between 3 μm and 6 μm for Cr radiation on Fe (ASTM E2860-12, 2012; NOYAN; COHEN, 1987). The measurement range for these spots was from $2\theta = 149.1°$ to $2\theta = 162.5°$. The reason for this range is that, in addition to the peak position information, the shape of the profile was also of interest for the line broadening analysis described further. A general recommendation of a range of five times FWHM was tried to be followed (HAUK, 1997). For the 1 mm spots, the measurements were made at $\phi = 0°$ and $\phi = 90°$. Measurements at $\phi = 45°$ were not conducted, because the number of measurement points was high and the experiments were very time consuming for obtaining a satisfactory peak signal. The measurement range for these spots was narrower, from $2\theta = 151.8°$ to $2\theta = 159.6°$, because the interest was on the diffractogram peak position. From these smaller spots, the stress tensor was determined, but it was assumed the approximation $\sigma_{12} = \sigma_{33} = 0$.

After the measurements, the obtained profiles were treated for accurate 2θ peak positioning. First, the background was defined. When the sample material consisted mainly of ferrite (before the heat treatment step), both tails of the profile were well defined and with the same background intensity. In this case, the background was determined by selecting four points of each of the profile's extremities to perform a linear fit. After heat treatment, the samples' material consisted predominantly on martensite, and the correspondent profiles were considerably broadened, as described in the literature (HAUK, 1997). In this case, the background was defined as a constant line built with four points of the left extremity. The reason for this is that the right peak tail was not completely reachable due to the limitation of the goniometer on measuring angles 2θ higher than 163°.

Following the background definition, other profiles treatments were conducted. No absorption correction is necessary in the χ-mode (NOYAN; COHEN, 1987), but the curves were corrected with the *Lorentz* and polarization factors. The *Lorentz* and polarization factors account trigonometric terms that describes the dependence of the diffracted intensity on the diffraction angle (NOYAN; COHEN, 1987). The polarization effects must be corrected only when the incident beam is unpolarized, which is the case in this study. In sequence, the $K\alpha_2$ radiation peak was removed by the *Rachinger* method (RACHINGER, 1948), considering a $K\alpha_2/K\alpha_1$ intensity ratio of 0.5. After all these corrections, the peak positions were determined through a modified *Lorentzian* fit, which is generally used in the practice of profile fitting (NOYAN; COHEN, 1987). The fluxogram in Figure 3.5 summarizes the curves treatment for peak location. For the validation of the chosen optics, RS measurement and determination procedures, a free-stress ferrite sample was measured before the execution the RS mapping experiments.

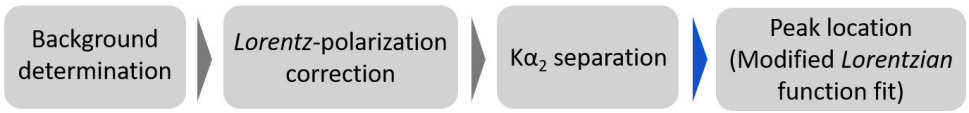

FIGURE 3.5 – Fluxogram of curves treatment steps for residual stress determination

3.2.2 Line broadening method

Differently from the residual stress mapping, which provide average or macro RS, the line broadening analysis provide information of what happens in the micro scale. As exposed in section 2.2.3, the broadening of X-ray profiles occur due to instrumental influences, microstrains (and therefore micro residual stresses) and crystallite size distributions. The intention of the line broadening analysis here performed is to correlate the microstress information obtained with the heterogeneity of macro RS assessed through mapping. Since the macro RS represent an average of several crystalline grains, their deviations (or heterogeneity) can be assessed through the intensity of microstresses distributions (REGO, 2016). The RS mapping is a time consuming method and may be impractical for industrial applications. Additionally, it provides information of how the macrostresses vary in areas of millimeters size. The stress deviations, however, may occur in the microscale. The line broadening methods, in contrast, are much simpler and just a few diffraction profiles may be enough for obtaining microstress information. In the following paragraphs, the method for broadening analysis of this study is described.

As exposed in Section 2.2.3, the broadening of X-ray profiles occur due to instrumental influences, microstrains (and therefore micro RS) and crystallite size distributions. The line broadening analysis can be performed in the real space or in the *Fourier* space. The *Fourier*-space methods make no assumption on the shape of the profiles and therefore

they may provide more accurate information. However, these *Fourier* methods require higher experimental and mathematical efforts (GENZEL, 1997; BALZAR, 1999). The real-space methods, in turn, are less accurate, but simpler and more rapid and adequate for practical purposes (LANGFORD, 1978; GENZEL, 1997). These methods in the real space are best applied when trying to identify trends of microstructural changes by comparing specimens belonging to a series of experiments (SCARDI *et al.*, 2004), which is the case of the present study. Therefore, the real-space method was the choice for the line broadening analysis of the gear teeth, and its application is here detailed.

According to Jones (1938), the observed profile ($h(x)$) can be considered as the convolution of the physical ($f(x)$) and instrumental ($g(x)$) profiles, as in Equation 3.3.

$$h(x) = \int_{-\infty}^{\infty} f(y)g(x-y)dy \tag{3.3}$$

Each of these profiles, in turn, can be considered to follow a $Voigt$ function, which is the result of the convolution of *Gauss* and *Cauchy* (or *Lorentzian*) functions (LANGFORD, 1978; SUORTTI *et al.*, 1979). These assumptions are the basis for the method of $Voigt$ analysis, which is often referred as integral breadth method (GENZEL, 1997; SCARDI *et al.*, 2004). The broadening parameters used in this analysis are the full width of half maximum (FWHM) and the integral breadth (net profile area/maximum intensity, β). As the curves have to be symmetrical for this function assumptions, the profiles investigated were treated in terms of $K\alpha_2$ separation.

Particle size broadening follows approximately a *Cauchy* function, whereas broadening due to microstrains are more nearly *gaussian* (WARREN, 1959; GUPTA; ANANTHARAMAN, 1971; LANGFORD, 1978; LANGFORD *et al.*, 1988). By using empirical equations proposed by (DELHEZ *et al.*, 1982), the integral breadths of the *Cauchy* (β_C) and *Gauss* (β_G) components of the profiles were determined (Equations 3.4 and 3.5), considering a maximum error of 1% (DELHEZ *et al.*, 1982).

$$\left(\frac{\beta_C}{\beta}\right)_{h,g} = 2.0207 - 0.4803\left(\frac{\text{FWHM}}{\beta}\right) - 1.7756\left(\frac{\text{FWHM}}{\beta}\right)^2 \tag{3.4}$$

$$\left(\frac{\beta_G}{\beta}\right)_{h,g} = 0.6420 + 1.4187\left(\frac{\text{FWHM}}{\beta} - \frac{2}{\pi}\right)^{0.5} - 2.2043\left(\frac{\text{FWHM}}{\beta}\right) + 1.8706\left(\frac{\text{FWHM}}{\beta}\right)^2 \tag{3.5}$$

For obtaining the instrumental profile, there are two approaches. On both options, the shape of the correspondent curves must have minimal influence of crystallite size and strain, and the preparation of the samples is non-trivial. The first one consists on

preparing of a standard sample with the same composition of the material investigated, with a crystallite size above 1 μm and with practically no lattice imperfections. For metals, suitable specimens can be obtained by normalising rather than powder (GENZEL, 1997). During the measurements, the same optics have to be used for the investigated and standard samples. It would be ideal to have a standard specimen of the same material investigated, however due to difficulties and time involved on the preparation, this is seldom achieved (BERKUM *et al.*, 1995). Therefore, in the second approach, a standard of another material can be prepared or obtained, such as the certified specimen of LaB_6 (NIST SRM 660). By doing this, the lines of standard and studied specimens usually do not coincide, but by using analytic models the instrumental profile can be synthesized at any angle of interest. The *Caglioti* function represented by Equation 3.6 can be used for this purpose (CAGLIOTI *et al.*, 1958):

$$\mathrm{FWHM}^2(2\theta) = U\tan^2\theta + V\tan\theta + W \tag{3.6}$$

By finding the U, V and W constants with the profiles of the standard specimen, the instrumental FWHM can be determined. The *Cauchy* and *Gauss* integral breadths can also be predicted for any 2θ, by using Equations 3.7 and 3.8 (LANGFORD *et al.*, 1991).

$$\beta_C(2\theta) = A/\cos\theta + B\tan\theta \tag{3.7}$$

$$\beta_G^2(2\theta) = C/\cos^2\theta + D\tan^2\theta \tag{3.8}$$

In this study, the instrument profiles were obtained from a previous calibration of the diffractometer with a standard specimen, through the second approach mentioned. After finding the *Cauchy* and *Gauss* integral breadths of the observed and instrumental curves, these breadths of the physical profile were isolated by Equations 3.9 and 3.10, as a consequence of the convolution.

$$\beta_C^f = \beta_C^h - \beta_C^g \tag{3.9}$$

$$(\beta_G^f)^2 = (\beta_G^h)^2 - (\beta_G^g)^2 \tag{3.10}$$

Following the studies of Scherrer (1918) and Stokes and Wilson (1944), the average crystallite size and microstrain were determined by Equations 3.11 and 3.12.

$$< N >= \frac{\lambda}{\beta_C^f \cos\theta} \tag{3.11}$$

$$\varepsilon = \frac{\beta_G^f}{4 \tan \theta} \tag{3.12}$$

The average size $<N>$ represents a volume weighted size perpendicular to the diffracting lattice planes considered. It is generally smaller than the grain size of the specimen, because the grains can be composed of a number of coherently diffracting domains (DELHEZ *et al.*, 1987). ε is the intensity or range of microstrains, resultant from the extreme values of lattice spacings, as described in Stokes and Wilson (1944) and Langford *et al.* (1988).

The described procedure can be applied to single profiles. However, when more reflections are available, it is recommended to determine size and strains effects from the variation of the physical integral breadths with the diffraction planes (GENZEL, 1997), which was tried to be done in this study. The profiles analyzed consisted on the curves from the measurements of the RS mapping with spots of 3 mm for $\psi = 0^+$, $\psi = 0^-$ and $\phi = 0°, 45°$ and $90°$. The three spots of 3 mm for each sample measured the peak around $2\theta = 156°$, which corresponds to the (211) plane of ferrite or martensite (ASTM E2860-12, 2012; ALEXANDRU; BULANCEA, 2002). Therefore 18 profiles of the (211) reflection were used per sample, and the average broadening parameters were calculated from them. A verification that the mentioned parameters did not change with ϕ was performed before those calculations, as done by REGO (2016). Additionally, wide range scans from $2\theta = 55°$ to $2\theta = 140°$ were conducted. The peaks correspondent to the (011) and (022) planes of ferrite/martensite were then also explored. Figure 3.6 summarizes the procedure of the line broadening analysis employed.

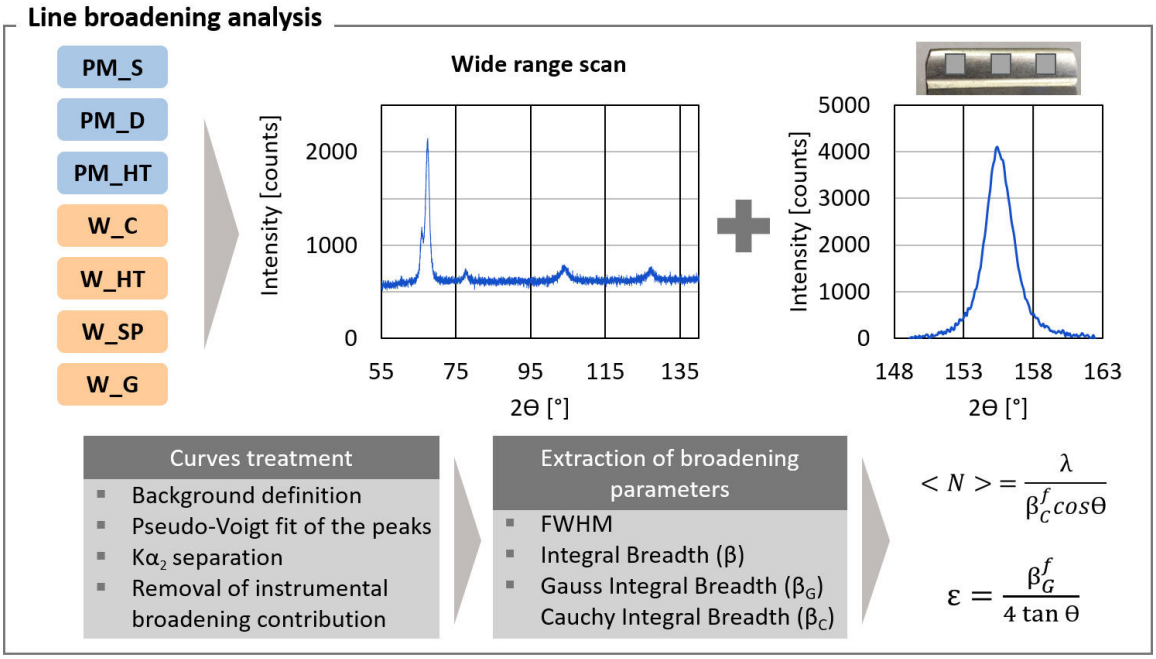

FIGURE 3.6 – Line broadening analysis procedure

The curves treatments, instrumental effects removal, *Voigt* fitting and extraction of broadening parameters were performed in the software *Panalytical Highscore*, which contains dedicated algorithms and routines for this purpose. The evolution of broadening and microstructural parameters such as FWHM, $<N>$ and ε was finally investigated along the powder metallurgy and wrought steel gears manufacturing chains. The results were then confronted with those of the RS mapping and those of the correlational surface integrity features experiments, described ahead.

3.3 Correlational surface integrity assessment

To support the RS heterogeneity results of the PM chain, correlational surface integrity evaluations were performed. These evaluations were based on metallography, topography analysis and hardness mapping of the workpieces, at the same regions where the RS heterogeneity was assessed. For the metallography, samples were cut in the transverse direction and then mounted in bakelite resin, ground, polished and finally etched with a 3% Nital solution. The metallography images were then produced with an optical microscope *Carl Zeiss Ultraphot III*. Relevant information that these imagens can provide are identification of phases, grain size, grain distribution, preferred grain orientation and densification depth. These microstructural properties are directly associated to the line broadening parameters FWHM, <N> and ε support the analysis of micro RS. The macro RS variations can also be explained by microstructural heterogeneity in the regions considered. Additionally, these images permit the microstructure evolution assessment with the manufacturing steps and the comparison between the manufacturing chains. Figure 3.7 illustrates this analysis.

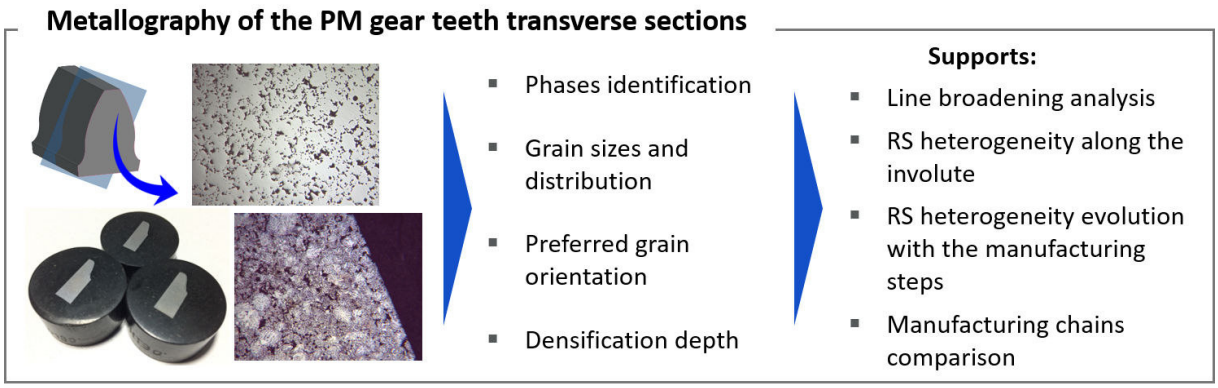

FIGURE 3.7 – Metallography analysis

For the hardness mapping, the specimens prepared for metallography were polished and submitted to micro indentation hardness tests in a microindenter *EMCO-TEST Durascan 70*. Samples correspondent to manufacturing steps before the heat treatment

were tested with a *Vickers* indenter and 0.05 kg of load (HV 0.05). After heat treatment, the surfaces of the samples were hardened and the test load was increased to 0.1 kg (HV 0.1). The mapping consisted on measuring the hardness along the surface depth according to the standard DIN EN ISO 6507-1 (DIN, 2006) at the dedendum, pitch and addendum regions of the teeth, as shown in Figure 3.8. The mapping along the regions of the involute would be correlated with microstructural and RS heterogeneity observations. The mapping in the surface depth would also provide additional information for inferring what could be expected for the RS heterogeneity along the depth.

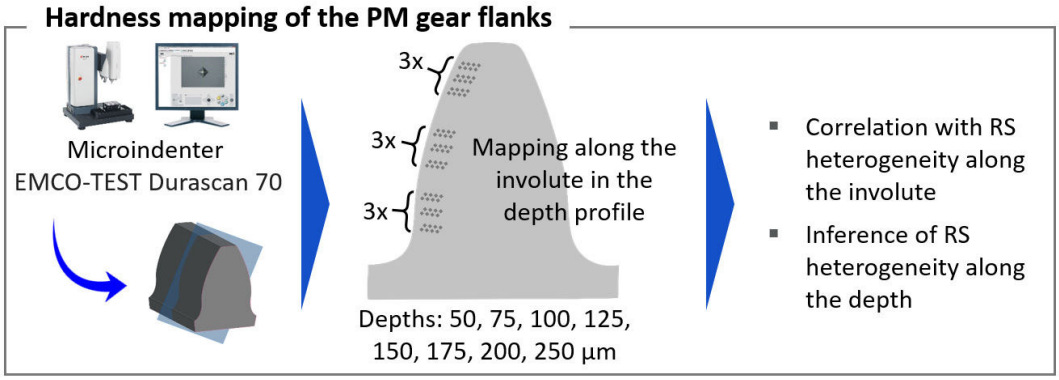

FIGURE 3.8 – Hardness mapping

The topography analysis was performed in a scanning electron microscope *Vega3 Tescan* and by profilometry in a chromatic aberration confocal microscope *Cyber CT100*. Scanning electron microscope (SEM) images were produced from the dedendum, pitch and addendum regions of the workpieces, by means of secondary and backscattered electrons. These images permitted the qualitative analysis at high magnifications of the topography of the flank surface of the specimens. For a quantitative analysis, the profilometer was used for the three dimensional measurement of squared 1x1 mm spots at the dedendum, pitch and addendum regions of the teeth. These spots were used for correlation with the RS mapping according to investigation of similar regions. The sensor employed in this case had a lateral resolution of 1 μm and a depth resolution of 0.1 μm. For the extraction of roughness parameters, polynomial filters were applied to remove the curvature of the tooth profile. Figure 3.9 shows a schematic of the topography analysis.

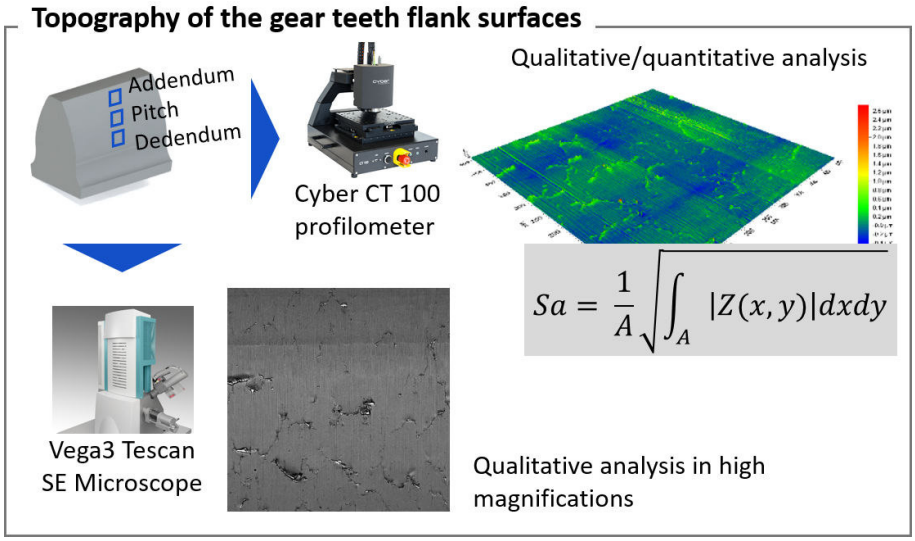

FIGURE 3.9 – Topography analysis

In regard of the statistics of the research, this assessment was applied to the RS mappings, line broadening analysis and hardness mappings. The errors for these experiments were accounted as one standard deviation. The standard deviation of the RS mappings are the result of the curve fitting needed for the RS calculations. In the case of the line broadening analysis, the statistical calculations were based on the results extracted from 18 samples of each manufacturing step. The sample size for the hardness mapping was three measurements results for each region analyzed. In the next section, all the previous mentioned RS and correlational surface integrity experiments have their results analyzed and discussed in an integrated approach.

4 Results and discussion

This chapter is divided into two sections related to each of the research questions presented in the "Objective and approach" section in Chapter 1. In section 4.1, the results and discussion are directed to the methodology analysis. The RS heterogeneity methods are investigated in terms of their capabilities and compared to answer the first research question of this study. In section 4.2, the residual stresses heterogeneity assessment methods are applied to the workpieces correspondent to subsequent steps of the powder metallurgy and wrought steel chains. The results are exposed and the heterogeneity parameters are analyzed and correlated with other surface integrity features, such as microstructure, topography and hardness. This approach allows the characterization of the RS evolution along the manufacturing steps. First, the PM results are discussed separately in detail, and then the PM and wrought steel chains are compared. The answer to the second research question is then given. A summary of the exposal of results and discussion to answer the questions is presented in Figure 4.1.

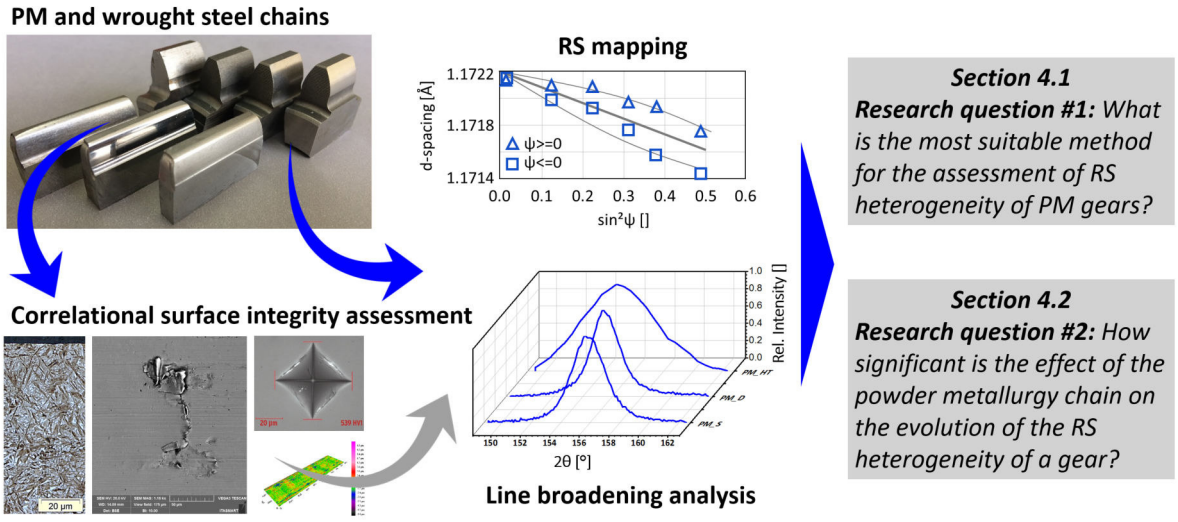

FIGURE 4.1 – Structure of the results presentation

4.1 Evaluation of the methods for the assessment of RS heterogeneity

The RS mapping and the line broadening analysis methods provide information of macro- and microstresses, respectively. The purpose of testing each of these methods is that the general practice in the gear technology field of analyzing punctually the macrostresses is not enough for fatigue behavior comprehension, as explained in the literature review. The RS mapping is a method that can provide information of how macro RS vary along the surface. However, due to the fact that the RS mapping method is highly time consuming, it is proposed in the literature that the macro RS heterogeneity can be alternatively assessed through the intensity of micro RS (KLOCKE *et al.*, 2016; REGO, 2016). The line broadening analysis can be used for obtaining these micro RS with the same macro RS data. Therefore, the punctual macro RS measurement can also provide information of heterogeneity without additional experimental effort. These two heterogeneity assessment methods were then tested and validated in wrought steel gears and discs in the literature (KLOCKE *et al.*, 2016), but in this present study they were applied to PM gears with modifications that provided additional relevant information.

In this Master Thesis, the RS mapping method is modified in such a way that the macro RS variation can be clearly identified according to the regions of the gear flank's surface, which was not previously described in the literature. The results that are presented in the next section show that the macro RS can vary along the lead profile, along the involute profile and can also vary in a diffuse manner. From the analyses, it could be also observed that the micro RS can vary along the lead profile. Therefore, the comprehension of gears RS heterogeneity is expanded, as it can be classified according to the level of RS considered (macro or micro) and according to the region where it is manifested (along the lead, along the involute and diffuse). These concepts of gears RS heterogeneity are illustrated in Figure 4.2.

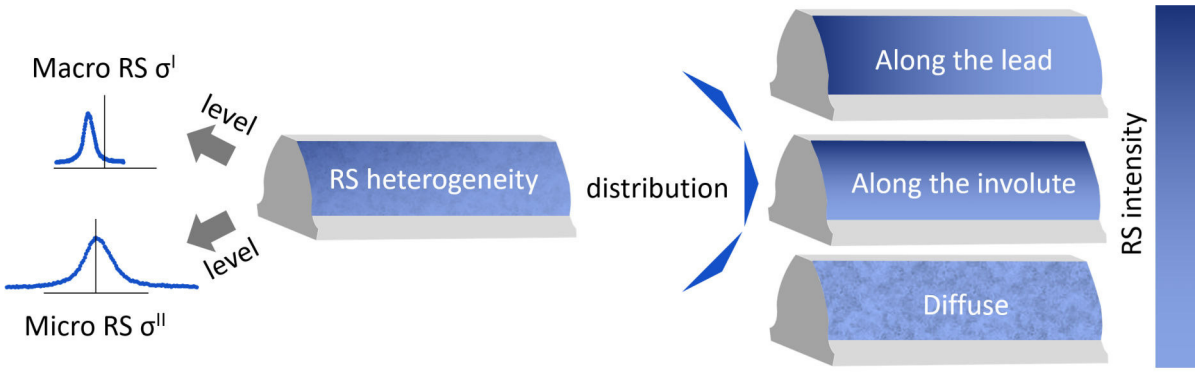

FIGURE 4.2 – Classification of the gears surface residual stresses heterogeneity according to levels (macro and micro) and distribution

The RS heterogeneities along the lead and along the involute were found to be especially relevant to PM gears, more than in the case of wrought steel gears, as it will be discussed in detail in section 4.2. In terms of the methods capabilities for the assessment of RS heterogeneities along the lead, through the RS mapping it was possible to identify variations in form of gradients of macro RS. The line broadening analysis showed similar trends in terms of microstresses. Figure 4.3 exposes examples of these heterogeneities found in the PM chain. In these examples, it could be observed that macro RS variations along the lead is generally associated to different micro RS intensities. After sintering, the lower the compressive macro RS (negative values), the lower was the broadening parameter FWHM and the microstrain. After surface densification, the macro RS differences were decreased, while the broadening parameter FWHM did not change its pattern considerably. After heat treatment, however, the macro- and micro RS gradients were again evidenced. Therefore, when analyzing a PM process step, FWHM and the micro RS can be suitable indicators of RS heterogeneity.

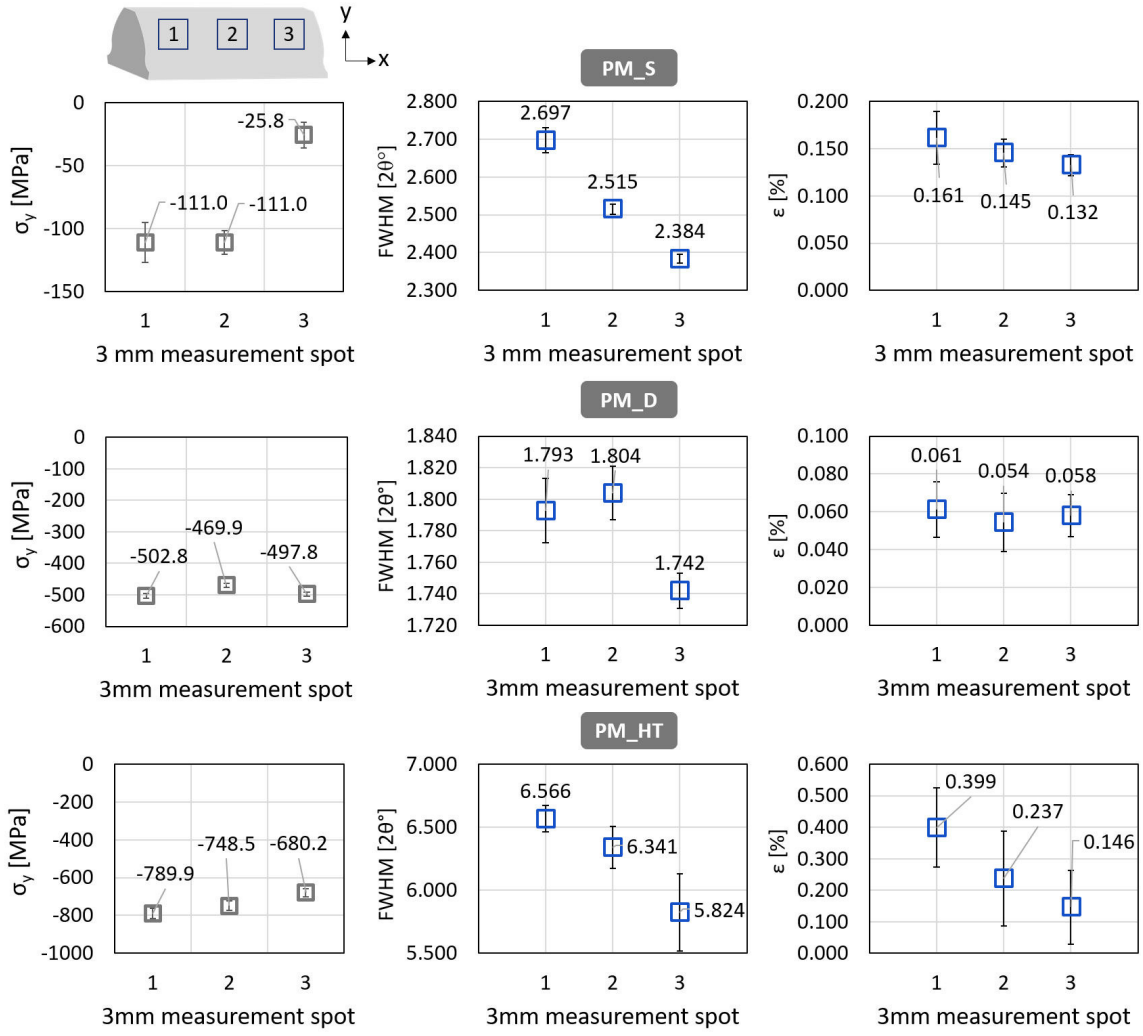

FIGURE 4.3 – Variations of the macro RS σ_y and the broadening parameters FWHM and ε along the lead profile of PM gears, according to each manufacturing step

In regard to the analysis of heterogeneity along the involute and diffuse, it was previously shown in the literature that the RS variation in adjacent regions of a gear surface may be correlated to microstrain intensities (which are indicators of micro RS intensities) (KLOCKE *et al.*, 2016). The previous study validated this correlation when comparing the shot peening step with different process parameters in order to induce different RS heterogeneities. In this dissertation, however, different process steps and manufacturing chains were compared and no direct correlation between the 1 mm spots RS variation and the broadening parameters FWHM and microstrain could be observed. Figure 4.4 shows this analysis for the PM and wrought steel chains. In this figure, only the microstrains are compared, because FWHM presented similar behavior. Therefore, it can be concluded that when comparing different process steps, the micro RS intensities alone are not enough to characterize the RS heterogeneity. Thus, both RS mapping and line broadening methods were applied in this study for the analysis of the RS heterogeneity evolution along the manufacturing chains.

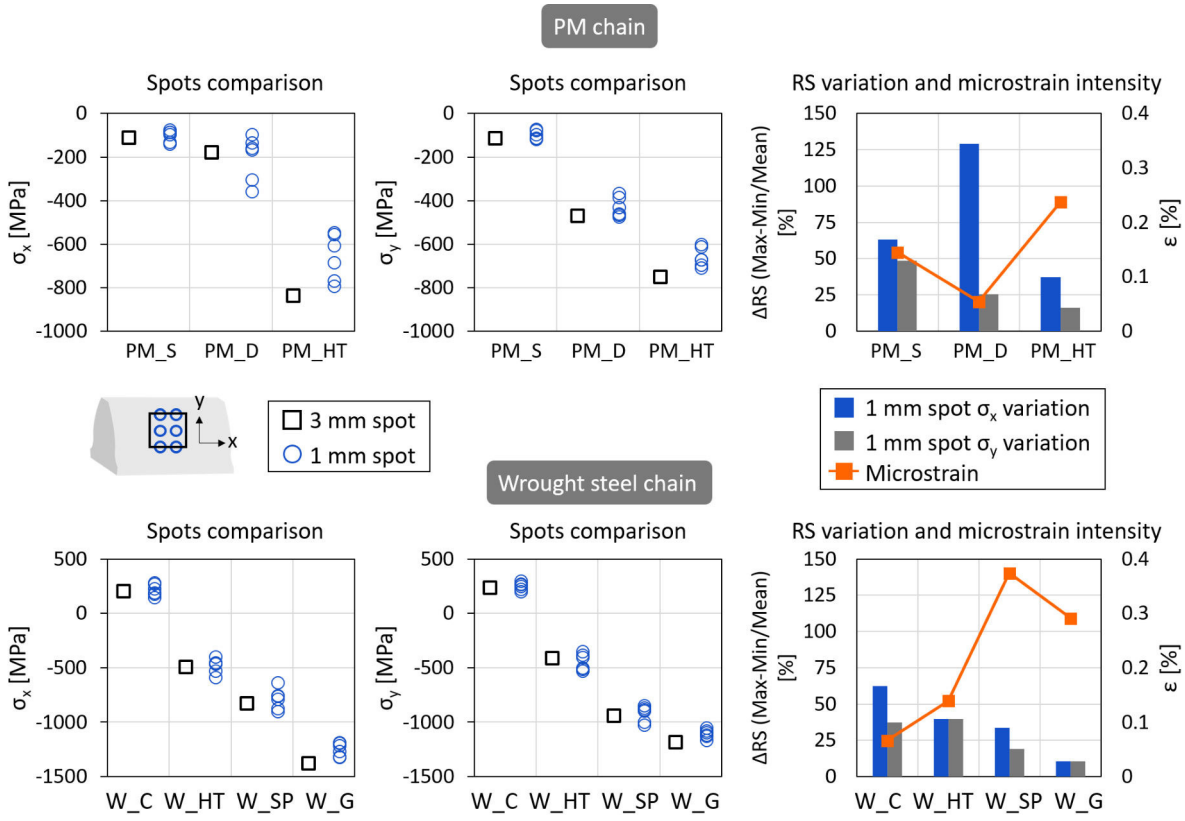

FIGURE 4.4 – Comparison between the RS variations and the microstrain intensities in the PM and wrought steel chains

The answer to the first research question of this dissertation is then given. The most suitable method for the RS heterogeneity assessment of PM gears depends if the analysis is of a single process step or between process steps or manufacturing chains. It was shown that the RS heterogeneity along the lead profile of a single step can be better identified

through the line broadening analysis. The macro RS variation is generally associated to different microstrain intensities. Additionally, there are cases when the macro RS do not vary considerably but the broadening indicates heterogeneity that can be again evidenced in the next process step in a macro level. Therefore, the line broadening analysis showed to be the most suitable method in this case, because it provides information which the RS mapping cannot provide and it is experimentally simpler. When comparing different process steps, however, the microstrain intensities cannot be used alone for characterizing the RS heterogeneity. In this case, the variations of macro and micro RS must be analyzed separately. It means that if the microstrain intensities are higher in a step, the macro RS variations will not be necessarily higher in comparison to other process step. Different process steps and manufacturing chains are generally associated to different microstructure characteristics (porosity, hardening, phases, anisotropy) and, consequently, different mechanical properties (for example, E and ν). Hence, both RS mapping and line broadening analysis are recommended for comparing different manufacturing steps and chains. Figure 4.5 illustrates the answer to the first research question here provided.

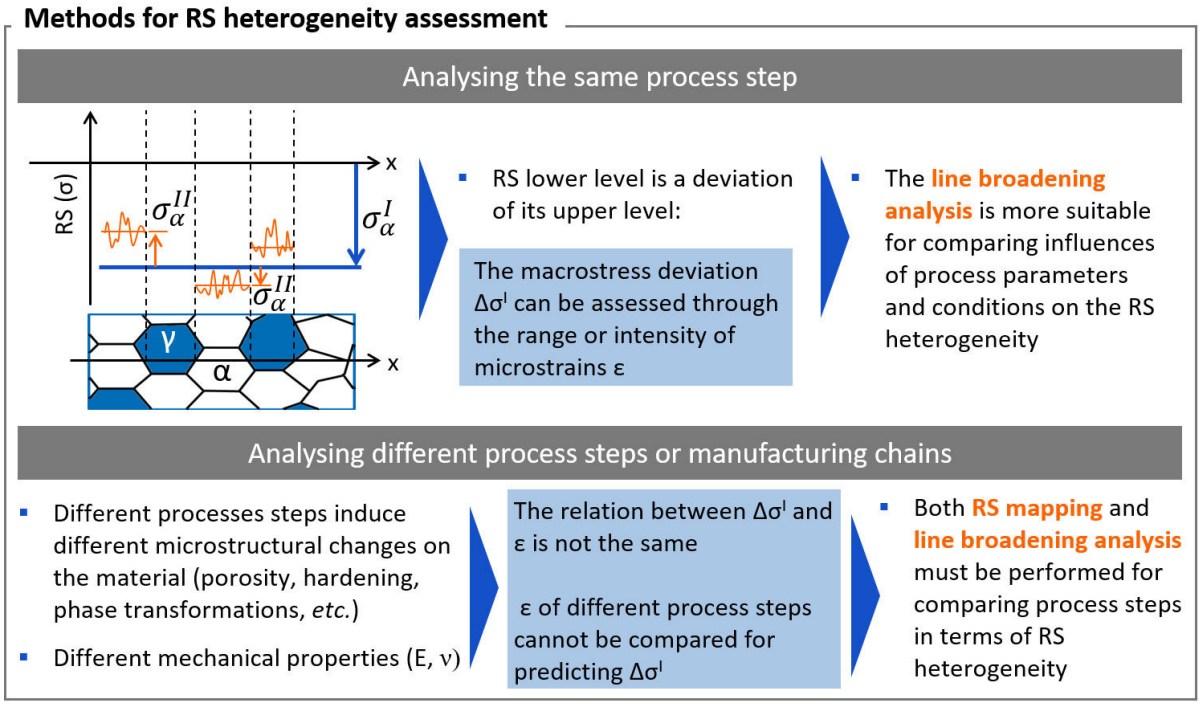

FIGURE 4.5 – The answer to the first research question of this study on the most suitable method for RS heterogeneity assessment

In the present study, multiple peaks were available for the line broadening analysis, as illustrated in Figure 4.6. It can be seen clearly the change of the diffraction peaks broadening with the manufacturing steps. These broadenings were quantified in terms of integral breadths and a method of multiple line analysis was applied for obtaining microstructural information, the *Williamson-Hall* method. This method was tried to be used with the

(011), (002) and (211) peaks of αFe to provide information about the crystallite sizes and microstrains. However, due to anisotropy, when the results of different peaks were plotted, they did not follow the straight line pattern necessary for the application of this method. Hence, all the broadening analyses were based on the single line method with the (211) αFe peaks. The reason for this choice is that the peaks associated to higher 2θ angles are more sensitive to broadening effects, as shown in Figure 4.7.

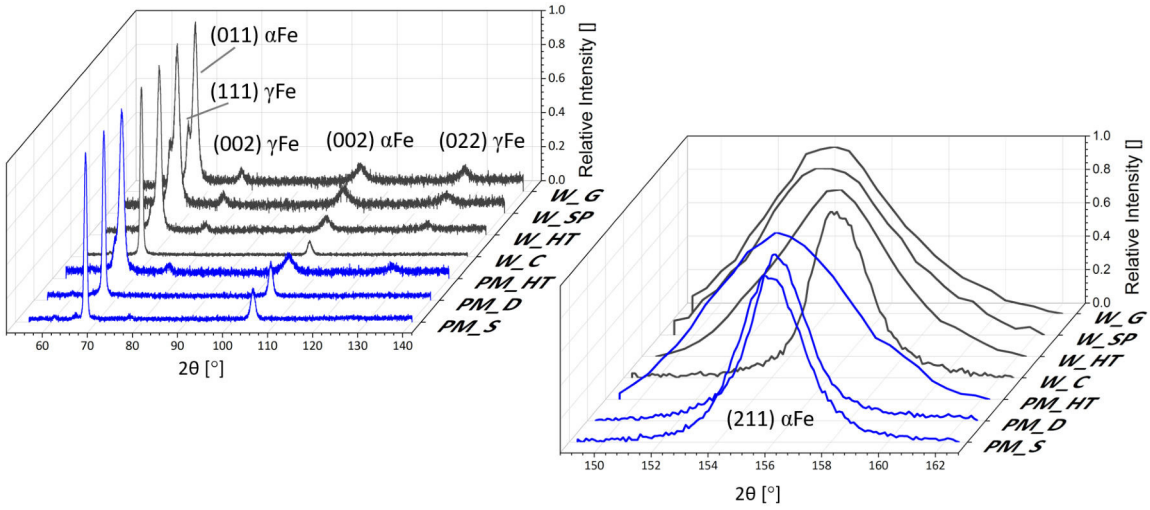

FIGURE 4.6 – Multiple peaks available for the line broadening analysis of this study

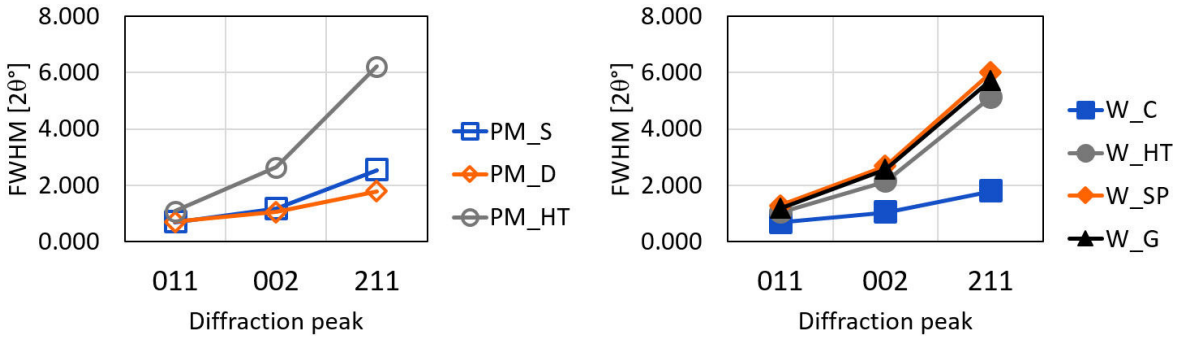

FIGURE 4.7 – Sensitivity of the different peaks of αFe to broadening. The peaks of higher 2θ angles (211) are the most sensitive

Based on the methodology analysis here presented, the residual stress mapping and the line broadening analysis were applied to the different steps of the PM and wrought steel manufacturing chains. The answer to the second research question of this Master Thesis on the evolution of RS heterogeneity of PM gears is then given in the next section.

4.2 Evolution of RS heterogeneity in the gears manufacturing chains

4.2.1 Powder metallurgy chain

In this subtopic, the results are presented and discussed in detail according to each step of the powder metallurgy manufacturing chain (sintering → surface densification → heat treatment). The results include residual stress mapping, line broadening analysis, metallography, topography and hardness mapping.

RS heterogeneity after sintering

The gear tooth representative of the sintering step of the powder metallurgy chain had its surface mapped along the lead profile, and these results are shown in Figure 4.8. The RS values of the three measurement squared spots of 3 mm size are plotted according to the region. The error bars correspond to a confidence interval equal to one standard deviation. Only the normal stresses σ_x and σ_y are presented, because the shear stresses values were approximately zero and $\sigma_z = 0$ was considered in the calculations. The complete stress tensors with standard deviations of all measurements of this study are registered in the Appendix A. The results of this RS mapping indicate that the macro RS σ_x and σ_y vary along the lead profile. The third spot presented values with a lower magnitude than the others.

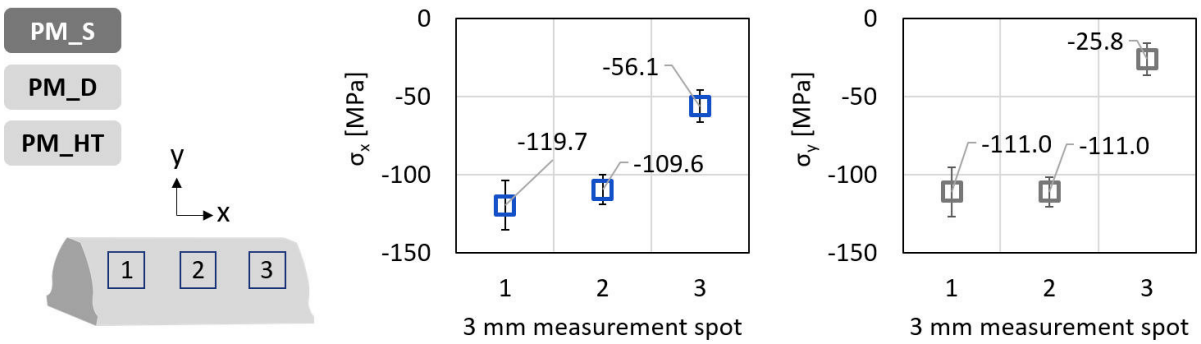

FIGURE 4.8 – Results of the residual stress mapping along the lead of the gear tooth after sintering

To eliminate the hypothesis that this finding was due to measurement errors, the experiment was repeated at this third spot. The same trend of a less compressive stress was found. Therefore, the different RS values may be a consequence of the sintering and the previous manufacturing step, compaction. As shown in the literature review, the applied stresses during compaction are not uniform along the gear teeth width, and the resultant RS heterogeneity may have been propagated after sintering. This explanation is then illustrated in Figure 4.9. Whether this finding will have effect on the final product

and be of relevance in terms of affecting the fatigue behavior, it must be investigated in the further PM process steps.

FIGURE 4.9 – RS heterogeneity along the PM gear lead profile as a result of the compaction step

Analyzing the line broadening parameters of the (211) αFe peaks, it can also be observed heterogeneity in terms of microstresses along the lead profile, as show in Figure 4.10. The spots with higher compressive macro RS are also associated to wider difractogram profiles, represented by FWHM. For a more detailed investigation, the broadening effects were separated in crystallite size <N> and microstrain ε. The crystallite sizes did not change with the region. A trend associating the more compressive spots with higher microstrain range could be perceived. Therefore, the broadening differences may be due to microstrain effects. Of the three broadening parameters, however, FWHM was the one that showed this differentiation more clearly. From this analysis it can be concluded that, in the case of the specimen considered, the same loads that induced more intense macro RS in some spots also induced a higher intensity of microstresses. Therefore, two levels of heterogeneity can be identified. The first one is a macro RS heterogeneity, based on the differences in macro RS found. And the second level is a micro RS heterogeneity, based on the different ranges of microstrains found. In this case, association between both levels of heterogeneity was seen.

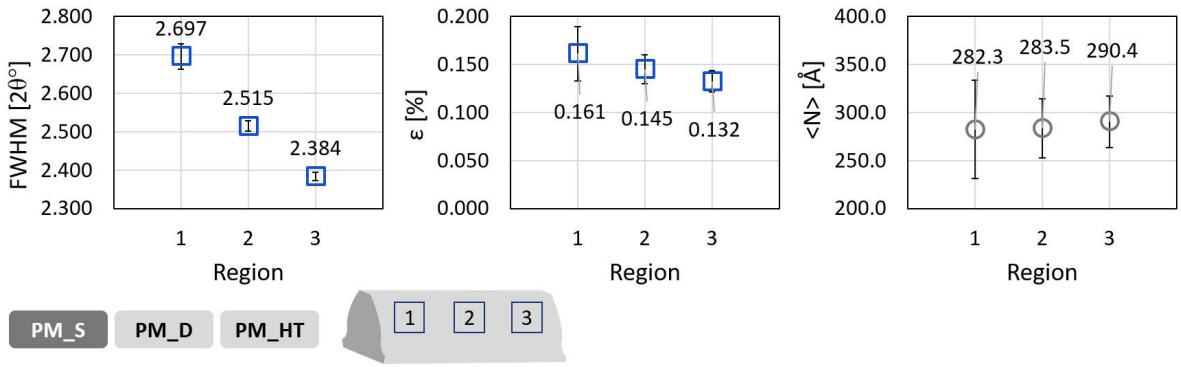

FIGURE 4.10 – Line broadening analysis along the lead of the gear tooth after sintering

The RS mapping was also performed along the involute profile, as shown in Figure 4.11. The measurements correspond to two columns of three squared spots of 1 mm side distributed along the involute. The results are then separated according to the dedendum, pitch and addendum regions of each column. The error bars were suppressed to simplify the visualization, but the maximum uncertainty in this case was ± 25 MPa. It can be observed that RS vary not only along the profile, but the values depend on the column of measurement.

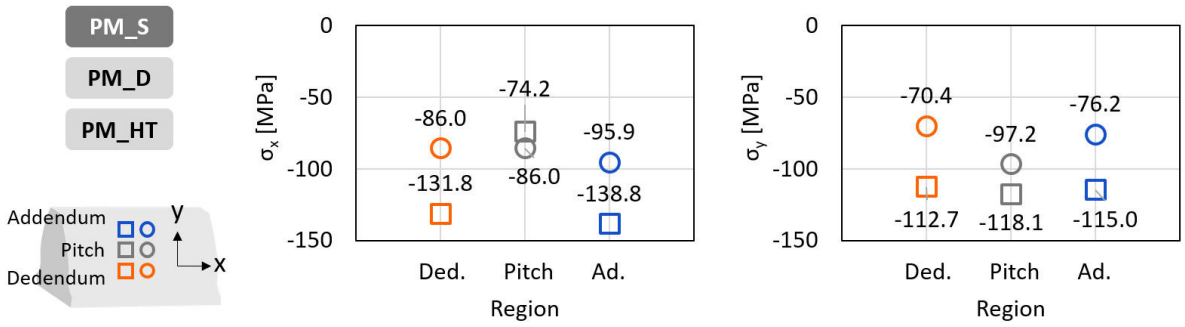

FIGURE 4.11 – Results of the residual stress mapping along the involute of the gear tooth after sintering

The topography investigation results support these RS variations. The images of Figure 4.12 show that the pores distribution is not homogeneous. There are regions with higher concentration of pores than the others, along the lead and the involute profiles. In Figure 4.12 a) it can be seen that the pores concentration is not the same for the 1 mm measurement spots. Additionally, the heterogeneity in pores distribution on the lead profile can be confirmed not only visually, but also by an image analysis software, as in Figure 4.12 b). Therefore, it is another evidence that the pores are more concentrated in the right side regions of the lead profile, which correspond to the spot of lower compressive RS. This finding reinforce the argument that the lead RS heterogeneity is due to the non-uniform loading along the gear tooth width during compaction. The heterogeneous bands of pores along the involute shown in Figure 4.12 c) also explain the diffuse heterogeneity of the 1 mm spots. The roughness mapping exposed in Figure 4.13, in turn, indicates that the spatial roughness also vary along the involute for a column of three 1 mm squared spots, which may be associated to the porosity heterogeneity mentioned.

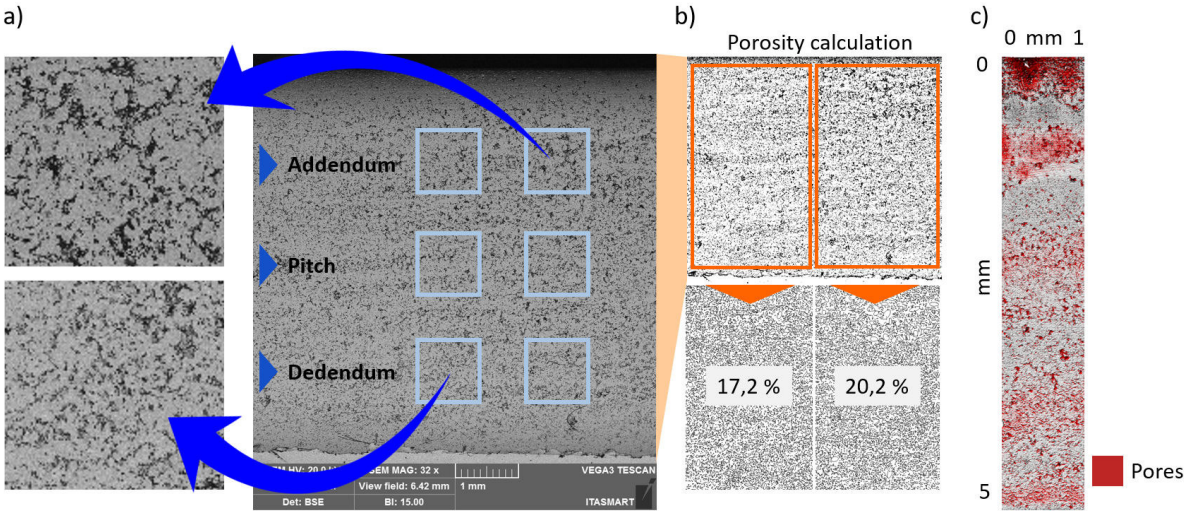

FIGURE 4.12 – Topography analysis of the flank of the sintered gear tooth. a) SEM image showing heterogeneous pores distribution. b) Different porosity distribution along the lead profile, as calculated by an image analysis software. c) The bands of pores evidenced in a profilometry image

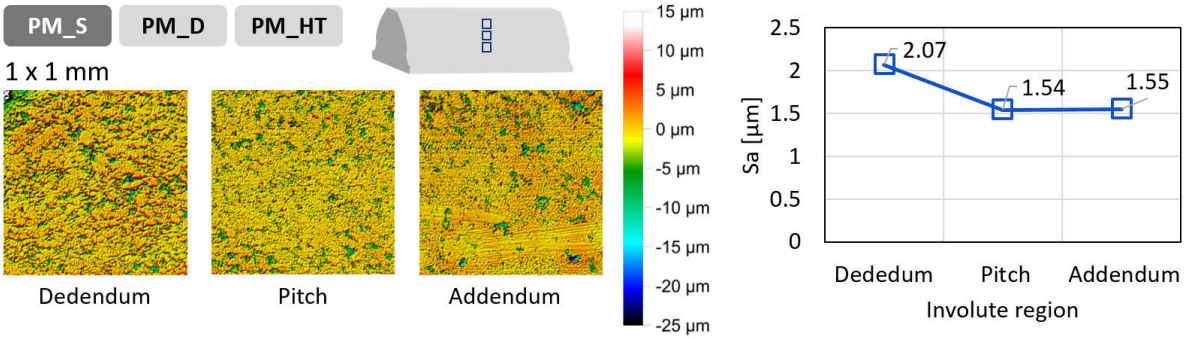

FIGURE 4.13 – Roughness mapping along the involute of the sintered gear tooth

In order to verify if this heterogeneity also exist along the depth, the hardness was mapped through microindentations at the dedendum, pitch and addendum regions until a depth of 250 μm. The results are plotted in Figure 4.14. The confidence interval correspond to one standard deviation. The curves indicate no tendency of hardness differentiation. As the RS intensities are not high, their heterogeneity may not be correlated with a significative change in hardness. Hence, a recommendation for future studies is that further RS measurements should be performed for the analysis of heterogeneity along the depth, using material layer removal through electropolishing.

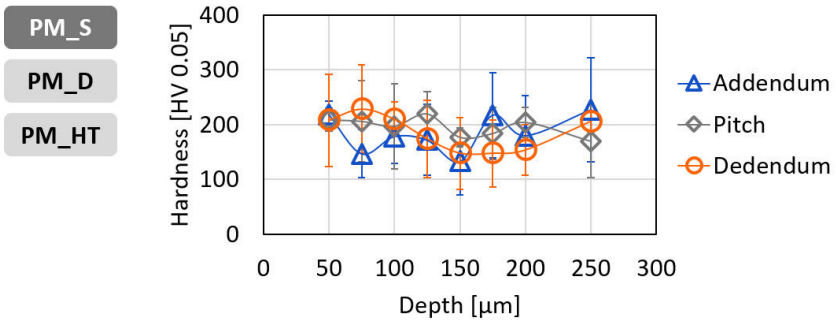

FIGURE 4.14 – Hardness mapping along the involute of the sintered gear tooth

RS heterogeneity after surface densification

After the surface densification step, the porosity at the surface is reduced to practically zero up to a depth of the order of one millimeter. Figure 4.15 shows this transition from the sintering to the surface densification step. The mechanical loads of the process increase the magnitude of the compressive RS at the surface. This increase, however, preferably occurs in the involute profile direction, which is due to the kinematics of the load application. The RS mapping along the lead profile of the densified specimen exposes this effects and the results are shown in Figure 4.16.

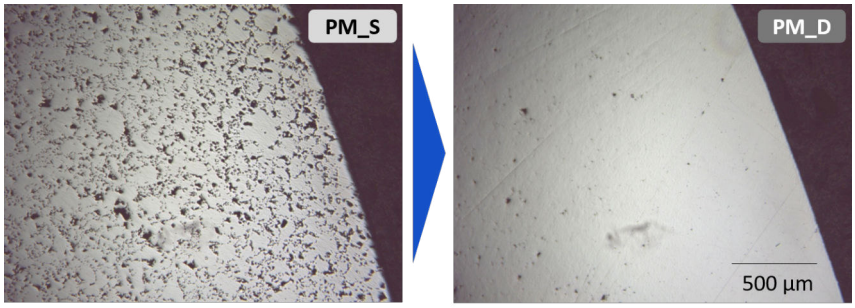

FIGURE 4.15 – Metallography showing the transition from sintering to surface densification. 50x magnification

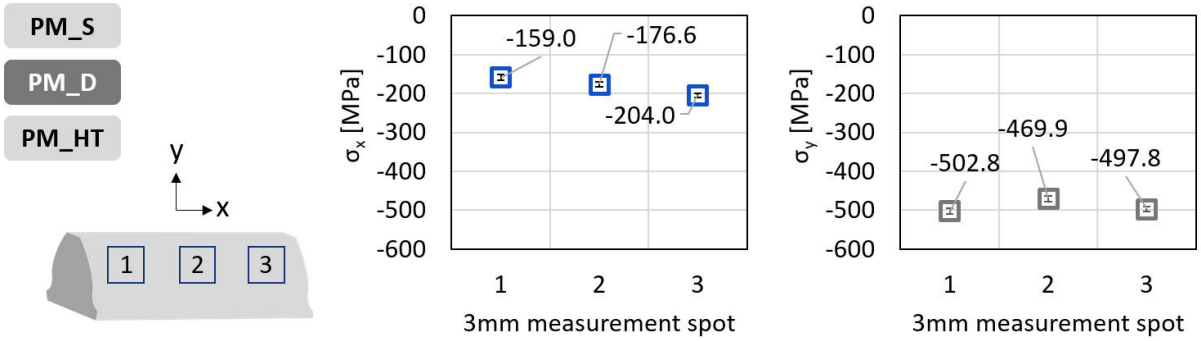

FIGURE 4.16 – Results of the residual stress mapping along the lead of the gear tooth after surface densification

After any load application on the material, RS are redistributed to reach an equilibrium. The influence of a previous step cannot be neglected as it may influence the final RS state, as already described in the literature review. This effect can be slightly perceived in the σ_x chart of the 3 mm spots. The spot 3 with lower compressive stresses after sintering also presented a difference out of the error bars in comparison with the others. It suggests therefore that the heterogeneity resultant of sintering may be carried out after surface densification.

The line broadening analysis also showed that the third spot is different from the others, as exposed in Figure 4.17. The broadening parameters FWHM and ε decreased for all the spots, while the crystallite size did not change. It means that the broadening change from sintering to surface densification may be attributed to microstrains influence. It also means that the surface densification has the effect of making the microstrains more homogeneous than those of a porous surface. Furthermore, the spot 3 that presented a narrower range of microstrains after sintering, continued being more homogeneous in terms of FWHM and, therefore, microstrains (although the ε parameter in the graph was not sensitive).

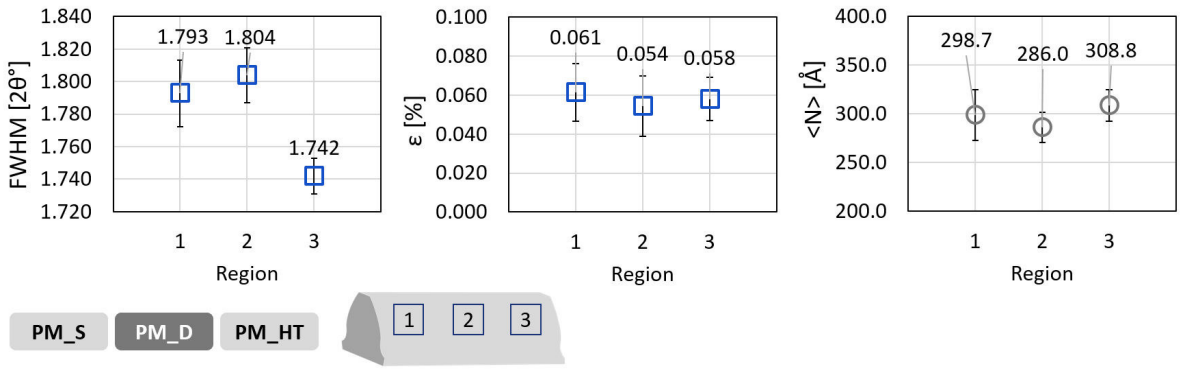

FIGURE 4.17 – Line broadening analysis along the lead of the gear tooth after surface densification

When analyzing the RS distribution along the involute, heterogeneity was also observed after densification. But this time, it is manifested differently from what happens after sintering. Figure 4.18 exposes the results of the RS mapping performed with six 1 mm spots along the involute profile. There is no significant RS differentiation according to the spots column, but they vary with the region on the involute, for both σ_x and σ_y. The RS intensity at the dedendum tends to be inferior in comparison with the other regions. This is consistent with the depth of the densified layer, which is shorter at the dedendum, as exposed in Figure 4.19. For σ_x, the stresses are more intense at the addendum, and for σ_y, at the pitch region. These findings are in accordance with the surface densification kinematics, which is associated to different load applications along the involute.

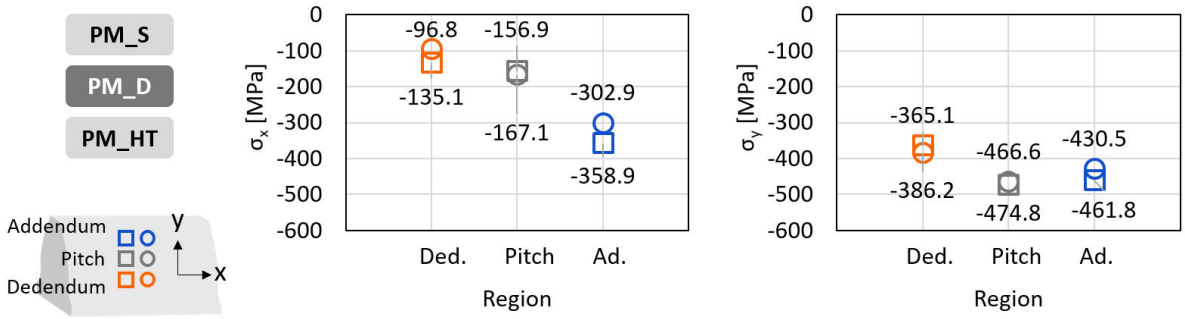

FIGURE 4.18 – Results of the residual stress mapping along the involute of the gear tooth after surface densification

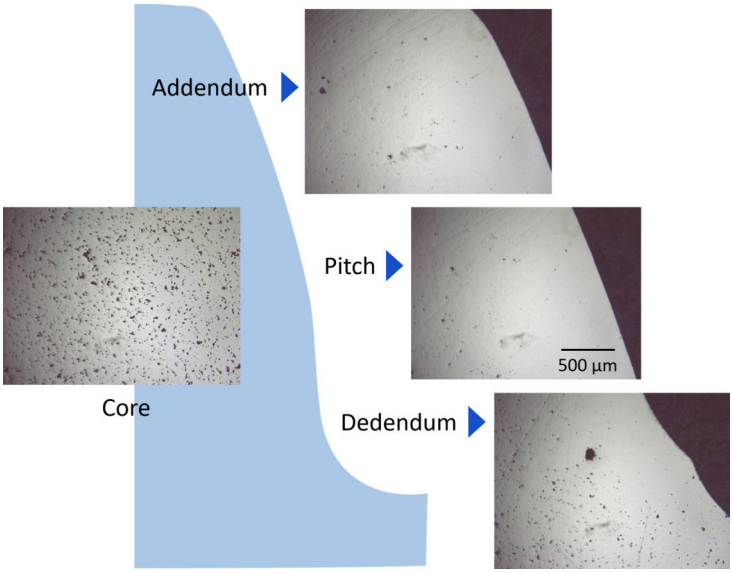

FIGURE 4.19 – Metallography showing the different surface densification depths along the involute. 50x magnification

The correlational surface integrity assessment also supports these RS results. The comparison of the bainitic microstructures of the sintering and surface densified specimens shows how the materials grains are deformed unequally along the involute, as can be seen in Figure 4.20. At the addendum, a preferable grain orientation points towards the tip of the tooth. At the dedendum, the orientation points towards the root. At the pitch region, the grains are compressed without being preferably oriented. The hardness mapping also presents a trend of variation along the involute, as show in Figure 4.21. The tendency is not exactly the same, the pitch region has lower hardness values in comparison with the extremities. Even so, it is another evidence that the flank surface is heterogeneous.

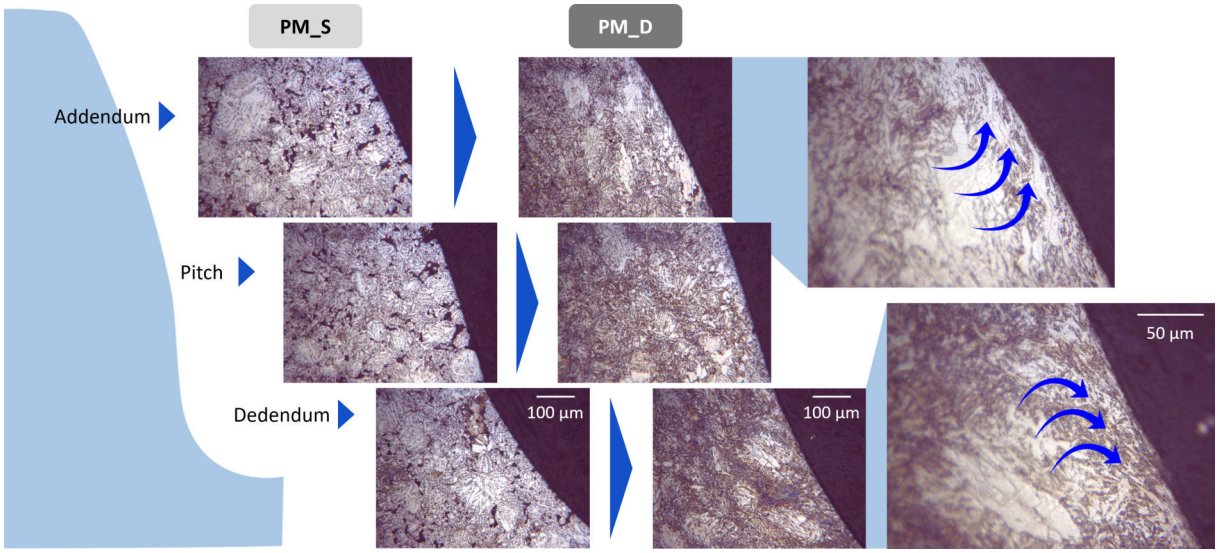

FIGURE 4.20 – Metallography showing the non-lamellar bainitic microstructure evolution from sintering to surface densification (200x magnification). In detail, the different grain orientation at the addendum and dedendum of the surface densified gear tooth (500x magnification)

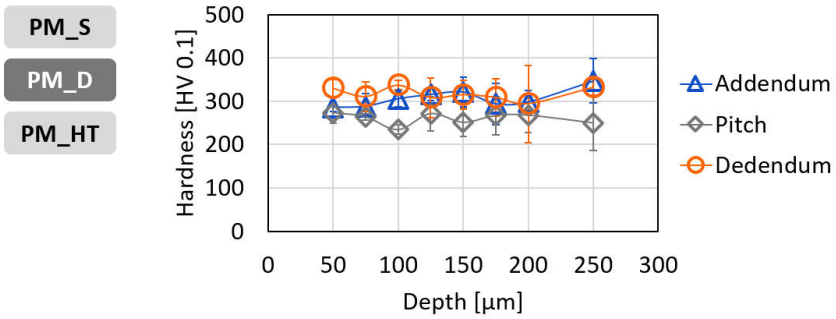

FIGURE 4.21 – Hardness mapping along the involute of the surface densified gear tooth

The topography investigations reinforce the previous findings. The SEM images shows that the surface topography is different from the dedendum to the addendum, as in Figure 4.22 a). At the dedendum, material overlaps can be seen pointing towards the root; at the pitch region, there is still some residual porosity; and at the addendum, overlaps point towards the tip. To quantify these topography differences, the surface roughness parameter *Sa* of the three regions was measured, and this analysis is shown in Figure 4.22 b). The results then indicate that the dedendum roughness is higher than that of the other regions.

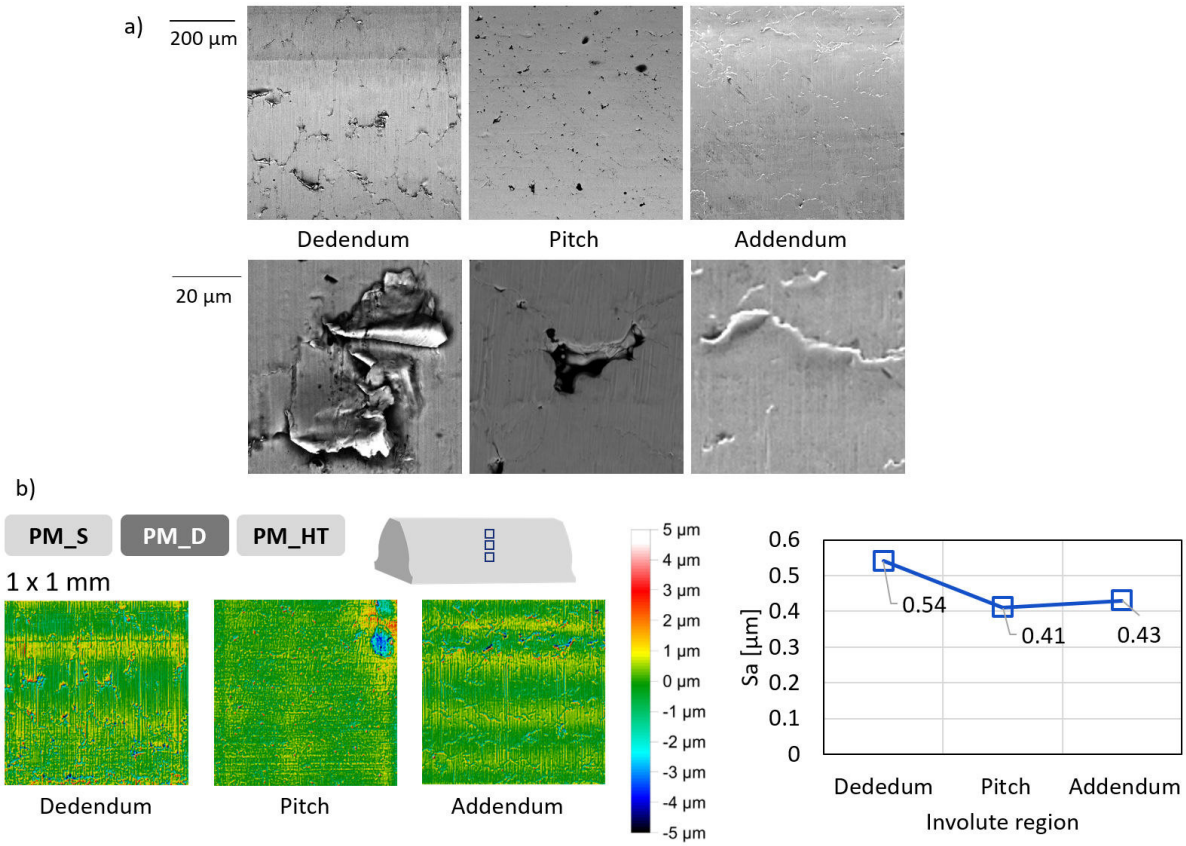

FIGURE 4.22 – Topography results of the surface densified gear tooth. a) SEM images. b) Profilometry images and roughness mapping

RS heterogeneity after heat treatment

The heat treatment induced an increase of compressive RS at the surface of the PM gear sample. In terms of heterogeneity along the lead, it was detected after sintering and was slightly evident after surface densification. After heat treatment, however, this heterogeneity became again pronounced, and at the same 3 mm spot of the prior steps. Figure 4.23 shows these results of RS mapping. These evidences, therefore, reinforce the argument that the previous steps have influence on the final RS state of gears.

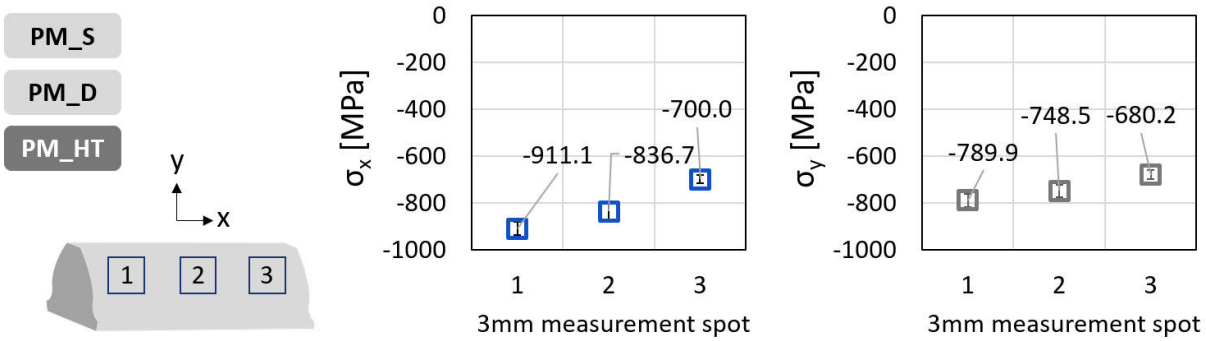

FIGURE 4.23 – Results of the residual stress mapping along the lead of the gear tooth after heat treatment

The line broadening analysis shows the same trend, as exposed in Figure 4.24. The diffractogram profiles became broader due to effects of crystallite size reduction and the microstrains range increase. The crystallite size decrease is compatible with the transformation of the microstructure to martensite, which is finer than the previous bainite. The heterogeneity of microstrains along the lead also became more evident. FWHM and ε are lower for the same spot that was different after sintering and after surface densification.

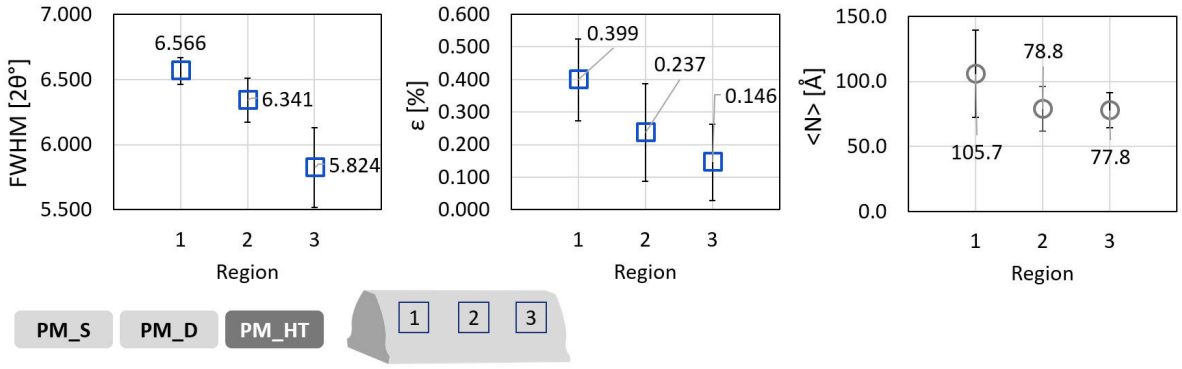

FIGURE 4.24 – Line broadening analysis along the lead of the gear tooth after heat treatment

Along the involute profile, the RS heterogeneity of the surface densification step is also propagated after heat treatment, as show in Figure 4.25. The RS σ_x at the dedendum is less compressive than at the other regions. Therefore, all the RS heterogeneities in macro and micro levels are carried out from the sintering to the heat treatment steps. These findings highlight the importance of analysing the evolution of the RS heterogeneities, instead of focusing on the last manufacturing steps, as already proposed by (REGO, 2016). The analysis of the evolution of RS along the chain not only explains the final RS state, but also allow the identification of the causes of heterogeneities. With this knowledge, therefore, the RS heterogeneity can be controlled through interventions on the appropriate manufacturing steps for reaching an optimized RS state.

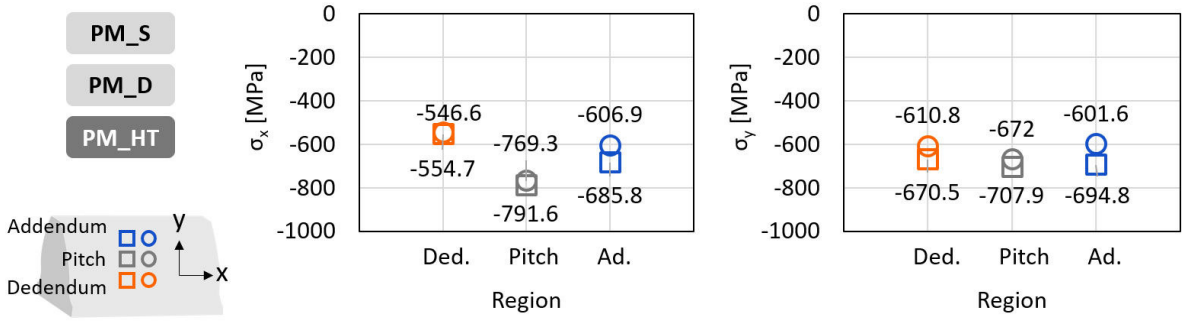

FIGURE 4.25 – Results of the residual stress mapping along the involute of the gear tooth after heat treatment

The metallography analysis shows that the preferential grain orientation induced by surface densification remains after heat treatment. In Figure 4.26, it can be observed that the bainitic structure that existed after sintering and surface densification evolves to a martensitic structure at the surface. Retained austenite can also be identified as white areas with a diffuse border to the martensite. Their appearance at the surface of carburized steels is due to the carbon effect of stabilizing this phase (HÖGANÄS, 2015). At the addendum and mainly at the dedendum, it can be seen that these austenite areas are oriented the same way the bainitic structure was in these areas before. Therefore, the surface microstructure is heterogeneous after heat treatment and, consequently, also the RS, as it was found in the experiments.

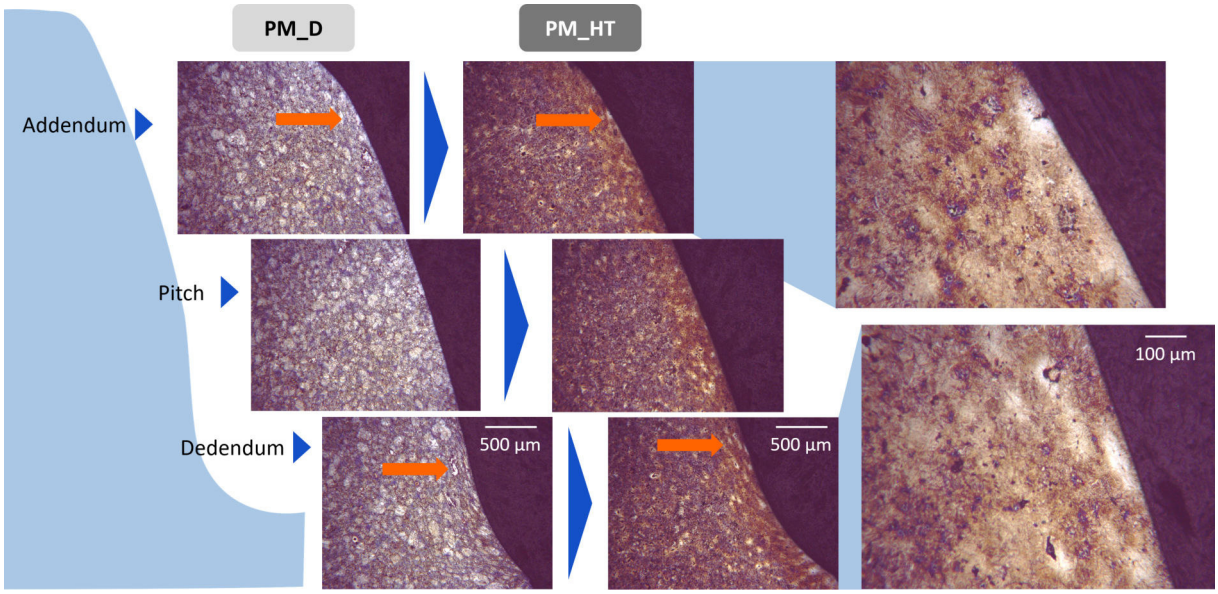

FIGURE 4.26 – Metallography showing the microstructure evolution from surface densification to heat treatment (50x magnification). Oriented grains are indicated by the arrows. In detail, the different orientation of the retained austenite at the addendum and dedendum of the heat treated gear tooth (200x magnification)

The hardness mapping along the involute showed no trend of distinction of the regions along the depth, as in Figure 4.27. The topography analysis, however, indicate an increase of the surface roughness along the entire involute in comparison to the previous step. A slight tendency of roughness increase from the dedendum to the addendum can be perceived, as exposed in Figure 4.28. Differently from the surface pattern of the densification step, which was characterized by marks in the involute direction, after heat treatment marks in all directions were additionally found. The marks in the involute direction in this last step can be attributed to the densification process. The marks in the other directions, however, may be a consequence of the heat treatment itself. Another hypothesis is that those random marks are a result of the compaction die surface pattern, which could have been polished, for example. The subsequent steps after compaction could have

hidden those marks, while the associated RS remained. After heat treatment, those RS may have been relaxed, causing the marks to be again evidenced. This last hypothesis is connected to the history of the material processing influencing the final product features.

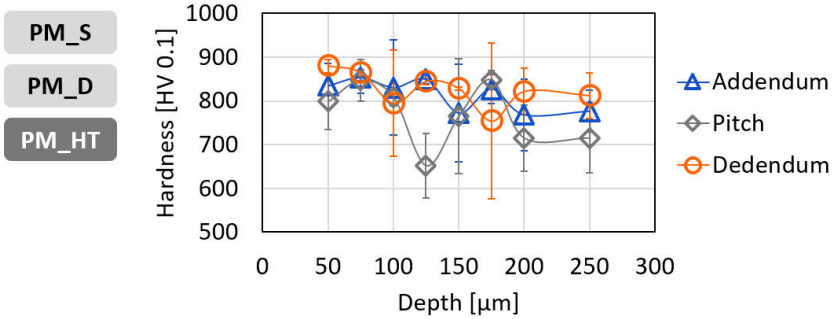

FIGURE 4.27 – Hardness mapping along the involute of the heat treated gear tooth

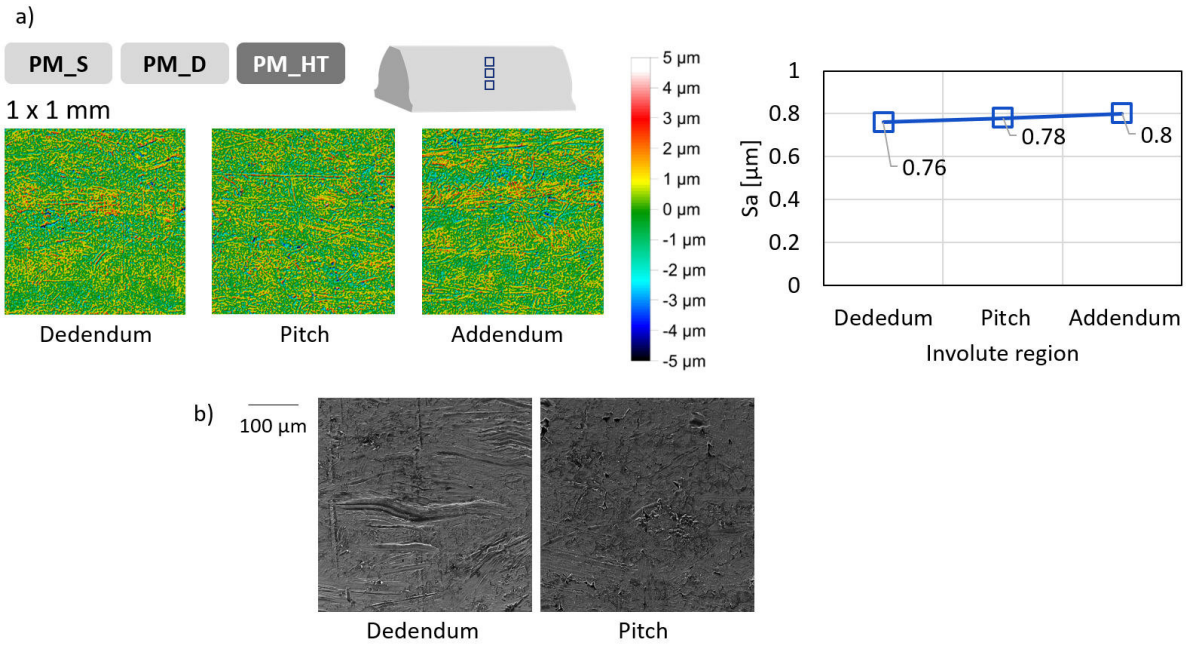

FIGURE 4.28 – Topography results of the heat treated gear tooth. a) Profilometry images and rougness mapping. b) SEM images showing randomly oriented marks

4.2.2 Manufacturing chains comparison

In this section, the PM and wrought steel manufacturing chains are compared. In order to know how significant is the effect of the PM chain on the RS heterogeneity of gears, it is necessary to have the conventional chain as reference. The comparison is then divided between the specimens correspondent to the steps before heat treatment and after heat treatment of each manufacturing chain, due to the similarity of microstructure. Figure 4.29 then shows the RS distribution along the lead profile of the sintered and

surface densified specimens of the PM chain and of the wrought steel cut specimen. It can be perceived that the cut specimen is associated to RS heterogeneity along the lead profile, more than the surface densified specimen and less than the sintered specimen. This finding in the wrought steel sample could be due to blank misalignment during cutting or preferential region of lubricant fluid application during machining. Therefore, the RS heterogeneity along the lead profile is not exclusive of PM gears, though the reasons are different.

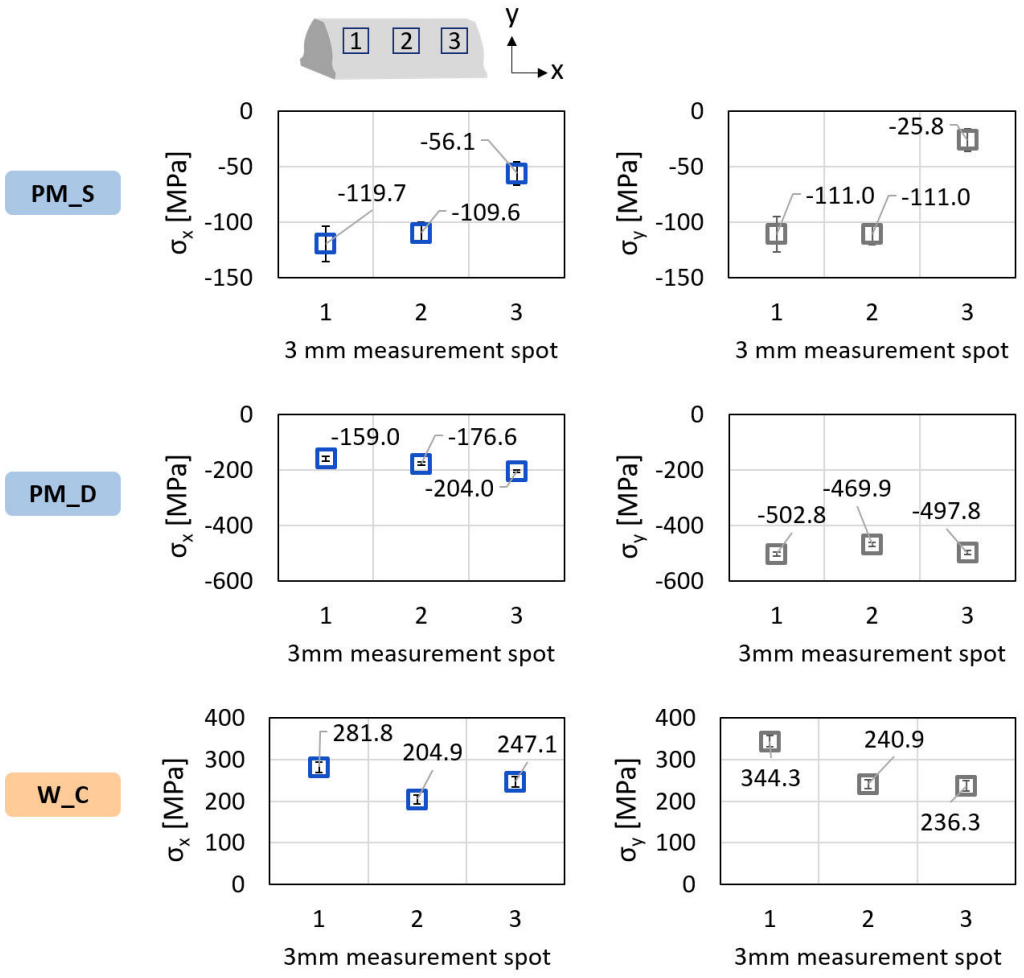

FIGURE 4.29 – Comparison of RS heterogeneity along the lead of PM and wrought steel specimens before heat treatment

The line broadening analysis results of Figure 4.30 also reveals heterogeneity in the microscale along the lead of the cut specimen. The regions can be differentiated in terms of FWHM. It is not clear, however, if the differentiation is due to microstrain or crystallite size contributions. Nevertheless, it indicates that the macro RS heterogeneity is associated to a microstructural heterogeneity also in the wrought steel chain.

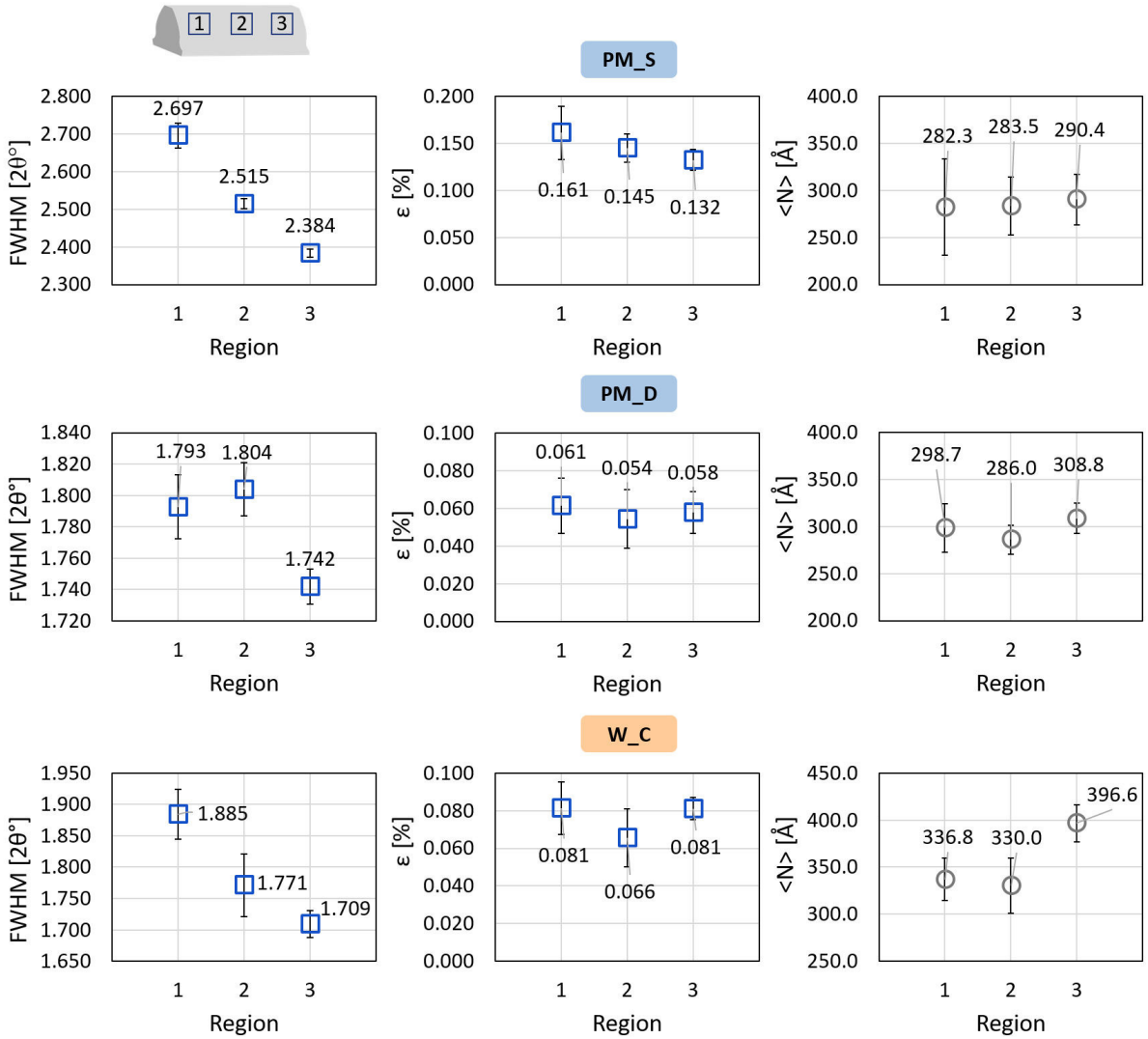

FIGURE 4.30 – Line broadening analysis results along the lead of PM and wrought steel specimens before heat treatment

The RS mapping results along the involute profile of the specimens before heat treatment are shown in Figure 4.31. RS heterogeneity along the involute can also be observed for the cut specimen. The RS are less intense at the pitch region in comparison to the dedendum and addendum, which may be a consequence of the loads and kinematics of the cutting process. The shear stresses differences along the involute are also more pronounced in the wrought steel chain. This result, therefore, shows that RS heterogeneity along the gears involute does not exist only in the PM chain, but in the conventional route as well. These heterogeneities, however, have different distributions.

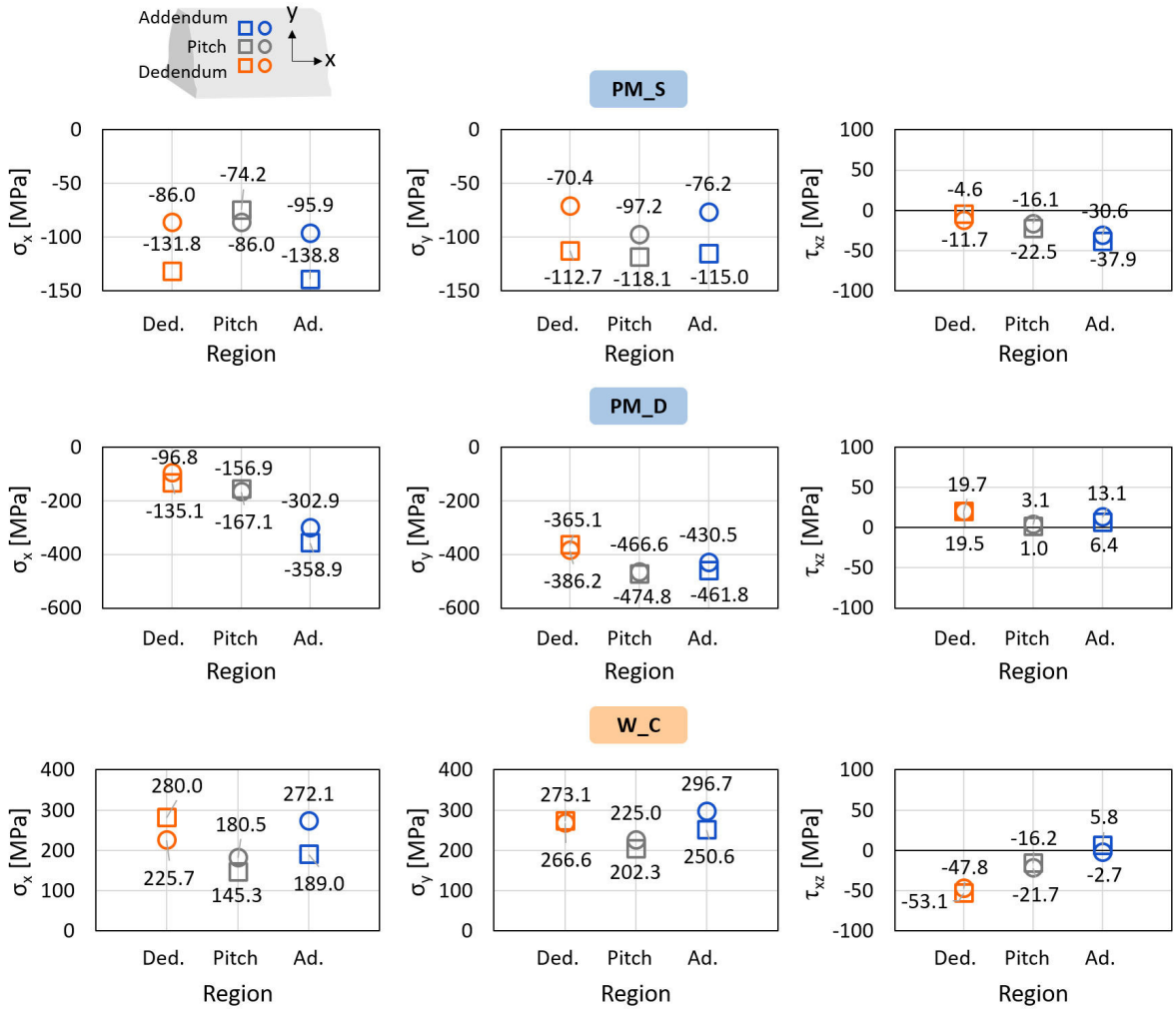

FIGURE 4.31 – Comparison of RS heterogeneity along the involute of PM and wrought steel specimens before heat treatment

The last steps of the manufacturing chains are in sequence compared. Figure 4.32 exposes the RS heterogeneity along the lead of the correspondent gear samples. The heat treated specimens of both manufacturing chains present a gradient of RS which was seen in the previous steps. Again, the previous RS states are influencing the final state. The lead gradient is, however, more pronounced in the PM chain, for both σ_x and σ_y. The shot peening and grinding results may not be suitable for direct comparison, but they can provide information of what could be expected if these finishing processes were applied to PM gears. The shot peening process increases the compressive RS, but seems to preserve the gradient found after heat treatment, the differences between the spots are similar for the heat treated and shot peened specimens. After grinding, however, the RS become more compressive, but the RS gradient at the surface is not anymore perceived. According to the study of Rego (2016) on the RS interaction between processes of gear manufacturing, however, the RS state in the depth profile after grinding in this case is not expected to be the same. As the previous RS states were different and submitted to

similar loads, the RS redistribution to reach the equilibrium is not expected to be the same. This motivates further studies on the RS heterogeneity in the depth profile to be performed, since the RS at the subsurface have a relevant role in the fatigue of gears (MITSUBAYASHI *et al.*, 1994).

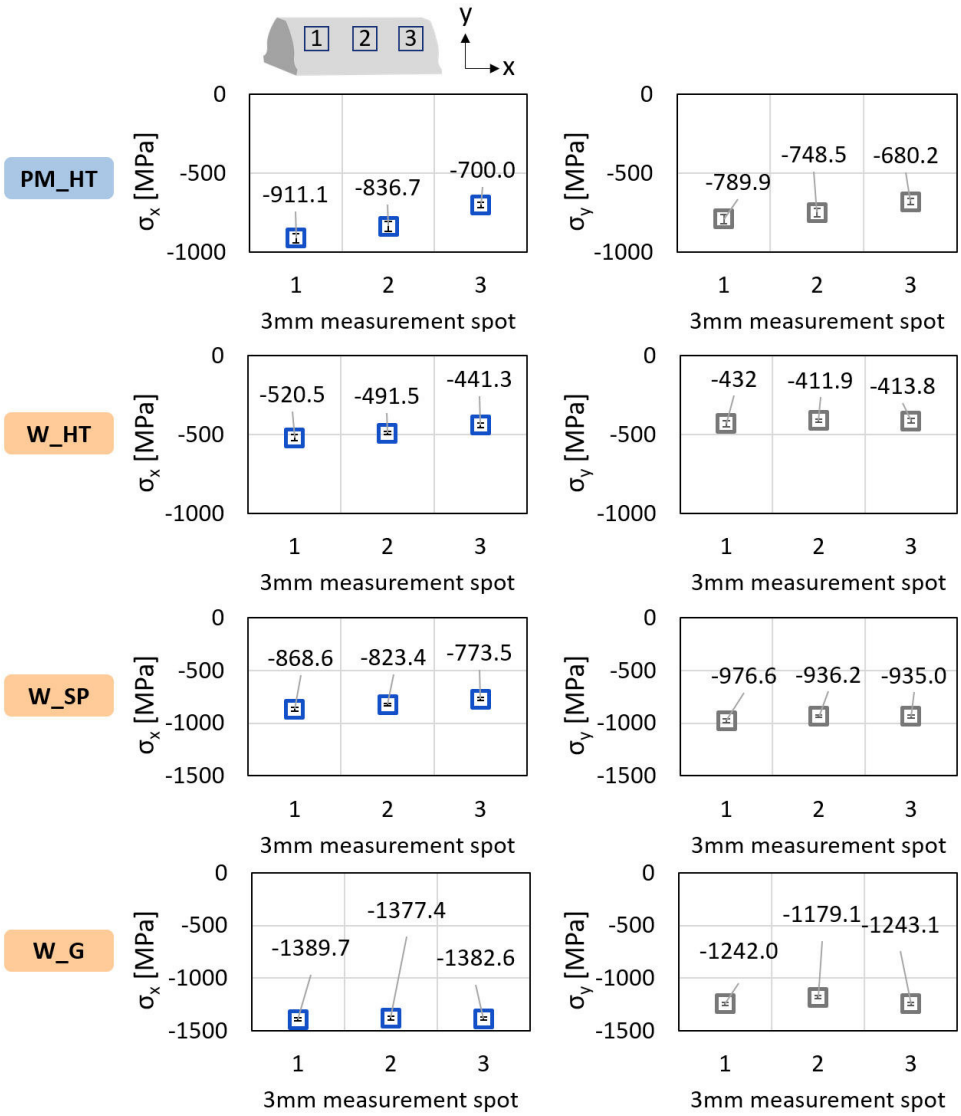

FIGURE 4.32 – Comparison of RS heterogeneity along the lead of PM and wrought steel specimens after heat treatment

Regarding the line broadening analysis along the lead, after heat treatment the propagation of the broadening could also be observed, and the differentiation is clearly in terms of micro RS, as shown in Figure 4.33. After shot peening and grinding, however, the broadening and micro RS are equalized. As mentioned in the last paragraph, different macro RS depth profiles are expected for the three spots after shot peening and grinding, and the same is expected for the micro RS. The variation of the broadening along the depth after shot peening has already been described in the literature (ZHAN *et al.*, 2012). As the previous analysis showed that the macro RS heterogeneity is associated to micro

RS heterogeneity, different macro RS depth profiles are expected to be associated with different micro RS profiles.

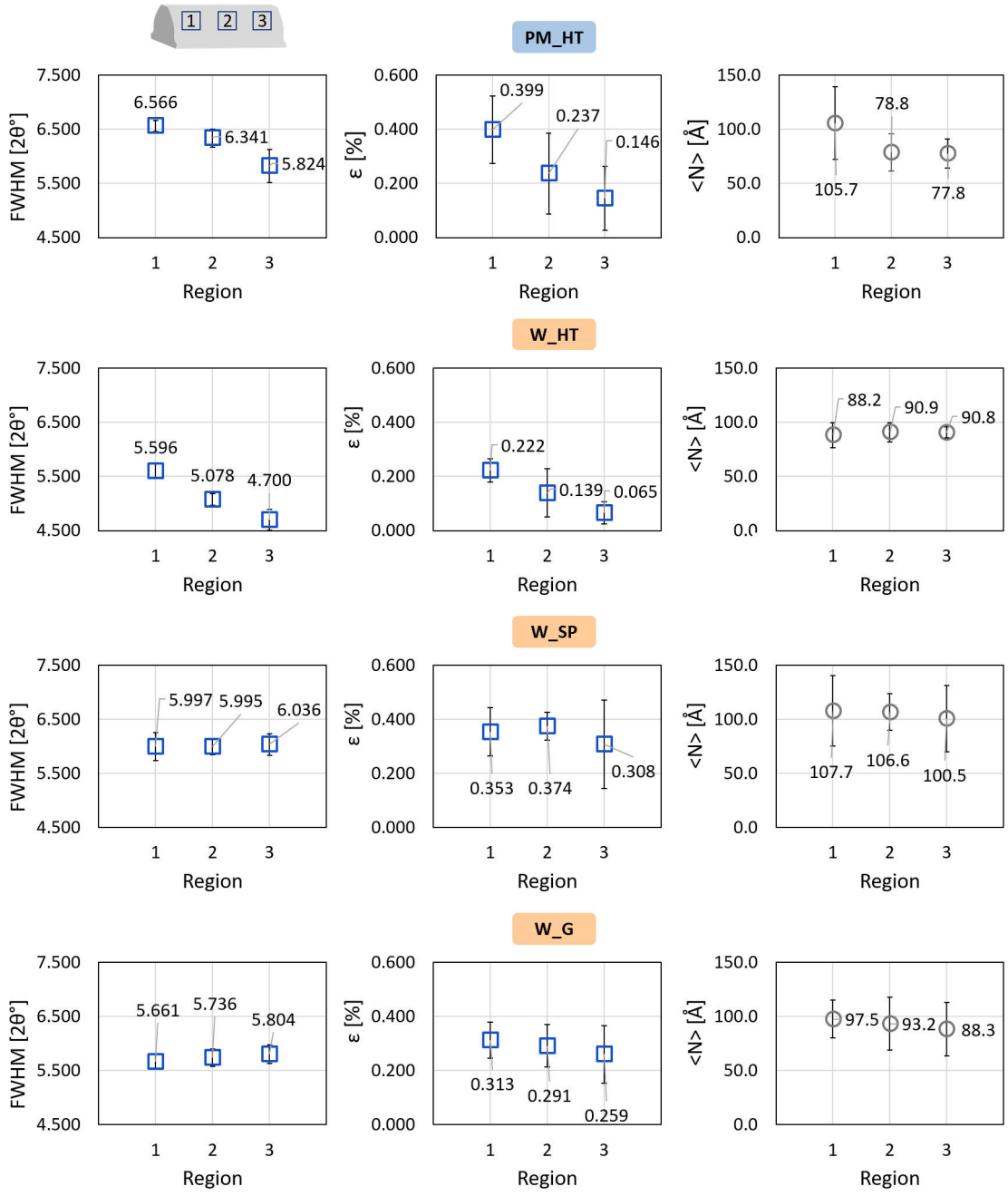

FIGURE 4.33 – Line broadening analysis results along the lead of PM and wrought steel specimens after heat treatment

The RS heterogeneity along the involute profile of the specimens after heat treatment is shown in Figure 4.34. It can be noticed that this heterogeneity exits for heat treated specimens of both manufacturing chains. However, in the PM chain, the more compressive normal RS were found at the pitch region. In the wrought steel case, however, the normal RS tend to be more compressive from the dedendum to the addendum. The differentiation

of normal stresses in the wrought steel chain can also be seen according to the measurement columns. This may be due to the peaks and valleys generated by cutting, which may be associated to different RS intensities that were propagated after heat treatment. The shot peening step, in turn, induced a similar effect observed along the lead, it increased the compressive normal RS intensities but did not change considerably the differences between the regions. Furthermore, the grinding step eliminated the differences in normal RS at the surface again. For both manufacturing chains, differentiation of shear RS along the involute also occur. The shear RS increase from the dedendum to the addendum and the difference become more pronounced with the advance of the process steps.

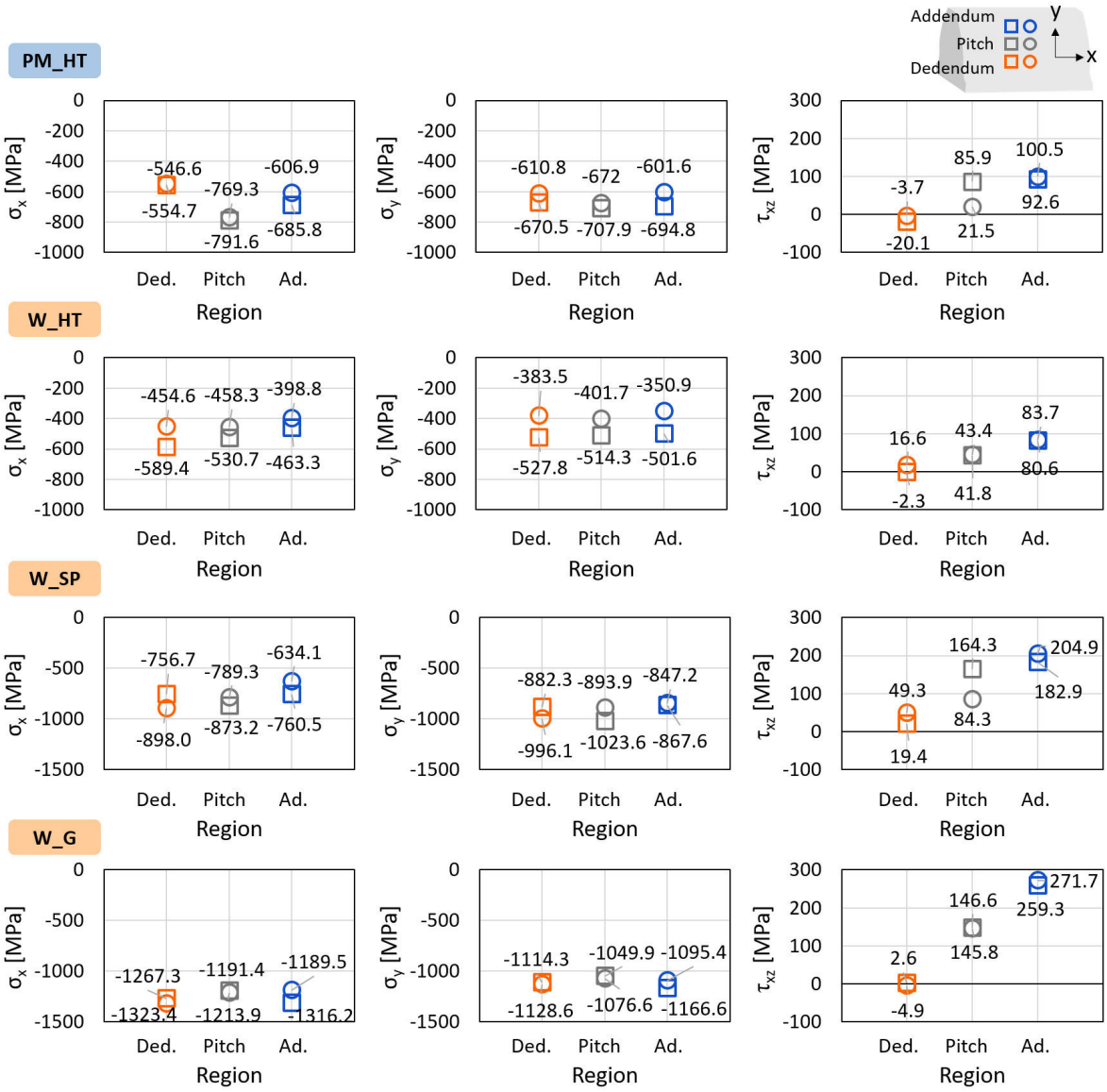

FIGURE 4.34 – Comparison of RS heterogeneity along the involute of PM and wrought steel specimens after heat treatment

In the next subsection, all the findings on the evolution of RS heterogeneities described are summarized, and the second research question is then answered.

4.2.3 Summary

From the previous results and analyses, RS heterogeneity was identified since the beginning of the PM manufacturing chain. A RS gradient along the lead profile was found and attributed to the compaction process. Other RS heterogeneities distributions in macro and micro levels could also be observed along the chain. After sintering, diffuse RS heterogeneity was connected to non-uniform porosity distribution. In the next step, surface densification, a defined RS gradient along the involute profile was observed and connected to the process kinematics. After heat treatment, it was found that the previous RS heterogeneities were propagated. Furthermore, the macro RS heterogeneity was always associated to heterogeneity of micro RS. Figure 4.35 summarizes these effects on the RS heterogeneity along the PM chain.

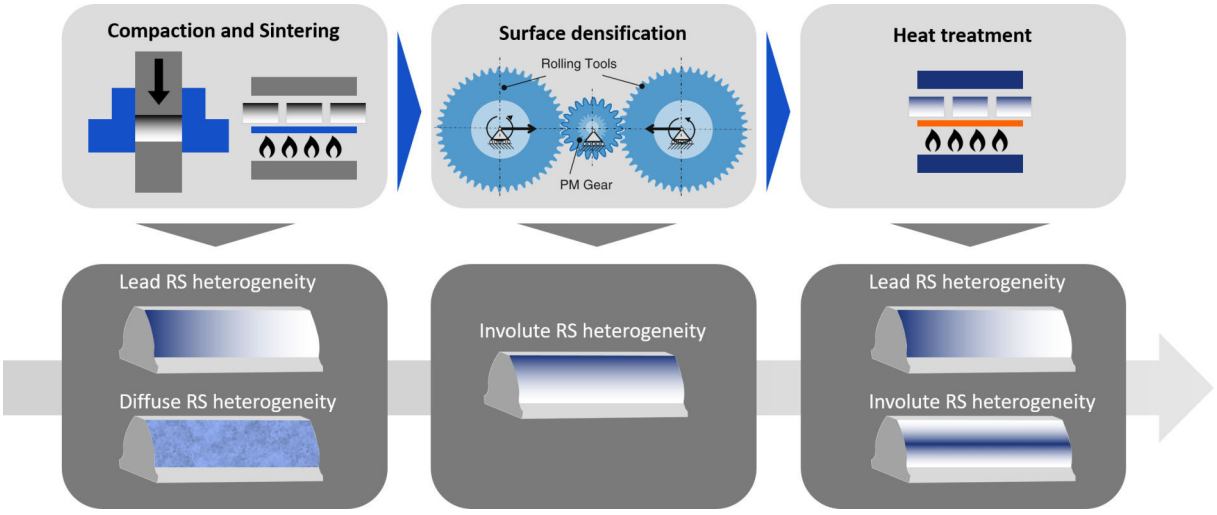

FIGURE 4.35 – Evolution of the RS heterogeneity along the PM manufacturing chain

The comparison with the wrought steel chain showed that the RS stress heterogeneity along the surface is not exclusive of the PM chain. All the RS heterogeneity levels and distributions were also identified in the conventional route and propagated after heat treatment, but were more pronounced in the PM specimens. The grinding step, however, equalized the macro and micro RS stresses of all forms of distributions at the surface. Analogously, the same effect would be expected if grinding were applied to the PM chain. Nevertheless, due to the influence of the previous RS state on the final state, RS heterogeneity is expected to be found in the depth profiles after grinding. This information about the subsurface is of relevance for fatigue behavior and, therefore, is a motivation for the continuation of the research.

Therefore, the answer to the second research question on the significance of the effect of the PM chain on the RS heterogeneity of gears was given. Each PM manufacturing step induces a characteristic RS heterogeneity distribution manifested in both macro and micro

RS levels, which propagates even after heat treatment. The heterogeneities associated to the PM chain studied were more pronounced than those of the wrought steel chain investigated and had different distribution patterns. Figure 4.36 illustrates the combination of the RS stress gradients found in the PM chain, highlighting the regions that tend to have lower RS and may, as consequence, be more susceptible to fatigue effects. This last conclusion however, depends on the information of the RS heterogeneity in the subsurface as well. Besides the residual stresses, the applied stresses also determine the fatigue behavior. The applied stresses on gears, in turn, are higher at the dedendum region, due to the fact that the surface is rolled in one direction and pushed in another (KRAMER, 2012; MAZZO, 2013). Figure 4.37 then shows the region that tends to be critical for the PM gears investigated.

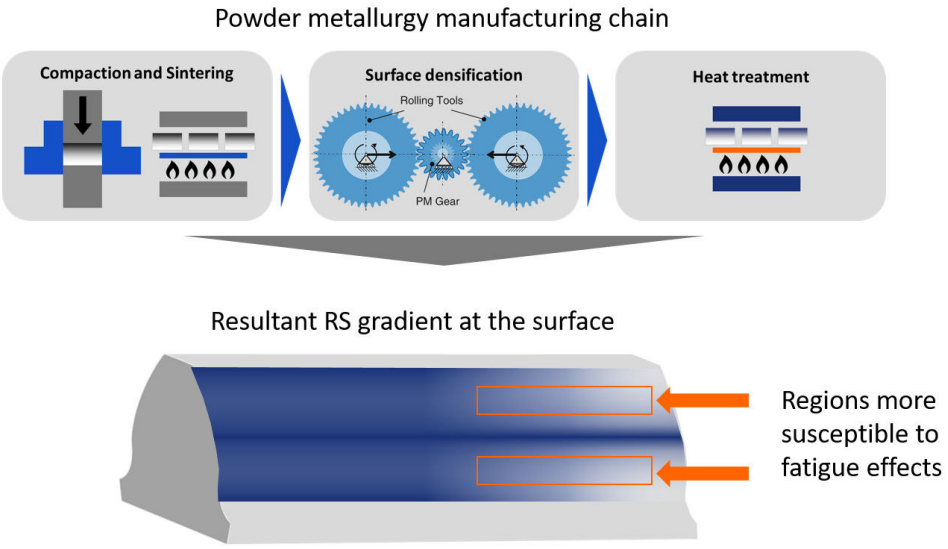

FIGURE 4.36 – Resultant residual stress gradient at the surface of the gear tooth flank of the powder metallurgy manufacturing chain

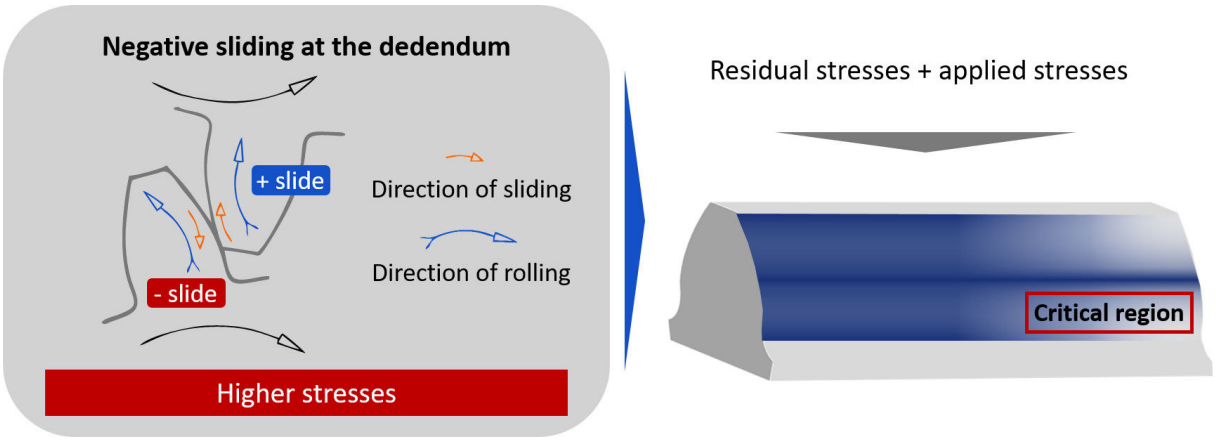

FIGURE 4.37 – Resultant residual stress gradient at the surface of the gear tooth flank of the powder metallurgy manufacturing chain

Regarding the occurrence of weaker regions on the flank of PM gears, there are two alternative solutions for this problem. The first alternative is to change the process steps parameters and conditions in order to decrease the RS heterogeneity effects. The second alternative would be to perform microgeometry corrections on the gear flank to have a suitable contact pattern between the gears, with the higher loads applied to the regions with higher compressive RS. Another aspect to be considered is that the fatigue behavior of PM gears may be more sensitive to misalignments. If the gears contact pattern causes higher loads on critical regions due to misalignments, premature failure can occur. Therefore, PM gears may also require special attention during assembly.

5 Conclusions and outlook

The powder metallurgy implementation on automotive transmission gears can be associated to economical, ecological and performance benefits. The heterogeneous microstructure of gears manufactured by powder metallurgy, however, is connected to a heterogeneous state of residual stresses on the surface of these components. Due to the relevance of such stresses to the fatigue behavior, the assessment of their heterogeneity is of fundamental importance for the PM gears lifetime optimization. The conventional methods of RS evaluation applied by the industry, however, do not consider variations that may occur at the surface. Therefore, the present study focused on answering two research questions concerning RS heterogeneity on PM gears. The first question is related to which method is more appropriate for this heterogeneity assessment. The second one is on the significance of the effect of the PM chain on the evolution of RS heterogeneity of gears.

Through RS mapping and X-ray diffraction line broadening analysis methods applied to gear teeth of PM and wrought steel, the answers to these questions were given. It could be identified that the RS heterogeneity of gears is manifested according to RS levels (macro and micro RS) and distribution (along the lead, along the involute and diffuse). When analyzing the RS heterogeneity correspondent to the process steps, it could then be observed association between macro RS and micro RS heterogeneities. However, when comparing different process steps and manufacturing chains, in which microstructural differences exist, the macro RS heterogeneity cannot be directly predicted by microstrains information.

The most suitable method for gears RS heterogeneity assessment, therefore, depends if a single process step is being considered or if the analysis is based on the comparison between manufacturing steps or chains. When analyzing the RS heterogeneity after a single process step, the most suitable assessment method was found to be the line broadening analysis, because it is simpler and provides information of microstrains, which can be used to predict the macro RS heterogeneity. When comparing process steps and manufacturing chains, however, both methods must be applied for a complete understanding of the macro and micro RS states. The first research question of this study was, therefore, answered, and the correspondent conclusions gave basis to the methods application to answer the next question.

Each of the PM chain steps was found to be associated to a characteristic RS heterogeneity. The compaction and the surface densification steps of this chain induce RS gradients along the gears flank surface that are clearly defined. Furthermore, after the heat treatment step, the influences of these RS gradients could still be perceived. Hence, it can be concluded that the PM chain has significant effects on the evolution of RS heterogeneity of gears, more pronounced and defined than in the reference wrought steel chain. The answer to the second research question was then given. The evolution could also be characterized, because the final RS state was found to be a consequence of the previous states. These findings allow then the identification of the regions more susceptible to fatigue effects in PM gears. The reasons for these probable weaker regions could be understood, which is even more important, and appropriate interventions on the PM manufacturing chain can be applied if necessary.

Although in the wrought steel chain the RS heterogeneity on the surface vanished after grinding, the previous steps influences cannot be directly neglected. The residual stress state relevant to the fatigue behavior is situated along the depth, where failures may initiate and propagate in form of cracks. Therefore, the continuation of this study involves the investigation of the RS heterogeneity evolution in the surface depth of PM gears. All these analyses are directed to a broader fatigue comprehension. Hence, another step in this line of research is to evaluate the influence of the RS heterogeneity state of PM gears on the fatigue behavior of such components. This can be done by inducing different RS heterogeneities through the variation of process parameters and submitting the gears to fatigue tests. This will allow the correlation between manufacturing parameters, surface integrity and fatigue performance, contributing to make the application of the concept of "Design for residual stresses" possible for PM gears.

In the present thesis, therefore, it was demonstrated that the RS heterogeneity of PM gears can be assessed through X-ray diffraction methods, which was the hypothesis to be proved. Through the answer to the research questions, the objective of this dissertation on the comprehension of the RS heterogeneity of PM gears could then be achieved. PM gears for automotive transmissions exist for more than a decade, and among the reasons for their non-implementation in mass production is the lack of scientific knowledge for the improvement of their lifetime, which this study contributed to diminish. This Master Thesis, hence, is a small step on making PM gears for automotive transmissions feasible. The consequences of the knowledge here generated, finally, can benefit not only the powder metallurgy and automotive industries, but also the society in general.

Bibliography

AGMA. **ANSI/AGMA 1012-G05**: Gear nomenclature, definition of terms with symbols. Alexandria, USA: American Gears Manufacturers Association, 2011.

ALBAN, L. E. Failure of gears. In: **ASM Handbook Volume 11: Failure analysis and prevention**. Materials Park: ASM International, 2002. v. 11, p. 2558–2603.

ALEXANDRU, I.; BULANCEA, V. Effect of cryogenic cooling of residual stresses, structure and substructure. In: TOTTEN, G.; HOWES, M.; INOUE, T. (Ed.). **Handbook of residual stress and steel deformation**. Materials Park: ASM, 2002.

ANDERSON, G. L.; IMBROGNO, P. G. Improved power density through use of powder-forged helical gears in transmissions. **SAE Technical Papers**, 2014.

ASHBY, M.; SHERCLIFF, H.; CEBON, D. **Materials: engineering, science, processing and design**. Jordan Hill: Butterworth Heinemann, 2007.

ASTAKHOV, V. Surface integrity - definition and importance in functional performance. In: DAVIM, J. P. (Ed.). **Surface integrity in machining**. London: Springer, 2010. p. 1–35.

ASTM E2860-12. **Standard method for residual stress measurement by X-ray diffraction for bearing steels**. West Conshohocken, US: American Society for Testing and Materials, 2012.

BALZAR, D. X-ray diffraction line broadening: modeling and applications to high-Tc superconductors. **Journal of research of the National Institute of Standards and Technology**, v. 98, n. 3, p. 321–353, 1993.

BALZAR, D. Voigt function model in diffraction line broadening analysis. In: SNYDER, R. L.; BUNGE, H. J.; FIALA, J. (Ed.). **Microstructure analysis from diffraction**. [S.l.]: International Union of Crystallography, 1999.

BARBOSA, V. C.; BREITSCHAFT, A. M. S.; MENDONÇA, J. P. R. F.; MOREIRA, L. M.; MORAES, P. C. G. Uma visualização do princípio de huygens-fresnel na obtenção de um padrão de difração. **Revista Brasileira de Ensino de Física**, v. 34, n. 3, p. 3301, 2012.

BEHNKEN, H. Some basic relations to the stress analysis using diffraction methods. In: HAUK, V. (Ed.). **Structural and residual stress analysis by nondestructive methods**. Amsterdam: Elsevier, 1997. p. 39–65.

BELSAK, A.; FLASKER, J. Method for detecting fatigue crack in gears. **Theoretical and Applied Fracture Mechanics**, v. 46, p. 105–113, 2006.

BERKUM, J. G. M.; SPRONG, G. J. M.; KEIJSER, T. H.; DELHEZ, R.; SONNEVELD, E. J. The optimum standard specimen for X-ray diffraction line-profile analysis. **Powder diffraction**, v. 10, p. 129–139, 1995.

BOLJANOVIC, V. **Metal shaping processes**: Casting and molding; particulate processing; deformation processes; and metal removal. New York: Industrial press, Inc., 2010.

BONETTI, G.; NAVAZIO, A.; ZINGALE, P. Gears for demanding applications: a comparison between cast iron, wrought steels and PM steels. **SAE Technical Papers**, 2000.

BOUCHARD, P. J.; WHITERS, P. J. Identification of residual stress length scales in welds for fracture assessment. In: YOUTSOS, A. G. (Ed.). **Residual stress and its effect on fatigue and fracture**. Dordrecht: Springer, 2006.

CAGLIOTI, G.; PAOLETTI, A.; RICCI, F. P. Choice of collimators for a crystal spectrometer for neutron diffraction. **Nuclear instruments**, v. 3, p. 223–228, 1958.

CALLISTER, W. D.; RETHWISCH, D. G. **Fundamentals of materials science and engineering**: An integrated approach. 4th. ed. USA: John Wiley e Sons, Inc., 2007.

CAMPBELL, F. C. **Metals fabrication**: Understanding the basics. Materials Park: ASM International, 2013.

CAPUS, J. M. Surface densified PM gears: new hope in new transmissions. **Metal Powder Report**, v. 61, p. 18, 20–21, 2006.

CAPUS, J. M. PM gears: RWTH Aachen points a way forward. **Metal Powder Report**, v. 63, p. 12–15, 2008.

CHIAVERINI, V. **Metalurgia do pó**. 4th. ed. São Paulo: ABM, 2001.

COCKROFT, J. K.; BARNES, P. **Powder Diffraction on the WEB**: School of Crystallography, Birkbeck College, University of London. 2001. Retrieved from: <http://pd.chem.ucl.ac.uk/pd/welcome.htm>. Date accessed: May 15, 2017.

CULLITY, B. D.; STOCK, S. R. **Elements of X-ray diffraction**. 3rd. ed. Harlow: Pearson, 2014.

DAVIS, J. R. **Surface hardening of steels**: Understanding the basics. Materials Park: ASM International, 2002.

DAVIS, J. R. **Gear materials, properties and manufacture**. Materials Park: ASM International, 2005.

DELHEZ, R.; KEIJSER, T. H.; MITTEMEJER, E. J. Determination of crystallite size and lattice distortions through X-ray diffraction line profile analysis. **Fresenius Zeitschrift für Analytische Chemie**, v. 312, p. 1–16, 1982.

DELHEZ, R.; KEIJSER, T. H.; MITTEMEJER, E. J. Role of X-ray diffraction analysis in surface engineering: investigation of microstructure of nitrided iron and steels. **Surface Engineering**, v. 3, n. 4, p. 331–342, 1987.

DIN. **DIN EN ISO 6507-1**: Metallic materials - Vickers hardness test - Part i: Test method. Berlin: Deutsches Institut für Normung, 2006.

DING, Y.; RIEGER, N. F. Spalling formation mechanism for gears. **Wear**, v. 254, p. 1307–1190, 2003.

EMPYREAN REFERENCE MANUAL. **Panalytical Empyrean X-ray Diffraction System**. 2010.

ENGSTRÖM, U.; MILLIGAN, D. Opportunities to replace wrought steel gears with high performance PM gears in automotive applications. **SAE Technical Papers**, 2006.

FIELD, M.; KAHLES, J. F. The surface integrity of machined and ground high strength steels. **DMIC Report 210**, p. 54–77, 1964.

FITZPATRICK, M. E.; FRY, A. T.; HOLDWAY, P.; KANDIL, F. A.; SCHAKLETON, J.; SUOMINEM, L. **A national measurement good practice guide**: determination of residual stresses by X-ray diffraction. United Kingdon: ASM International, 2005.

FLODIN, A. Powder metal gear technology: a review of the state of the art. **Power transmission engineering**, p. 38–43, 2016.

GENZEL, C. Line broadening by non-oriented residual micro RS. In: HAUK, V. (Ed.). **Structural and residual stress analysis by nondestructive methods**. Amsterdam: Elsevier, 1997. p. 435–460.

GRÄSER, E. Materialfluss beim Dichtwalzen. In: 55. ARBEITSTAGUNG "ZAHNRAD- UND GETRIEBEUNTERSUCHUNGEN" DES WZL, 2013. Aachen, Germany: WZL, 2013.

GRIFFITHS, B. **Manufacturing surface technology**: Surface integrity and functional performance. London: Penton Press, 2001.

GUMMESON, P. U. High pressure water atomization. In: BURKE, J. J.; WEISS, V. (Ed.). **Powder metallurgy for high performance application**. Syracuse: Syracuse University Press, 1972.

GUPTA, R. K.; ANANTHARAMAN, T. R. An X-ray diffraction study of deformation in HCP rare-earth metals. **Journal of the less common metals**, p. 353–360, 1971.

HAUK, V. **Structural and residual stress analysis by nondestructive methods**. Amsterdam: Elsevier, 1997.

HAUK, V.; NIKOLIN, H. J. The evaluation of the distribution of residual stresses of the I. kind (RS I) and of the II kind (RS II) in textured materials. **Textures and microstructures**, v. 8-9, p. 693–716, 1988.

HEYN, E. Internal strains in cold wrought metals and some troubles caused thereby. **The Journal of the Institute of Metals**, v. 12, p. 3–37, 1914.

HÖGANÄS. **Metallography**: Höganäs handbook for sintered components. 2015.

ICHIKAWA, R. U. **Aplicações do método de Warren-Averbach de análise de perfis de difração**. Dissertação de Mestrado — IPEN - Universidade de São Paulo, São Paulo, 2013.

IERVOLINO, F.; BULLA, L. Compactação. In: **A metalurgia do pó: alternativa econômica com menor impacto ambiental**. São Paulo: Grupo Setorial de Metalurgia do Pó, 2009.

INOUE, T. Metallo-thermo-mechanical coupling in quenching. In: HASHMI, S. (Ed.). **Comprehensive Materials Processing**. [S.l.]: Elsevier, 2014.

JAMES, W. B.; NARASIMHAN, K. S. Warm compaction and warm-die compaction of ferrous PM materials. **Höganäs Corporation**, 2013.

JENKINS, R.; SNYDER, R. **Introduction to X-ray powder diffractometry**. United States: Wyley, 1996.

JONES, F. W. The measurement of particle size by the X-ray method. **Royal Society (London)**, A166, 1938.

KAUFFMANN, P. **Walzen pulvermetallurgisch hergestellter Zahnräder**. Doctoral Thesis — RWTH Aachen, Aachen, 2012.

KAUFFMANN, P. Pulvermetallurgie: Potential für die Getriebeproduktion. In: GETPRO KONGRESS. Würzburg, 2015.

KHODAEE, A.; SUNDARAM, M. C.; ANDERSSON, M.; MELANDER, A.; STRONDL, A.; HEIKKILÄ, I.; MIEDZINSKI, A.; NYBORG, L.; AHLFORS, M. Innovative powder based manufacturing of high performance gears. In: WORLDPM, EUROPEAN POWDER METALLURGY ASSOCIATION - EMPA, 2016. Hamburg, 2016.

KLOCKE, F.; BRECHER, E.; BRUMM, M. **Zahnrad- und Getriebetechnik**. Aachen: Apprimus Verlag, 2014.

KLOCKE, F.; BRINKSMEIER, E.; WEINERT, K. Capability profile of hard cutting and grinding processes. In: CIRP ANNALS - MANUFACTURING TECHNOLOGY V. 54, 2005. [S.l.]: Elsevier, 2005.

KLOCKE, F.; GOMES, J.; LÖPENHAUS, C.; REGO, R. R. Assessing the heterogeneity of residual stress for complementing the fatigue performance comprehension. **Journal of Strain Analysis**, v. 51, n. 5, p. 347–357, 2016.

KLOCKE, F.; GORGELS, C.; GRÄSER, E.; KAUFFMANN, P. PM gear testing. In: PM WORLD CONGRESS, 2010. [S.l.], 2010.

KLOCKE, F.; GORGELS, C.; KAUFFMANN, P.; GRÄSER, E. Influencing densification of PM gears. In: SCHUH, G.; NEUGEBAUER, R.; UHLMANN, E. (Ed.). **Future trends in production engineering. Procedings of the first conference of the German Academic Society for Production Engineering (WGP), Berlin, Germany, 8th-9th June 2011**. Berlin: Springer, 2013.

KLOCKE, F.; SCHÖDER, T.; KAUFFMANN, P. Fundamental study of surface densification of PM gears by rolling using FE analysis. **Production Engineering**, v. 1, n. 2, p. 113–120, 2007.

KRAMER, P. **An investigation of rolling-sliding contact fatigue damage of carburized gear steels**. Master Thesis — Colorado School of Mines, Golden, 2012.

LANGFORD, J. I. A rapid method for analysing the breadths of diffraction and spectral lines using the Voigt function. **J. Appl. Cryst.**, v. 11, p. 10–14, 1978.

LANGFORD, J. I.; CERNIK, R. J.; LOUËR, D. The breadth and shape of instrumental line profiles in high-resolution powder diffraction. **J. Appl. Cryst.**, v. 24, p. 913–919, 1991.

LANGFORD, J. I.; DELHEZ, R.; KEIJSER, T. H.; MITTEMEJER, E. J. Profile analysis for microcrystalline properties by the Fourier and other methods. **Aust. J. Phys.**, v. 41, p. 173–187, 1988.

LAWCOCK, R.; BUCKLEY-GOLDER, K.; SARAFINCHAN, D. Testing of high endurance PM steels for automotive transmission gearing components. **SAE Technical Papers**, 1999.

LECHNER, G.; NAUNHEIMER, H. **Automotive Transmissions**: Fundamentals, selection, design and application. New York: Springer, 1999.

LÖHE, D.; LANG, K.; VÖHRINGER, O. Residual stresses and fatigue behavior. In: TOTTEN, G.; HOWES, M.; INOUE, T. (Ed.). **Handbook of residual stress and steel deformation**. Materials Park: ASM, 2002.

LÖPENHAUS, C. Trends in gear manufacturing. In: WZL GEAR CONFERENCE IN THE USA, 6th., 2016. [S.l.], 2016.

MAITRA, G. M. **Handbook of gear design**. 2nd. ed. New Delhi: Tata McGraw-Hill, 1994.

MAZZO, N. **Engrenagens cilíndricas: da concepção à fabricação**. São Paulo: Blucher, 2013.

MCGUINN, J. The global gear industry: insights, projections, facts and figures. **Gear technology**, 2011.

Metal Powder Industries Federation. **PM Industry Roadmap**: Technology update for the powder metallurgy industry. 2012.

MITSUBAYASHI, M.; MIYATA, T.; AIHARA, H. Phenomenal analysis of shot peening: analysis of fatigue strength by fracture mechanics for shot peened steel. **JSAE Technical Papers**, v. 15, p. 67–71, 1994.

NARASIMHAN, K. S.; BORECZKY, E. New transmission technologies on gear requirements for global powder metal industry. **SAE Technical Papers**, 2006.

NEUGEBAUER, R.; KLUG, D.; HELLFRITZSCH, U. Description of the interactions during gear rolling as a basis for a method for the prognosis of the attainable quality parameters. **Production Engineering**, v. 1, 2007.

NIGARURA, S.; PARAMESWARAN, R.; SCOTT, M.; DENNERT, C. A comparison of wrought steel gears and surface-densified powder metallurgy gears. **Gear solutions**, 2015.

NIGARURA, S.; PARAMESWARAN, R.; SCOTT, M.; DENNERT, C. Wrought steel gears and surface densified powder metallurgy gears - a comparison. **PMG Sinter**, 2015.

NOYAN, I. C.; COHEN, J. B. **Residual stress**: Measurement by diffraction and interpretation. New York: Springer, 1987.

ORLANDIN, J.; CARVALHO, M.; MAZZA, P.; PEGORER, R. Pós metálicos. In: **A metalurgia do pó: alternativa econômica com menor impacto ambiental**. São Paulo: Grupo Setorial de Metalurgia do Pó, 2009.

RACHINGER, W. A. A correction for the $\alpha_1\alpha_2$ doublet in the measurement of widths of X-ray diffraction lines. **J. Sci. Instrum.**, 1948.

RADZEVICH, S. P. **Dudley's handbook of practical gear design**. 2nd. ed. New Delhi: CRC Press, 2004.

RAKHIT, A. K. **Heat treatment for gears**: A practical guide for engineers. Materials Park: ASM International, 2000.

RAMAKRISHNAN, P. Residual stresses in powder-metal processing. In: TOTTEN, G.; HOWES, M.; INOUE, T. (Ed.). **Handbook of residual stress and steel deformation**. Materials Park: ASM, 2002.

RAU, G.; SIGL, L. S.; KREHL, M. Highly loaded PM gears produced by selective surface densification. **SAE Technical Papers**, 2003.

REGO, R. R. **Residual stress interactions in-between processes of the gear manufacturing chain**. Thesis of Doctor of Science in Materials and Manufacturing Processes — Instituto Tecnológico de Aeronáutica, São José dos Campos, 2016.

SALAK, A.; RIECANSKY, V. **Ferrous powder metallurgy**. Cambridge: Cambridge International Science Publishing, 1995.

SCARDI, P.; LEONI, M.; DELHEZ, R. Line broadening analysis using integral breadth methods: a critical review. **Journal of Applied Crystallography**, v. 37, p. 381–390, 2004.

SCHATT, W.; WIETERS, K.; KIEBACK, B. **Pulvermetallurgie**: Technologien und Werkstoffe. Cambridge: Springer, 2006.

SCHERRER, P. Bestimmung der Grösse und der inneren Struktur von Kolloidteilchen mittels Röntgenstrahlen. **Nachrichten von der Gesellschaft der Wissenschaften zu Göttingen**, p. 98–100, 1918.

SCHOLTES, B. Residual stress analysis - an useful tool to assess the fatigue behavior of structural components. In: ADVANCES IN X-RAY ANALYSIS. Germany: International Centre for Diffraction Data, 2000.

SHACKELFORD, J. F. **Introduction to materials science for engineers**. USA: Pearson, 2014.

SIGL, L. S.; RAU, G.; DENNERT, C. When the going gets tough PM gears can cope. **Metal Powder Report**, v. 62, n. 10, p. 22–26, 2007.

SIGL, L. S.; RAU, G.; KREHL, M. Properties of surface densified PM gears. **SAE Technical Papers**, 2005.

SIMCHI, A.; NOJOOMI, A. A. Warm compaction of metallic powders. In: CHANG, I.; ZHAO, Y. (Ed.). **Advances in powder metallurgy: properties, processing and applications**. Cambridge: Woodhead publishing, 2013. p. 86–108.

SKOGLUND, P.; LITSTRÖM, O. Improvement of powder metallurgy gears for engines and transmissions. **SAE Technical Papers**, 2013.

SLATTERY, R.; HANEJKO, F. G.; RAWLINGS, A. J.; MARUCCI, M.; NARASIMHAN, K. S. High performance gears using powder metallurgy technology. **Gear Technology**, 2004.

SPIESS, L.; TEICHERT, G.; SCHWARZER, R.; BEHNKEN, H.; GENZEL, C. **Moderne Röntgenbeugung**: Röntgendiffraktometrie für Materialwissenschaftler, Physiker und Chemiker. 2nd. ed. Mörlenbach: Vieweg+Teubner, 2014.

STOKES, A. R.; WILSON, A. J. C. The diffraction of X-rays by distorted crystal aggregates - i. **Proceedings of the Physical Society**, v. 56, n. 3, p. 174–181, 1944.

STREHL, R. **Tragfahigkeit von Zahnrädern aus hochfesten Sinterstählen**. Doctoral Thesis — RWTH Aachen, Aachen, 1997.

SUORTTI, P.; AHTEE, M.; UNONIUS, L. Voigt function fit of X-ray and neutron powder diffraction profiles. **J. Appl. Cryst.**, v. 12, p. 365–369, 1979.

THÜMMLER, F.; OBERACKER, R. **An introduction to powder metallurgy**. London: The Institute of Materials, 1993.

TROSS, N. **Tragfähigkeitssteigerung von PM Zahnrädern**. Master Thesis — RWTH Aachen, Aachen, 2016.

UPADHYAYA, G. S. **Powder metallurgy technology**. Cambridge: Cambridge International Science Publishing, 2002.

WARREN, B. X-ray studies of deformed metals. **Progress in Metal Physics**, v. 8, p. 147–202, 1959.

WHITERS, P. J.; BADHESIA, H. K. D. H. Residual stress part I - measurement techniques. **Materials Science and Technology**, v. 17, p. 355–365, 2001.

WHITTAKER, D. Powder metallurgy for gear production: current status and potential future trends. **Materials & design**, v. 12, n. 2, p. 97–100, 1991.

WHITTAKER, D. World PM2016: trends in automotive powertrains and their impact on the future of PM applications. **Powder Metallurgy Review**, v. 5, n. 4, p. 35–45, 2016.

ZHAN, K.; JIANG, C. H.; JI, V. Uniformity of residual stress distribution on the surface of S30432 austenitic stainless steel by different shot peening processes. **Material Letters**, v. 99, p. 61–64, 2013.

ZHAN, K.; JIANG, C. H.; WU, X. Y.; JI, V. Surface layer characteristics of s30432 austenite stainless steel after shot peening. **Material Transactions**, v. 53, n. 5, p. 1002–1006, 2012.

Appendix A - RS values

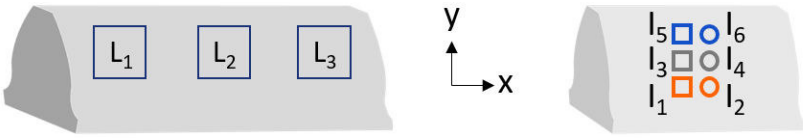

Assumption: $\sigma_z = 0$

TABLE A.1 – PM_S residual stresses values

Spot	σ_x	Δ	σ_y	Δ	τ_{xy}	Δ	τ_{xz}	Δ	τ_{yz}	Δ
L_1	-119.7	15.8	-111.0	18.6	1.4	0.2	-16.0	4.7	6.7	3.8
L_2	-109.6	9.5	-111.0	9.2	7.9	5.6	-19.2	4.7	-2.5	2.6
L_3	-56.1	10.3	-25.8	10.6	0.7	0.1	-10.0	0.6	-5.0	2.6
I_1	-131.8	19.7	-112.7	19.7	0.0	0.0	-4.6	5.2	-4.9	5.2
I_2	-86.0	22.5	-70.4	22.5	0.0	0.0	-11.7	5.9	9.9	5.9
I_3	-74.2	19.2	-118.1	19.2	0.0	0.0	-22.5	5.1	5.1	5.1
I_4	-86.0	25.7	-97.2	25.7	0.0	0.0	-16.1	6.8	0.8	6.8
I_5	-138.8	13.6	-115.0	13.6	0.0	0.0	-37.9	3.6	-2.7	3.6
I_6	-95.9	15.9	-76.2	15.9	0.0	0.0	-30.6	4.2	-0.2	4.2

TABLE A.2 – PM_D residual stresses values

Spot	σ_x	Δ	σ_y	Δ	τ_{xy}	Δ	τ_{xz}	Δ	τ_{yz}	Δ
L_1	-159.0	7.4	-502.8	7.2	-9.0	0.1	7.8	1.9	11.0	1.8
L_2	-176.6	6.9	-469.9	7.2	12.2	0.5	6.8	1.9	9.0	1.9
L_3	-204.0	5.2	-497.8	6.1	42.7	1.0	6.0	1.7	7.2	1.6
I_1	-135.1	16.6	-365.1	15.0	-20.7	1.3	19.7	4.4	15.0	3.4
I_2	-96.8	10.6	-386.2	10.1	-12.4	0.4	19.5	2.7	7.0	2.4
I_3	-156.9	10.1	-474.8	9.8	-7.6	0.2	1.0	2.6	2.5	2.5
I_4	-167.1	16.8	-466.6	17.0	4.1	0.7	3.1	4.2	9.7	4.3
I_5	-358.9	11.0	-461.8	11.2	6.6	1.5	6.4	2.6	12.2	3.0
I_6	-302.9	11.4	-430.5	12.0	5.6	1.2	13.1	2.8	4.6	3.1

TABLE A.3 – PM_HT residual stresses values

Spot	σ_x	Δ	σ_y	Δ	τ_{xy}	Δ	τ_{xz}	Δ	τ_{yz}	Δ
L_1	-911.1	28.3	-789.9	27.8	-1.9	3.9	-107.2	7.0	-4.1	7.1
L_2	-836.7	33.1	-748.5	26.5	-25.4	11.4	-80.4	7.0	18.8	8.2
L_3	-700.0	17.7	-680.2	20.0	28.8	10.0	-91.2	5.7	5.3	1.8
I_1	-554.7	80.0	-670.5	57.2	0.0	0.0	-20.1	23.7	-30.9	14.5
I_2	-546.6	79.9	-610.8	50.6	0.0	0.0	-3.7	23.1	-34.0	13.2
I_3	-791.6	48.3	-707.9	48.3	0.0	0.0	85.9	12.8	12.8	12.8
I_4	-769.3	52.8	-672.0	52.8	0.0	0.0	21.5	14.0	-10.8	14.0
I_5	-685.8	62.5	-694.8	62.5	0.0	0.0	92.6	16.5	-11.3	16.5
I_6	-606.9	59.8	-601.6	56.7	0.0	0.0	100.5	16.2	-1.7	15.0

TABLE A.4 – W_C residual stresses values

Spot	σ_x	Δ	σ_y	Δ	τ_{xy}	Δ	τ_{xz}	Δ	τ_{yz}	Δ
L_1	281.8	13.0	344.3	15.7	-50.2	7.0	-27.4	0.6	-33.4	4.3
L_2	204.9	10.7	240.9	13.0	-27.4	5.6	-17.5	0.6	-35.5	3.6
L_3	247.1	12.8	236.3	11.8	-25.7	7.3	-26.0	0.5	-34.5	0.2
I_1	280.0	18.5	273.1	18.5	0.0	0.0	-53.1	4.9	-36.1	4.9
I_2	225.7	13.2	266.6	13.2	0.0	0.0	-47.8	3.5	-34.3	3.5
I_3	145.3	16.8	202.3	16.8	0.0	0.0	-16.2	4.4	4.4	4.4
I_4	180.5	17.5	225.0	17.5	0.0	0.0	-21.7	4.6	-40.6	4.6
I_5	189.0	21.8	250.6	21.8	0.0	0.0	5.8	5.8	44.5	5.8
I_6	272.1	16.3	296.7	16.3	0.0	0.0	-2.7	4.3	-41.1	4.3

TABLE A.5 – W_HT residual stresses values

Spot	σ_x	Δ	σ_y	Δ	τ_{xy}	Δ	τ_{xz}	Δ	τ_{yz}	Δ
L_1	-520.5	20.3	-432.0	20.5	-0.6	1.7	38.9	5.0	8.2	5.0
L_2	-491.5	9.7	-411.9	11.1	-9.6	2.2	47.4	5.0	0.8	3.0
L_3	-441.3	14.4	-413.8	14.7	-0.5	3.8	34.9	2.2	-0.5	3.7
I_1	-589.4	31.0	-527.8	31.0	0.0	0.0	-2.3	8.2	-20.3	8.2
I_2	-454.6	23.2	-383.5	23.2	0.0	0.0	16.6	6.1	-11.2	6.1
I_3	-530.7	34.0	-514.3	34.0	0.0	0.0	41.8	8.6	8.6	8.6
I_4	-458.3	27.5	-401.7	27.5	0.0	0.0	43.4	7.3	-24.8	7.3
I_5	-463.3	39.7	-501.6	39.7	0.0	0.0	80.6	10.5	0.1	10.5
I_6	-398.8	35.5	-350.9	35.5	0.0	0.0	83.7	9.4	-33.7	9.4

TABLE A.6 – W_SP residual stresses values

Spot	σ_x	Δ	σ_y	Δ	τ_{xy}	Δ	τ_{xz}	Δ	τ_{yz}	Δ
L_1	-868.6	22.4	-976.6	20.1	-10.9	0.4	90.8	6.0	27.8	4.6
L_2	-823.4	13.2	-936.2	15.0	14.0	3.6	106.7	6.0	35.8	4.0
L_3	-773.5	14.4	-935.0	13.5	-8.9	0.3	108.2	2.9	28.9	3.2
I_1	-756.7	73.1	-882.3	73.1	0.0	0.0	19.4	19.3	-33.4	19.3
I_2	-898.0	65.3	-996.1	65.3	0.0	0.0	49.3	17.3	-22.8	17.3
I_3	-873.2	86.0	-1023.6	86.0	0.0	0.0	164.3	22.7	22.7	22.7
I_4	-789.3	67.7	-893.9	67.7	0.0	0.0	84.3	17.9	-17.4	17.9
I_5	-760.5	68.2	-867.6	68.2	0.0	0.0	182.9	18.0	-3.2	18.0
I_6	-634.1	66.8	-847.2	66.8	0.0	0.0	204.9	17.7	-6.9	17.7

TABLE A.7 – W_G residual stresses values

Spot	σ_x	Δ	σ_y	Δ	τ_{xy}	Δ	τ_{xz}	Δ	τ_{yz}	Δ
L_1	-1389.7	13.2	-1242.0	14.8	-15.9	3.3	40.0	3.0	-13.9	3.9
L_2	-1377.4	17.5	-1179.1	19.0	-14.7	3.1	49.2	3.0	-9.8	5.0
L_3	-1382.6	13.6	-1243.1	15.2	-14.3	3.5	46.0	4.1	-14.4	4.0
I_1	-1267.3	45.4	-1114.3	45.4	0.0	0.0	2.6	12.0	-26.8	11.9
I_2	-1323.4	53.0	-1128.6	53.0	0.0	0.0	-4.9	14.0	-33.2	14.0
I_3	-1191.4	35.7	-1049.9	35.7	0.0	0.0	146.6	9.4	9.4	9.4
I_4	-1213.9	38.3	-1076.6	38.3	0.0	0.0	145.8	10.1	-8.3	10.1
I_5	-1316.2	57.8	-1166.6	57.8	0.0	0.0	259.3	15.3	-9.4	15.3
I_6	-1189.5	41.8	-1095.4	41.8	0.0	0.0	271.7	11.1	-26.7	11.1

Annex A - Gears terminology

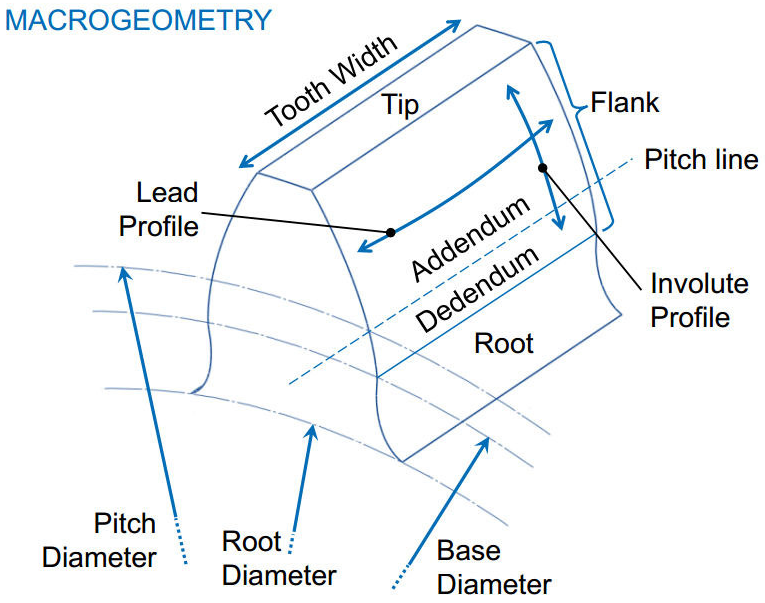

FIGURE A.1 – Gear nomenclature for macrogeometry (AGMA, 2011; MAZZO, 2013)

FOLHA DE REGISTRO DO DOCUMENTO

1. CLASSIFICAÇÃO/TIPO	2. DATA	3. DOCUMENTO Nº	4. Nº DE PÁGINAS
DM	08 de Agosto de 2017	DCTA/ITA/DM-071/2017	100

5. TÍTULO E SUBTÍTULO:

Residual stresses heterogeneity assessment of high performance powder metallurgy gears

6. AUTOR(ES):

Lucas Barreiros Robatto

7. INSTITUIÇÃO(ÕES)/ÓRGÃO(S) INTERNO(S)/DIVISÃO(ÕES):

Instituto Tecnológico de Aeronáutica - ITA

8. PALAVRAS-CHAVE SUGERIDAS PELO AUTOR:

Tensões residuais; Metalurgia do pó; Engrenagens

9. PALAVRAS-CHAVE RESULTANTES DE INDEXAÇÃO:

Tensão residual; Engrenagens; Metalurgia do pó; Fabricação de aço; Heterogeneidade; Metalurgia

10. APRESENTAÇÃO: (**X**) **Nacional** ( ) **Internacional**

ITA, São José dos Campos. Curso de Mestrado. Programa de Pós-Graduação em Engenharia Aeronáutica e Mecânica. Área de Materiais e Processos de Fabricação. Orientador: Prof. Dr. Anderson Vicente Borille. Defesa em 04/07/2017. Publicada em 2017.

11. RESUMO:

The implementation of powder metallurgy (PM) for high performance automotive transmission gears has the potential to replace the conventional wrought steel manufacturing chain in a near future. Several studies have shown the possible benefits of this implementation in terms of manufacturing costs, times and product performance. The main limitation of this transition is the inferior mechanical strength of the PM gears, which may implicate in shorter fatigue life. With the advance of the technique, however, the strength of PM gears have been improved, getting closer to that of the wrought steel ones. Nonetheless, the powder metallurgy chain has as characteristic effects of microstructural heterogeneity, due to the porosity and the grain orientation caused by surface densification. A consequence of this is a heterogeneous state of residual stresses (RS), that may affect the fatigue behavior of such gears. The present dissertation, then, has as objective the comprehension of the RS heterogeneity state of PM gears. It is based on the hypothesis that such heterogeneity can be assessed through X-ray diffraction methods. Hence, two research questions were formulated to guide this study. The first question is about the most suitable method for this assessment. The second question is about how significant is the effect of the PM chain on the RS heterogeneity of gears. According to these questions, RS mappings and X-ray diffraction line broadening analysis were applied to the surface of the flank of gear teeth correspondent to successive steps of the PM and wrought steel manufacturing chains. Correlational surface integrity assessments, such as metallography, topography analysis and hardness mapping, were also performed to support the RS results. From the methodology analysis, the line broadening was the most suitable method for investigating single process steps, and both methods are indicated for comparing different manufacturing steps and chains. It could then be observed that the RS heterogeneity of gears is manifested in two levels (macro and micro RS) and three types of distribution (along the lead, along the involute and diffuse). From the evolution of the heterogeneity along the PM chain, it was found that each of the process steps is associated to a characteristic RS heterogeneity. It could also be perceived that the heterogeneity of RS is propagated along the chains analyzed. Therefore, the present study contributes to the knowledge of PM gears for their lifetime optimization, whose consequences can benefit the powder metallurgy and automotive industries.

12. GRAU DE SIGILO:

(**X**) **OSTENSIVO** ( ) **RESERVADO** ( ) **CONFIDENCIAL** ( ) **SECRETO**